Theses and Dissertations--Chemistry
Chemistry

2014

A STUDY OF LIGNIN DEPOLYMERIZATION BY SELECTIVE CLEAVAGE OF THE C**α**-C**β** LINKAGES IN LIGNIN MODEL COMPOUNDS VIA BAEYER-VILLIGER OXIDATION & AN INVESTIGATION OF THE CHANNELING REACTION IN NITROGEN-DOPED MULTIWALLED CARBON NANOTUBES (N-MWCNTS)

Nikhil Dilip Patil
University of Kentucky, nikhilpatil22@gmail.com

STUDENT AGREEMENT:

I represent that my thesis or dissertation and abstract are my original work. Proper attribution has been given to all outside sources. I understand that I am solely responsible for obtaining any needed copyright permissions. I have obtained needed written permission statement(s) from the owner(s) of each third-party copyrighted matter to be included in my work, allowing electronic distribution (if such use is not permitted by the fair use doctrine) which will be submitted to UKnowledge as Additional File.

I hereby grant to The University of Kentucky and its agents the irrevocable, non-exclusive, and royalty-free license to archive and make accessible my work in whole or in part in all forms of media, now or hereafter known. I agree that the document mentioned above may be made available immediately for worldwide access unless an embargo applies.

I retain all other ownership rights to the copyright of my work. I also retain the right to use in future works (such as articles or books) all or part of my work. I understand that I am free to register the copyright to my work.

REVIEW, APPROVAL AND ACCEPTANCE

The document mentioned above has been reviewed and accepted by the student's advisor, on behalf of the advisory committee, and by the Director of Graduate Studies (DGS), on behalf of the program; we verify that this is the final, approved version of the student's thesis including all changes required by the advisory committee. The undersigned agree to abide by the statements above.

<div align="right">

Nikhil Dilip Patil, Student

Dr. Mark S. Meier, Major Professor

Dr. Dong-Sheng Yang, Director of Graduate Studies

</div>

ABSTRACT OF DISSERTATION

Nikhil D. Patil

The Graduate School

University of Kentucky

2014

A STUDY OF LIGNIN DEPOLYMERIZATION BY SELECTIVE CLEAVAGE OF THE Cα-Cβ LINKAGES IN LIGNIN MODEL COMPOUNDS VIA BAEYER-VILLIGER OXIDATION

&

AN INVESTIGATION OF THE CHANNELING REACTION IN NITROGEN-DOPED MULTIWALLED CARBON NANOTUBES (N-MWCNTS)

DISSERTATION

A dissertation submitted in partial fulfillment of the
requirements for the degree of Doctor of Philosophy in the
College of Arts and Science
at the University of Kentucky

By

Nikhil D. Patil

Lexington, Kentucky

Director: Dr. Mark S. Meier, Professor of Chemistry

Lexington, Kentucky

2014

ABSTRACT OF DISSERTATION

A STUDY OF LIGNIN DEPOLYMERIZATION BY SELECTIVE CLEAVAGE OF THE Cα-Cβ LINKAGES IN LIGNIN MODEL COMPOUNDS VIA BAEYER-VILLIGER OXIDATION

Lignin is amorphous aromatic polymer derived from plants and is a potential source of fuels and bulk chemicals. Herein, we present a survey of reagents for selective stepwise oxidation of lignin model compounds. Specifically, we have targeted the oxidative cleavage of Cα-Cβ bonds as a means to depolymerize lignin and obtain useful aromatic compounds. In this work, we prepared several lignin model compounds that possess structures, characteristic reactivity, and linkages closely related to the parent lignin polymer. We observed that selective oxidation of benzylic hydroxyl groups using TEMPO/O_2, followed by Baeyer-Villiger oxidation of the resulting ketones using H_2O_2, successfully cleaves the Cα-Cβ linkage in the model compounds. This process was also applied to depolymerization of Organosolv lignin. The deconstructed lignin was analyzed by a number of techniques, including ATR-IR, GPC, and ^{31}P NMR of suitably derivatized samples.

KEYWORDS: Lignin model compounds, Organosolv lignin, oxidative depolymerization, Cα-Cβ cleavage, β-O-4 linkages

AN INVESTIGATION OF THE CHANNELING REACTION IN NITROGEN-DOPED MULTIWALLED CARBON NANOTUBES (N-MWCNTS)

The reduction of nitrogen-doped multiwalled carbon nanotubes (N-MWCNTs) with Li/NH$_3$ results in deep longitudinal cuts in the nanotubes structure. As the N-MWCNTs are anisotropic, we were able to investigate whether the unzipping process proceeds with equal efficiency from the tip end or from the root (catalyst) end of the N-MWCNT structure. To accomplish this we prepared polymer filled aligned arrays of N-MWCNTs, then exposed one or the other end. Through this approach we were able to shield the sidewalls and either end of the nanotubes from the Li/NH3 solution We have found that when the top end of the N-MWCNTs array was exposed to the reaction mixture, very few nanotubes suffered significant 'unzipping'. However, when the root (substrate) side of the array is exposed to the reaction mixture, we observe the features characteristic of nanotubes with longitudinal cuts. Our finding provides some insight into the mechanism of the unzipping process, and provides evidence that the unzipping process has a directional preference-unzipping from the root end towards the tip end. And may provide a method for selective functionalization of the interior of tubes and create a new form of nanotube- based porous membrane.

Keywords: N-MWCNTs, unzipping, nitrogen-doped multiwalled carbon nanotubes, fracturing process, infiltration

<div style="text-align: right;">

Nikhil D. Patil
Student's Signature

04/29/2014
Date

</div>

A STUDY OF LIGNIN DEPOLYMERIZATION BY SELECTIVE CLEAVAGE OF THE Cα-Cβ LINKAGES IN LIGNIN MODEL COMPOUNDS VIA BAEYER-VILLIGER OXIDATION

&

AN INVESTIGATION OF THE CHANNELING REACTION IN NITROGEN-DOPED MULTIWALLED CARBON NANOTUBES (N-MWCNTS)

By

Nikhil D. Patil

<div style="text-align:right">

_____
Dr. Mark S. Meier
Director of Dissertation

_____
Dr. Dong-Sheng Yang
Director of Graduate Studies

_____
04/29/2014
Date

</div>

RULES FOR THE USE OF DISSERTATIONS

Unpublished dissertations submitted for the Doctor's degree and deposited in the University of Kentucky Library are as a rule open for inspection, but are to be used only with due regard to the rights of the authors. Bibliographical references may be noted, but quotations of summaries of parts may be published only with the permission of the author, and with the usual scholarly acknowledgments.

Extensive copying or publication of the dissertation in whole or in part also requires the consent of the Dean of the Graduate School of the University of Kentucky.

A library that borrows this dissertation for use by its patrons is expected to secure the signature of each user.

Name   Date

_____

_____

_____

_____

_____

_____

_____

_____

_____

DISSERTATION

Nikhil D. Patil

The Graduate School

University of Kentucky

2014

A STUDY OF LIGNIN DEPOLYMERIZATION BY SELECTIVE CLEAVAGE OF THE Cα-Cβ LINKAGES IN LIGNIN MODEL COMPOUNDS VIA BAEYER-VILLIGE OXIDATION

&

AN INVESTIGATION OF THE CHANNELING REACTION IN NITROGEN-DOPED MULTIWALLED CARBON NANOTUBES (N-MWCNTS)

―――――――――――――――――――――――

DISSERTATION

―――――――――――――――――――――――

A dissertation submitted in partial fulfillment of the
requirements for the degree of Doctor of Philosophy in the
College of Arts and Science
at the University of Kentucky

By
Nikhil D. Patil

Lexington, Kentucky

Director: Dr. Mark S. Meier, Professor of Chemistry

Lexington, Kentucky

2014

Dedicated to my beloved grandparents, Late Parshuram N. Patil and Vimal P. Patil

ACKNOWLEDGEMENTS

TABLE OF CONTENTS

LIST OF TABLES

LIST OF FIGURES

CHAPTER 1. GENERAL INTRODUCTION

1.1 Introduction

Fossil fuels are an easily available conventional source of liquid fuel in a contemporary world. The reserves of fossil fuels are being depleting rapidly due to an increase in consumption rate and rise in population. Therefore, an alternate fuel source is extremely necessary. The main advantage of liquid petroleum is that it can be easily stored, and it has low flash points. Because of this, it is conveniently used as a fuel in vehicles. In the USA, nearly 70% of crude oil consumption is devoured in vehicles.[1]

Renewable resources like biomass are important carbon feedstocks to generate fuel and chemicals. Biomass seems to have a significant potential for conversion into liquid fuels, which could finally replace fossil fuel. Renewable resources like biomass could provide an alternate source of liquid fuels, if methods can be developed for converting these materials into a form that is suitable for use. The US Department of Energy is aiming to replace 30% transportation fuel by biomass by 2030.[2] Correspondingly, many petrochemical companies like Shell, Dupont, BP, DOW and Conoco-Phillips are doing major research to produce biofuels and biochemicals from biomass.[3]

Biomass is organic matter derived from living organisms. Often, material derived from plants is referred to as biomass, and it is a renewable-energy source. In the photosynthesis process, energy from the sun is converted into chemical energy, to produce carbohydrate molecules. Through this process, atmosphere carbon is fixed into biomass. In olden days, biomass was burned and used as a conventional source of heat for cooking purposes. In this process, chemical energy stored in biomass is converted into heat. However, this traditional technique has low thermal efficiencies and enormous amounts of pollutant are introduced into the atmosphere. In order to use biomass effectively, it is important to

process them into liquid or gaseous fuel. Techniques to convert biomass into fuel and useful chemicals have been under intense study for many decades.

Biofuel is broadly classified in three categories: first-generation, second-generation and third-generation biofuels. First-generation biofuels have been derived from food crops like corn, sugarcane, jatropha, vegetable, coconut, and soybeans.[4] Two most common examples of first-generation biofuels are bio-derived alcohols and biodiesel.[5] Bio-derived alcohols are produced from sugar and starch via microorganism and enzymatic fermentation. Biodiesel is produced by trans-esterification of oil or fats. Second generation biofuels are derived from non-edible lignocellulosic biomass like agricultural waste and crop residue.[4,6] The DOE and USDA reports that the USA has an ability to generate 1.3 billion dry tons of agricultural and forest lignocellulosic waste per year.[7] The extraction of biofuel from lignocellulose biomass seems to be extremely challenging however, and second generation biofuel is considered to be the "next generation" of fuel, as edible food is consumed to generate first-generation biofuels. Second-generation biofuels are produced from significantly less-expensive waste materials.[3] In many developed countries, large investments have been made in the advancement of technology for economical production of biofuel.[2] Ethanol is commercialized in some countries, and its use as a component of motor fuels is increasing. Third generation biofuels are produced from algae and micro-organisms.[8] Production of third-generation fuels is still an underdeveloped research field.

More specifically, biomass consists of three major constituent cellulose, hemicellulose and lignin.[9,10] Cellulose is a linear polysaccharide with basic D-glucose units linked via β (1→4) linkages. Cellulose is a major constituent of wood, and it is mainly used in paper industries. Nowadays, the usage of cellulose in the production of ethanol is also commercialized in many countries. Subsequently, the use of ethanol as an additive to gasoline is increased appreciably. Hemicellulose is amorphous polysaccharides made from xylose, mannose, galactose, rhamnose, arabinose and glucose. It is known that hemicellulose can be easily hydrolyzed by dilute acid or base. On other hand, lignin is made of aromatic polymer with complex irregular structure. The liquefaction of lignin is still an undersized research area, because lignin resistant to most of the enzymes and

chemicals. The lignin is a recalcitrant, high molecular weight polymer, and at this time, efficient and inexpensive technique for its controlled depolymerization is not advanced.
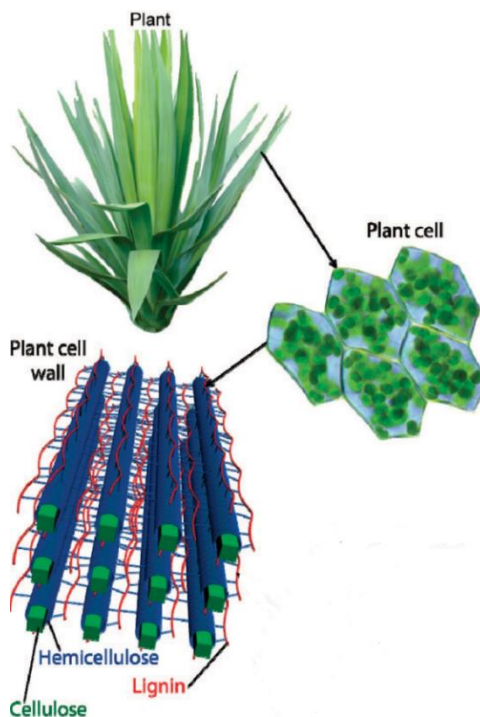
Figure 1. 1 Schematic representation of lignocellulosic material.[11] Reprinted with permission from reference.[10] Copyright (2010) American Chemical Society.

Lignin serves as a binder between cellulose and hemicellulose, and it provides mechanical strength and structural support. Lignin, being the second most abundant organic compound on earth after cellulose, is considered a potential source of fuels and bulk chemicals. The three major class of lignin are hardwood (angiosperm), softwood (gymnosperm) and grass/annual plant (graminaceous) lignin. The softwood has high lignin content, and annual plant has least lignin content.[10] Common industrial uses of lignin include board binder, concrete, disperse pesticides, board binder, and food additive. Currently, in the pulp and paper industry, unwanted lignin is separated from the biomass and burned as a low-grade fuel.

1.2   Lignin structure

1.2.1 Monolignol Biosynthesis

Lignin is a cross-linked phenolic polymer made from commonly occurring monoliginols: p-coumaryl alcohol (**H**), coniferyl alcohol (**G**) and sinapyl alcohol (**S**) (Figure 1.2). These monomeric precursors are distinguished based on methoxyl groups present at C3 and C5 in the aromatic ring. The monolignols are the monomeric lignin precursors, which are formed via the phenylpropanoid biochemical pathway.[12]
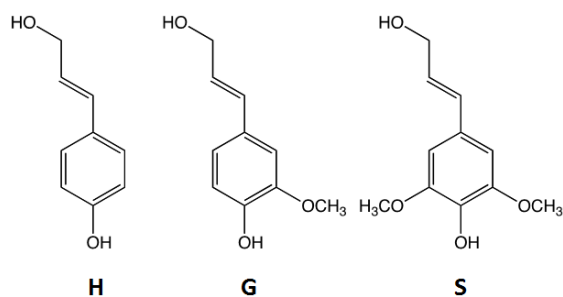
Figure 1. 2 Monolignol: p-coumaryl alcohol (H), coniferyl alcohol (G) and sinapyl alcohol (S).

The chemistry of the lignin has been study for 100 years, however the investigation of lignin structure is still an undergoing research area. In 1874, Tiemann and Haarmann first stated that coniferyl alcohol was basic structure unit of lignin polymer.[13] Klason and group prove that when coniferyl alcohol was heated with acidic sulfite solution, compounds were produced that had similar characteristics to that of lignin sulfonate.[13] Later, in 1968, Freudenberg and co-worker further confirmed the structure of lignin. In their experiment dehydrogenation of coniferyl alcohol produced polymer structure as native lignin.[14]

In the past, many researchers proposed that enzymatic catalytic one-electron oxidation of the monolignol initiates the lignin polymerization process, and currently this theory is accepted worldwide.[15] In the lignification process, monomer radicals interconnect via radical coupling reactions. The phenoxyl radical formed has fairly stable resonance structure as shown in figure 1.3, the delocalized radical potentially coupled through four

different center leads to various structure units.[16] The oxidation potentials and radical reactivity govern which linkage form favorably in phenol oxidative coupling.[17]
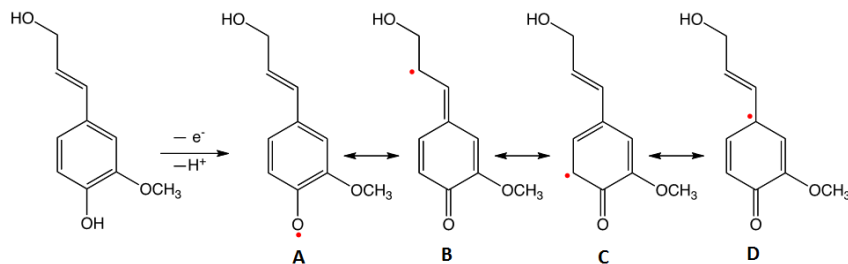
Figure 1. 3 Phenoxyl radical resonance structure.
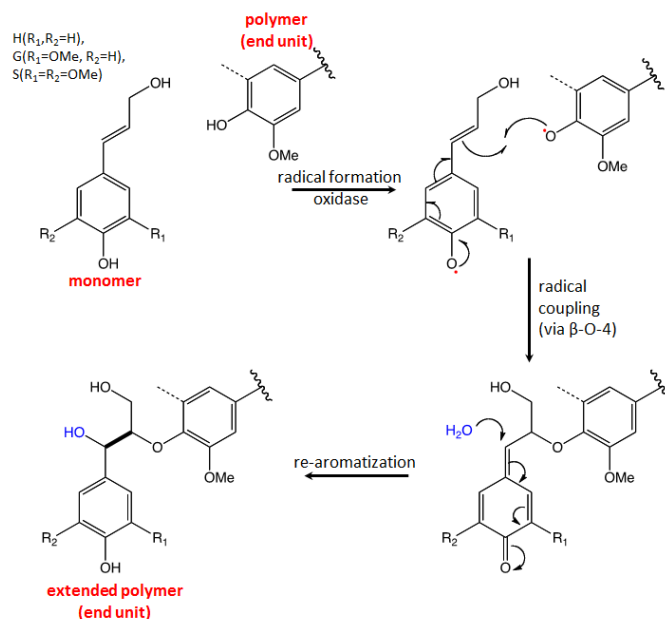
Figure 1. 4 β-O-4 linkage: endwise radical coupling reactions.[18,19]

The monomeric radical can cross-couple with an oligomer to form three types of linkages: dimerization to form β-O-4, β -5 and cross dimerization to form β- β linkages.[19] Additionally, 5-5 and 5-O-4 linkages are form by oligomer-oligomer coupling reaction. The β-O-4 and β -5 linkages produce a linear lignin macromolecule, via endwise polymerization. The 5-5 and 5-O-4 linkages are responsible for cross-links or branch polymerization, also known as random polymerization. Figure 1.4 is an example of β-O-4 linkage endwise polymerization. The first step is one electron oxidation of the monolignol, the second step is radical coupling of phenoxyl radical with coniferyl alcohol radical at β

position to form a quinone methide intermediate. In last step, the quinone methide intermediate reacts with a water molecule to form the β-O-4 linkage. This unit further undergo endwise coupling reaction.[19,20]

1.2.2 Linkages

Lignin is a phenylpropanoid polymer with a complex and irregular structure.[20] Lignification is a random polymerization process, and the polymer formed is cross linked, optically inactive, and the linkages do not have specific regularity.[20] Commonly occurring linkages between monomer units have been determined by breaking the lignin polymer into small subunits using techniques such as pyrolysis[21], oxidation, thioacidolysis,[22] and biodegradation.[23] The chemical structures of some structural moieties have been determined by wet chemical methods,[24] and by techniques such as gas chromatography-mass spectrometry (GC-MS)[21], nuclear magnetic spectroscopy (NMR)[24], Raman microprobe[25] and computational studies.[26] These studies have shown that the most common linkages found in lignin are β-O-4, 5-5, β-5, 4-O-5, β-1, and β-β, of which the β-O-4 linkage is prominent.[10,27] The 5-5, β-5, 4-O-5, β-1, and β-β are rigid towards most chemical and biological degradation processes.[17,18] The linkages formed via C−O bonds are results of reaction at phenolic hydroxyl group. Relatively, the reaction at C3 or C5 of benzene ring to forms C−C bonds linkages is less common. As S units are preoccupied by methoxy groups the percentage of C−O bonds outnumber.
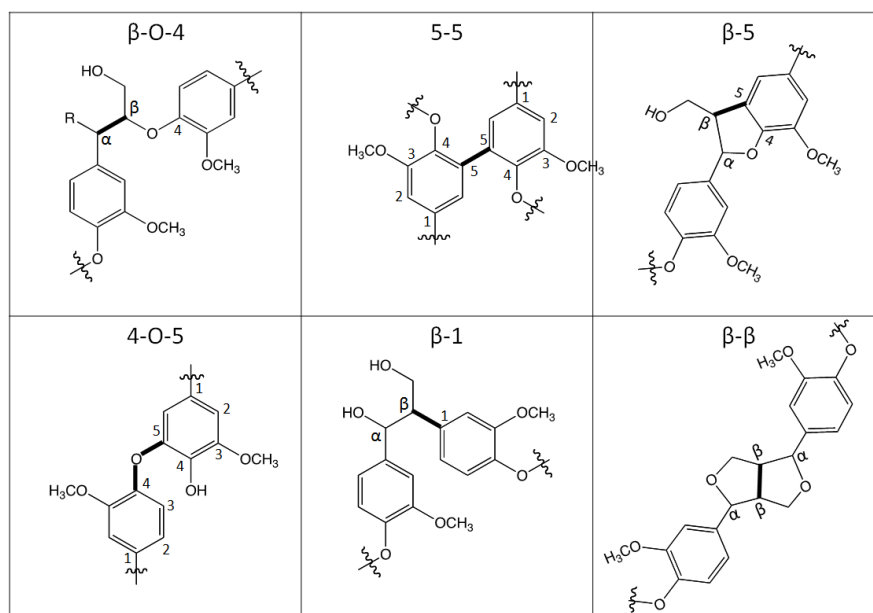
Figure 1. 5 Most common linkages found in lignin.

Based on analysis and theoretical yields of the oxidized product, the approximate percentage of linkages found in softwood and hardwood is represented in table 1.1.[28] The β-O-4 linkage is more than 50 % of the linkages in softwood and the ratio of *β–O–4* /*β–5* linkage is roughly 4:1.

Table 1. 1 Approximate percentage of different linkages found in softwood and hardwood.[28]

Linkage Type	Approximate percentage	
	Softwood	Hardwood
β-O-4	45-50	60
5-5	19-22	9
β-5	9-12	6
4-O-5	4-7	6.5
β-1	7-9	1
β-β	2-4	3

In the lignification process, cross-coupling reactions between the monolignol and the polymer end unit results in extension of the polymer. The polymer units P_S, P_G are shown

below undergoes cross coupling reactions with monolignols S and G to form the various linkages. The table 1.2 shows that β–O–4 linkages outnumber β–5 linkages. The polymer units' P$_S$ will not form β–5 linkages because C3 and C5 position is preoccupied by methoxy groups.

P$_G$ P$_S$
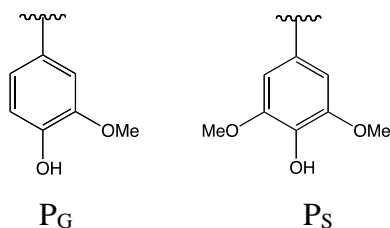
Table 1. 2 Lignification differs substantially from dimerization of polymer unit and monolignols.

Monolignol alcohol	Polymer units	β–O–4	β–5
G	P$_G$	✔	✔
G	P$_S$	✔	✖
G	P$_G$	✔	✔
G	P$_S$	✔	✖

In the study of artificial lignin synthesis, Syrjanen and Brunow found that when coniferyl alcohol is reacted with 4-(1-Hydroxyethyl)-2-methoxyphenol through dialysis tubing, the ratio of β–O–4 /β–5 product formed was 10:1, whereas in case of guaiacyl dimer only the β–O–4 trimer was found. Additionally, their experiment concludes that the monolignol addition rate changes the ratio of β–O–4 /β–5 linkages. The result suggest that the percentage of linkages in lignin is controlled by the availability of monolignol radicals.[18]

The molecular structure of lignin varies widely between plant species as well as between different plant tissues.[29,30] It is important to note that lignin can be made from more than three monomers, and because of mutations in plants, complex pattern of linkages is found in different plant tissues.[31]

1.2.3 Model structure of lignin

Lignin, being a high molecular weight cross-linked polymer, is insoluble in most of the organic solvents. In structure determination studies, solubility of lignin is increased by fragmenting the polymer into smaller monomeric units or by attaching polar functional groups to the parent backbone of the lignin. Significantly, chemically altered lignin samples have been used for structure determination studies. Therefore, the structure of lignin proposed by many researchers is not an exact structure. Moreover, lignin that is artificially synthesized by dehydrogenation polymerization of commonly occurring monolignols is assumed to have the same structure as native lignin. In 1968, Freudenberg and Neish proposed a structure for spruce lignin based on the similar dehydrogenation polymerization and this structure of lignin is shown in figure 1.6.
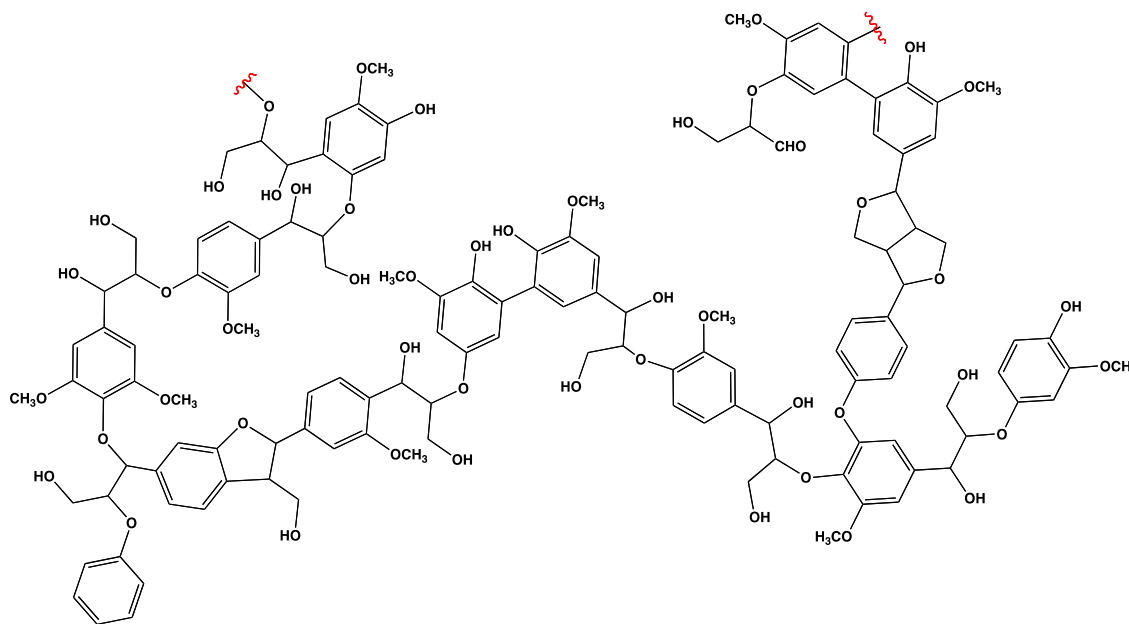
Figure 1. 6 Model structure of spruce lignin.[27] Image adapted with permission from reference.[27] Copyright 2003 Wiley Periodicals, Inc., A Wiley Company

The lignification in growing plant take place systematically such that composition of monomers differ in subcellular parts.[29,30] Softwood lignin mostly content guaiacyl sub-unit, hardwood lignin composed of both guaiacyl (G) and syringly (S) subunit. The grass/annual plant (graminaceous) lignin mainly composed of the p-coumaryl alcohol (H) subunit. The Argyropoulos group demonstrated that syringly (S) content in softwood is negligible whereas in hardwood S: G ratio in approximately 1 to 5. The ration of S, G and

H of enzymatic mild acidolysis lignin (EMAL) isolated from different wood species was determined using DFRC (derivatization followed by reductive cleavage)/^{31}P NMR (μmol/g) is shown in table 1.3.[32]

Table 1. 3 S: G: H ratio in select biomass.[32]

EMAL source	Lignin	sinapyl alcohol (**S**)	coniferyl alcohol (**G**)	p-coumaryl alcohol (**H**)
Douglas fir	Softwood	0	0.94	0.06
White fir		0	0.96	0.04
Redwood		0	0.95	0.05
Normal pine		0	0.98	0.02
Comp pine		0	0.91	0.09
E. Globulus	Hardwood	0.83	0.15	0.02

The ratio of monolignol sub-unit determines the type and number of cross linkages in lignin. Guaiacyl units can form three crosslink (*β–β, β–O–4 and β–5*), while syringly units can form only two kinds of crosslinks (*β–β and β–O–4*). Lignin samples from different plant tissue or from plants grown in dissimilar environment can have very different S/G ratios. The S/G ratio of lignin from stem tissues is from 1.6 to 2.5, and from root tissues that ratio is 1.1 to 2.[30] The S units are mainly coupled via weak ether bonds and this results in an unbranched structure. Funaoka et al. suggested that during the Kraft pulping process, the presence of syringyl units facilitates lignin delignification.[33] The S/G ratio can be increased by genetic engineering in order to simplify the pulping process.[34] Results reported by Pilate and group show that growth of these genetically modified plants is normal.[35] Further, Wang et al. demonstrated that genetic manipulation of switch grass yields phenotypically normal plants.[36]

1.3   Lignin isolation and types[37]
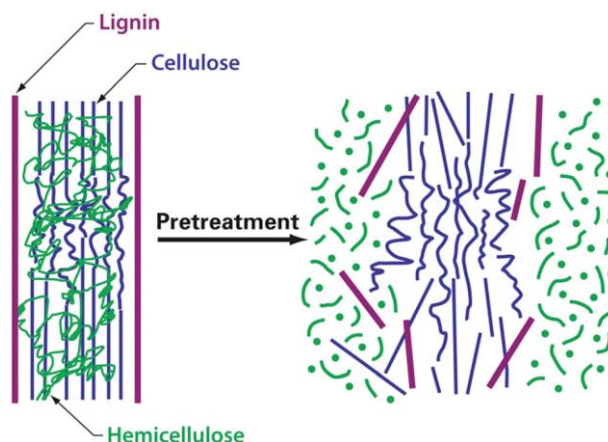
Figure 1. 7 Schematic representation of the lignocellulose material after pretreatment process. Image reprinted from reference,[38] adapted from Hsu, T. A.[39] Copyright 2012, Royal Society of Chemistry.

Lignin is chemically bonded to hemicellulose and non-lignin material. So as to isolate lignin from biomass, either lignin is dissolve selective or cellulose/hemicellulose is dissolve preferentially. Some of widely used methods to isolate lignin are given below.

(i) <u>Kraft lignin process</u>: In this method, wood chips are treated with sodium hydroxide and sodium sulfide for several hours at 170°C. Because of this ether linkages are fragmented and molecular weight lignin is lowered. The ionized phenol sodium salts increase the solubility of lignin in strongly basic solution. Kraft pulping is a widely used process in pulp and paper industries.

(ii) <u>Lignosulfonate Process</u>: In this process, biomass is treated with sulfur dioxide and hydrogen sulfite, such that sulfonic acid groups get attached to the lignin polymer to form lignosulfonates. The introduction of polar group increases the hydrophilicity of the polymer which in turn increases the solubility of polymer in aqueous solution. The molecular weight of lignin obtained by this method is higher that of Kraft lignin process. The lignosulfonate process is also used in paper industries to separate lignin from lignocellulose material.

(iii) <u>Organosolv Process</u>: In this process, lignocellulose biomass is treated with a mild acid in an aqueous organic solvent like methanol, ethanol, butanol, ethylene glycol and

tetrahydrofurfuryl alcohol. This method has several advantages over Kraft and lignosulfonate process. Firstly, the characterization of lignin is easier because lignin obtained by this process is soluble in some of the common polar organic solvent. Secondly, the original lignin structure remains largely unchanged in the extraction process and lignin is free from non-woody lignocellulose impurities. Lastly, the Organosolv process does not pollute water or generate a fishy odor as other pulping processes. Recently, this method is regularly used in bio-refinery as well as in pulp/paper industries.

(iv) Laboratory process: Various laboratory processes isolate the lignin with least altering the original structure. In this method, cellulose/ hemicellulose biomass is selectively dissolved using formic acid hydrolysis, H_2SO_4 hydrolysis, cellulose enzyme and milled wood processes.

It is hard to predict which method is better, as each method has advantages and disadvantages. Argyropoulos and group isolated lignin from a hardwood and from different species of softwood via three different methods. They found that lignin isolated from different species with the same method have different molecular weights, yields, as well as lignin structures.[32] A particular isolation processes may give a better yield for some species of plant, however it may not work properly for other species.[32] Each pretreatment process is known to bring out specific changes in structure of the native lignin, such that change in structural pattern of lignin isolated from particular method has resemblance. In order to study the depolymerization of lignin it is important to separate lignin without altering its structure. According to many researchers, abiotic and biotic stresses can help to increase lignin content as well as to change its chemical composition.[40-42] Biotic stresses are caused by other organism like virus, fungi or bacteria, and abiotic stresses occur due to factors such as temperature, UV-B radiation, or a nutrient deficiencies. Campbell and group study the effect of light on the biosynthesis of lignin, and found that light stimuli clearly lead to an increase in the S:G ratio.[43] Similarly, drought stress also increases the S:G ratio in Eucalyptus.[44] Thus, by increasing lignin content or by modifying the structure of lignin, the researcher can simplify the depolymerization process and raise the potential for lignin as a bioenergy feedstock material.

1.4 Fuel and Bulk chemicals from lignin

Crude oil, also known as petroleum, is extensively used in the internal-combustion engines. Crude oil basically consists of hydrocarbons derived from ancient biomass. It is a mixture of hydrocarbons that have different molecular weights and boiling points. In the fractional distillation process, hydrocarbons are separated into fractions with a narrow distribution of carbon atoms. Lower boiling fractions consist of gases which contain C1 to C4 carbon molecules. "Straight-run" gasoline is a blend of C5 to C10 hydrocarbons, and diesel fuel is typically made of compound with 12 to 20 carbon atoms. The valorization of lignin into monomeric aromatic molecules for use as a source of bulk chemicals and biofuel requires catalytic process that will fragment specific linkages efficiently. Fragmentation can be achieved by three common processes: catalytic oxidation reactions, catalytic reduction reactions and cracking.

(i) <u>Catalytic oxidation reactions</u>: Catalytic oxidation reactions: According to studies reported in the literature, the oxidative fragmentation paths has been useful in the determination of the structure of native lignin.[45-47] Effective oxidative depolymerization reactions include nitrobenzene oxidation, potassium permanganate/sodium periodate oxidation, and microbiological degradation.[48] These processes convert lignin into aromatic compounds with different functional groups, including aldehydes, acids, alcohols, allylic alcohols, and ethers. Lin and group demonstrated that aerobic oxidation of lignin by perovskite type oxide catalyst results in aromatic aldehydes.[49] Another group reported electrochemical depolymerization of Kraft lignin on Pt, Au, Ni, Cu and PbO_2 anodes.[50] The most studied homogeneous oxidation catalysts are porphyrin catalysts, Schiff-base catalysts, polyoxometalate based catalysts, and simple metal salt based catalysts.[51-53] Oxidative degraded small molecules tend to have higher oxygen content and because of this reason, their usability as bulk chemicals have been considered , although hydrocarbons can generated to produce biofuel.[10]

(ii) <u>Catalytic reduction reactions</u>: In 1938, Harris and group reported that hydrogenation of hardwood lignin generates nine or higher carbon atom compounds.[54] The catalytic hydrogenation of lignin and lignin model compounds aims to produce bio-oils and phenols. Hydrotreatment of lignin is emphasized as a way to upgrade the quality of the bio-oil.

Hydrotreatment lowers the oxygen content, and this helps to improve the thermal stability and reduces the volatility of the oil. Various reported heterogeneous and homogeneous catalysts used for hydrogenation of lignin, shows promising results.[55,56] The copper-dopes porous metal oxide heterogeneous catalyst effectively hydrogenate lignin into monomeric fuel additives.[57] Electrocatalytic hydrogenation of phenolic β–O–4 lignin model compounds with help of Ni and Pd cathodes has produced phenols.[58] Some homogeneous hydrogenation catalysts work in two phase reactions, using phase transfer catalyst (PTC). The examples of PTC catalysts are chloro(1,5-hexadiene)-rhodium for hydrogenation of arenes,[59] $RhCl_3$/ trioctylamine for reduction of disubstituted aromatics ring.[60] Ragauskas et al. reports a completely soluble catalyst for hydrogenative depolymerization of organosolv lignin with $Ru(PPh_3)_3Cl_2$ catalyst along with either Raney-Ni or Pt/C or using $NaBH_4/I_2$.[61] The reduction process has certain drawbacks, including high H_2 pressures and high temperatures, difficulty in recycling of the catalyst, and catalyst deactivation. These features make exploitation on an industrial scale is truly difficult.

(iii) <u>Cracking</u>: In this process, the polymer is broken down into small hydrocarbons by pyrolysis under inert atmosphere. Beste and Buchanan investigated the thermal transformation in lignin model molecules by flash vacuum pyrolysis via computational study.[62-65] According to their finding, fragmentation proceeds by free radical reactions, molecular rearrangements and concerted eliminations. Some strategies to increase the efficiency of the cracking process are fast pyrolysis, incorporating a catalyst, adding formic acid, or by modifying reactor designs.[10]

Various cracking catalysts reported in the literature have been successful in generating aliphatic as well as aromatic hydrocarbons. Catalytic hydrdeoxygenation of lignin using Fe/SiO_2 produces aromatic hydrocarbons,[66] Pd supported on SBA-15 catalysts to generate phenols,[67] calcium formate fast pyrolysis to generate alkylated phenols,[68] and deoxygenation of biomass via bimetallic Ni/ V catalyst.[69] The cracking process depends upon factors including the pyrolysis temperature, the catalyst, the heating rate and the feedstock. This makes the cracking process complicated and unpredictable.[70] In spite of all advantages in pyrolysis method, it is less selective than chemical treatment and biochemical depolymerization.

1.5   Lignin Model Compounds

The depolymerization of lignin polymer into its monomers is an interesting approach to generate bulk chemicals and biofuel. However, lignin being a very complex polymer, the study of its depolymerization has its challenges. The lignin obtained through all the above mentioned methods is not entirely pure, and it is insoluble in almost all organic solvents; because of this very few analytical methods are available to characterize the change in its functionality. On the other hand, the study of lignin model compounds is significantly simpler than oxidation of lignin itself and enables careful characterization of the products so that the issues of selectivity can be addressed. The small compounds generated by fragmentation of lignin model compounds could be separated by chromatographic techniques, and further identification is possible using conventional analytical methods like GC-MS and NMR. In our study, we synthesized six different lignin model compounds, providing examples of β-phenyl ethyl or β-O-4 linkages (Figure 1.8). These model compounds had similar linkages and functional groups as that of native lignin. We believe that if we are able to selectively cleave some common linkages in model compounds, the same process will be able to depolymerize native lignin. Compounds **1**, **2**, **3** and **5** do not have free phenolic -OH groups, while **4** and **6** are phenolic model compounds.
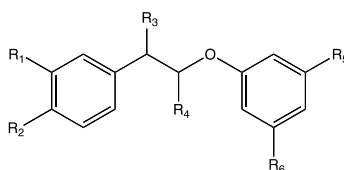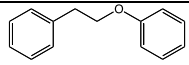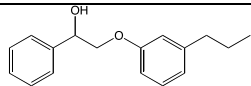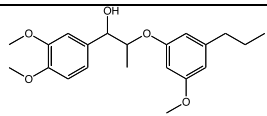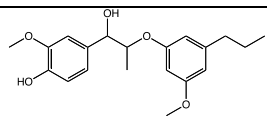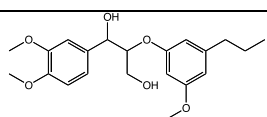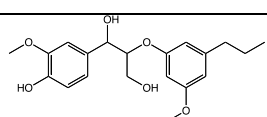
Figure 1. 8 β-O-4 linkage lignin model compounds used in this work. Substituents R_1, R_2, R_3, R_3, R_4, R_5 and R_6 are denoted in Table 1.4.

Table 1. 4 Structure of lignin model compounds.

LMCs	Structure	Substituent
1		$R_1 = R_2 = R_3 = R_3 = R_4 = R_5 = R_6 = H$
2		$R_1 = R_2 = R_4 = R_6 = H$, $R_3 = OH$, $R_5 = n\text{-Pr}$
3		$R_1 = R_2 = R_6 = OCH_3$, $R_3 = H$, $R_4 = CH_3$, $R_5 = n\text{-Pr}$
4		$R_1 = R_6 = OCH_3$, $R_2 = R_3 = OH$, $R_4 = CH_3$, $R_5 = n\text{-Pr}$,
5		$R_1 = R_2 = R_6 = OCH_3$, $R_3 = OH$, $R_4 = CH_2OH$, $R_5 = n\text{-Pr}$
6		$R_1 = R_6 = OCH_3$, $R_2 = R_3 = OH$, $R_4 = CH_2OH$, $R_5 = n\text{-Pr}$

The model molecules with methoxyl and phenolic hydroxyl group substituent on the aromatic ring serve as model compound for native lignin. Likewise, Cγ hydroxyl group resemble to propanoid substituent group. Given that different substituent groups are attached to the basic β-phenyl ethyl linkage, each of these molecules has distinct reactivity towards oxidants. A method for breaking apart some of the common linkages would be an extremely important step toward converting lignin from a solid polymer into small molecules that can be processed into fuels or utilized as platform chemicals. Of particular interest is an oxidation route, because there are a number of sites on the lignin polymer that should be possible to target with oxidizing agents, specifically benzylic C-H and C-OH bonds. Although an oxidative approach to lignin depolymerization comes at the cost of some of lignin's fuel potential, we believe that cutting a small percentage of the linkages can produce new materials that are much more amenable to processing.

1.6 Our depolymerization approach

Many researchers have studied the catalytic oxidation of lignin model compounds. In this study molecular O_2 and H_2O_2 is commonly used as oxidant. Molecular O_2 and H_2O_2 are highly desirable because they are inexpensive and no toxic byproducts are generated from the oxidizing agent itself.

Very recently, Toste's group reported the catalytic cleavage of C-O bonds using vanadium-oxo complexes.[71] Hanson, Baker and co-worker studied C-O and C-C bond cleavage using vanadium and copper catalysts.[72,73] Claudia and *et al.* reported the use of a lignin peroxidase biomimetic catalyst in oxidative degradation of lignin model compounds.[74] Of particular note is recent work by Stahl and co-workers, who were the first to report the use of TEMPO, and TEMPO derivatives, as catalysts for the oxidation of alcohol moieties in lignin model compounds and in the native lignin polymer.[75] Bozell and group reported Co-Schiff base-catalyzed oxidative cleavage of monomeric and dimeric lignin models.[76] The oxygenated aromatic compound obtain after catalytic oxidation of lignin could be used as bulk chemical or further process to non-oxygenated hydrocarbons petrochemical.

Step 1: Oxidation at benzylic hydroxyl group
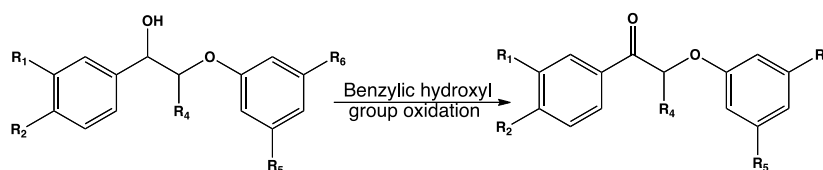
Step 2: Baeyer-Villiger oxidation to produce esters, followed by hydrolysis of esters to produce fragments
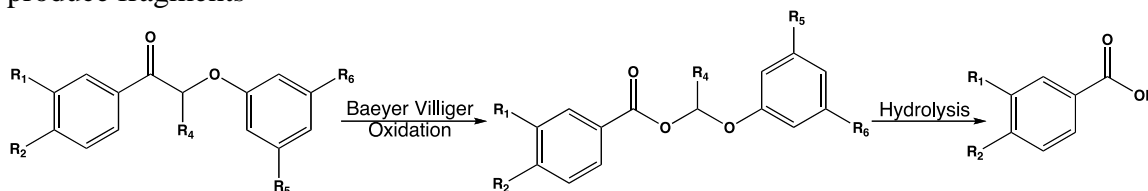
Figure 1. 9 Schematic representation of two step selective cleavage of the Cα-Cβ linkages.

It is known that β–O–4 linkage is more that 50% of the linkages in softwood as well as in hardwood. In this study, we are particularly targeting on β–O–4 linkages. We believe that

if we study catalytically breaking common linkages, we will be able to disassemble the lignin polymer. The depolymerization of lignin model compounds (LMCs) with identical linkage and reactivity as native lignin looks promising as a way to study depolymerization of lignin. We believe that oxidation has to be selective, which will result in useful molecules.

Herein, we present a method for selective stepwise oxidation of lignin under mild and practical condition using inexpensive oxidants such as H_2O_2 and molecular O_2. Specifically, we have targeted the oxidative cleavage of Cα-Cβ bonds as a means to depolymerize lignin and obtain useful aromatic compounds. In this work, we prepared several LMCs that have the structures, characteristic reactivity and linkages closely related to the parent lignin polymer. We observed that selective oxidation of benzylic hydroxyl groups using molecular O_2, followed by Baeyer-Villiger oxidation of the resulting ketones using H_2O_2, successfully cleaves the Cα-Cβ linkage in the model compounds. LMC was used to study oxidative cleavage reaction. Every molecule has distinct reactivity toward oxidant, as different substituent groups are attached to the basic β-phenyl ethyl linkage.

CHAPTER 2. SELECTIVE STEPWISE OXIDATION OF LIGNIN MODEL COMPOUNDS (LMCs)

2.1   Hydroxylation of benzylic methylene groups in lignin model compounds by an iron porphyrin catalyst

In photosynthesis, carbon dioxide is converted to organic molecules by the carbon fixation process. Plants synthesize their structural constituents from carbon dioxide in the presence of light and chlorophyll. The microorganisms are not able to degrade wood, because of lignin protective layer around cellulose and hemicellulose.[77] Lignicolous fungi is a wood-decay fungus which grows on dead wood. Wood-decaying fungus plays an important role within the ecosystem by degrading biomass back to carbon dioxide. These fungi are broadly classified in three major class: brown rot, soft rot and white rot. Every fungus has a characteristic degradation pattern. The brown rot and soft rot fungi favorably break down cellulose and hemicellulose in wood. White rot fungus preferentially degrades the lignin component in wood, causing left-over rotten wood to appear white and spongy.[78]

Kirk *et al.* have performed pioneering work on the biodegradation of lignin.[79] According to their studies, in the presence of H_2O_2 an extracellular enzyme from white rot fungus, Phanerochaete chrysosporium, is accountable for natural biodegradation of lignin.[23] In 1984, oxidases from ligninolytic cultures of Phanerochaete chrysosporium were isolated and identified as iron porphyrins and Mn^{+2}-dependent peroxidase.[51,80] The structure of the ligninase was further confirmed by crystallography.[81-83] Biodegradation of lignin and lignin model compounds was extensively studied by a variety systems using white rot enzyme.[84] Lignin peroxidase has been known to catalyze oxidation of several functional groups in lignin model compounds. The most common oxidation reactions executed by lignin peroxidase are hydroxylation of benzylic methylene groups,[85,86] benzyl hydroxyl group oxidation,[87] Cα-Cβ cleavage[78] and β-1, β-O-4, β-5 bond cleavages.[84,87] However, the use of lignin peroxidase is not economically convenient because depolymerized lignin eventually converts into carbon dioxide by further oxidation. In order to understand the mechanism of depolymerization reaction, individual enzyme need to be purified, which is

very costly process. It is believed that a synthetic metalloporphyrin catalyst is the ideal way to study selective oxidation process.[85]

Nowadays, metalloporphyrins are sold in many specialty chemical companies. The chemistry of synthetic porphyrins has been reviewed by many researchers in the areas of material science, catalysis and biological field.[88,89] Furthermore, introduction of substituents on the porphyrin ring or altering center metal ion provide an interesting way to modify the functionality of metalloporphyrins.[89] Synthetic metalloporphyrins with similar macrocyclic ligands and transition metals as in enzymes are highly studied as biomimetic catalyst for oxidation reactions.[85] In past, iron/magnesium porphyrin catalytic oxidation study of lignin model compound has been done using various oxidant like m-CPBA, H_2O_2, t-BuOOH and NaOCl. The biomimetic catalyst oxidation study of lignin model compound provides an insight for the depolymerization of native lignin polymer.
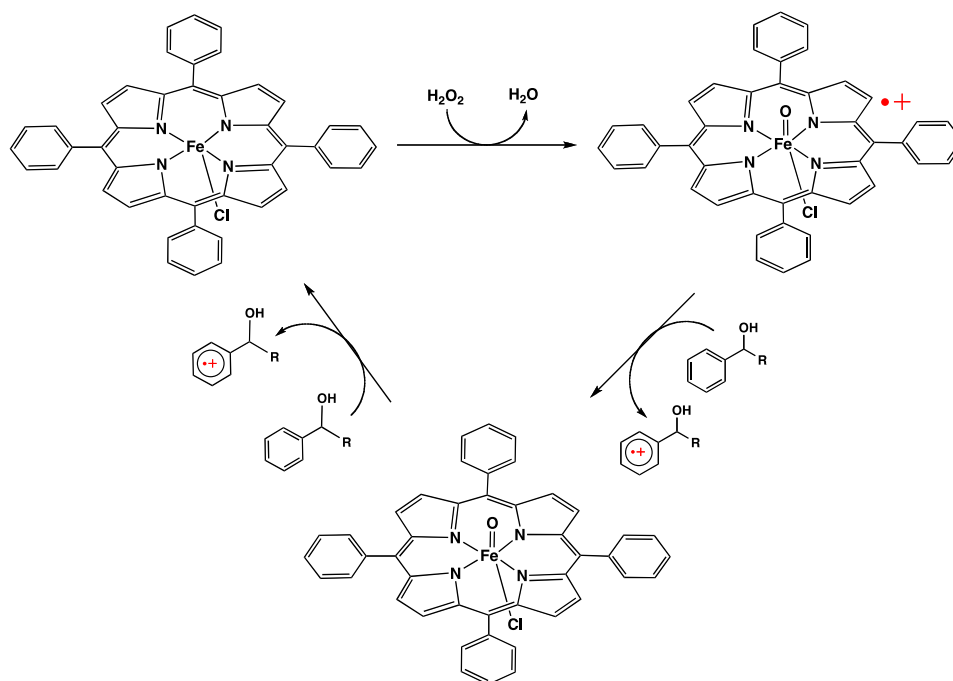
Figure 2. 1 Mechanism proposed for oxidation of LMCs by heme-porphyrin and H_2O_2.[74]

Figure 2.1 shows a simplified catalytic cycle of heme-porphyrin for oxidation of lignin model compounds. The proposed mechanism for hemi porphyrin catalytic cycle involves

oxidation of iron porphyrin to active catalyst-oxy(IV) iron porphyrin complex. (Compound I) by H_2O_2. The compound I oxidized lignin and itself get reduce to compound II. This is followed by successive another one electron oxidation to regenerate original catalyst.

The one-electron oxidized β-O-4 lignin model compounds form radical cation complex, and this complex then form benzylic radical intermediate through Cα-H deportation. The intermediate preferentially undergoes oxidation via two common pathways as shown in figure 2.2. In path a, aerobic conditions involves formation of hydroperoxy radical is followed by decomposition to produce ketone. In path b, first step is one electron oxidation to produce benzyl cation, which is followed by attacked of water to form benzyl alcohol. Although the detailed mechanism of the reaction requires further investigation.
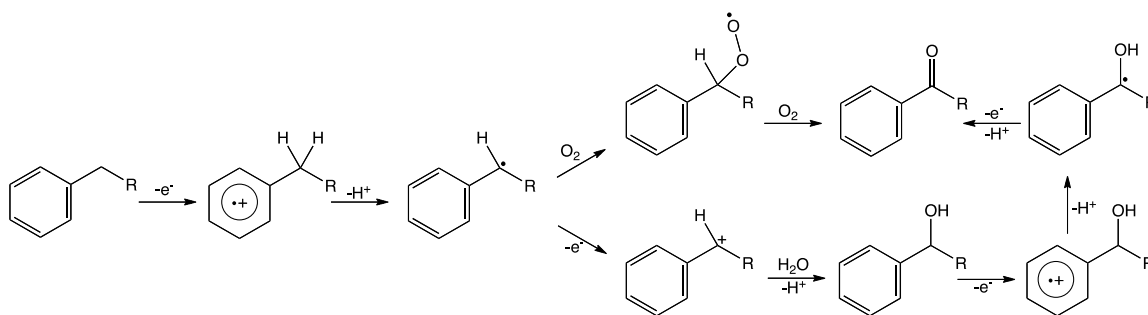
Figure 2. 2 Proposed mechanism for hydroxylation of benzylic methylene groups and oxidation of benzylic hydroxyl group.[87,90-92]

In order to carry out precise study of bond cleavage using iron porphrin catalyst, dimer model molecule allows thorough studies of oxidative cleavage reactions. The selective catalytic hydroxylation of benzylic methylene groups by lignin-degrading enzymes and by an iron tetraphenylporphyrin (TPP) chloride/tert-butylhydroperoxide (t-BuOOH) system has been reported in the literature.[83,93] We believe that hydroxylation at the Cα position of **1** is a key step in an effective oxidation process. In our study, we investigated the use of the previously reported iron porphyrin/tert-butylhydroperoxide (t-BuOOH)/pH 3 phosphate buffer system for catalytic hydroxylation of benzylic methylene groups (Figure 2.3, and Table 2.1).
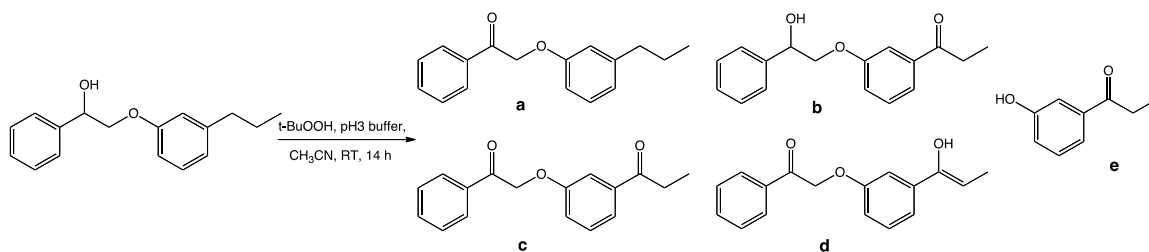
Figure 2. 3 Oxidation of the LMCs **2** by TPPFeCl and t-BuOOH.

Table 2. 1 Oxidation of **2** with and without TPPFeCl using different equivalent of t-BuOOH.

t-BuOOH (eq.)	TPPFeCl (eq.)	% smr	Yield^a (%)				
			a	b	c	d	e
1	No catalyst	97	2.5	0.5	-	-	-
1	0.01	60	18	9	11	-	-
5	0.01	11	26	12	18	8	16

The oxidation of benzylic C-H and C-OH groups in LMC **2** was carried out by treating **2** (50 mg, 0.2 mmol) with TPPFeCl, 70% aq soln of t-BuOOH, CH$_3$CN (0.5 mL) and 0.1N pH 3 phosphate buffer (1.5 mL) stirred at 25 °C for 14 h.[94] ^{a}Yields are for isolated pure products.

These reactions resulted in 3 major types of products, resulting from oxidation of benzylic hydroxyls or benzylic C-H bonds. The results in Table 3.1 indicate that catalyst plays important role in oxidation reaction, as when reaction was carried out without catalyst 97% of starting material was recovered. The oxidation of molecule **2** using 5 eq of t-BuOOH at fixed concentration of catalyst and reagent results in β-O-4 and O-phenyl bond cleavage.

Table 2. 2 Oxidation of **2** with TPPFeCl/t-BuOOH in presence PTC.

Phase transfer catalyst (PTC)	% Relative	Relative Yield[b] (%)		
	smr	a	b	c
-	63	29	4.5	3.6
Sodium dodecyl sulfate	61	30	4	3
Tetra butyl ammonium bromide	54	33	6	4
Tri methyl (tetra decyl) ammonium bromide	56	34	3	1

The oxidation of benzylic C-H and C-OH groups in LMC **2** was carried out by treating **2** (50 mg, 0.2 mmol) with TPPFeCl, PTC (1 mmol%), 70% aq soln of t-BuOOH, CH$_3$CN (0.5 mL) and 0.1N pH 3 phosphate buffer (1.5 mL) stirred at 25 °C for 14 h.[94] [b]Relative SMR and Yields are referred from GC-MS % area of the peaks, without calibration.

In order to explore the effect of a phase-transfer catalyst (PTC) on these heterogeneous reaction mixtures, three different PTCs were introduced into the reaction mixture. The results in Table 3.2 shows that PTC does not increases that rate of the reaction, as % conversation does not change much.

Table 2. 3 Oxidation of **2** with TPPFeCl/t-BuOOH in different proportion of buffer and MeCN.

MeCN (mL)	Phosphate Buffer (mL)	% Relative	Relative Yield[b] (%)		
		smr	a	B	c
0.5	1.5	63	29	4.5	3.6
1	1	72	28	-	-
1.5	0.5	86	14	-	-

The oxidation of benzylic C-H and C-OH groups in LMC **2** was carried out by treating **2** (50 mg, 0.2 mmol) with TPPFeCl (0.002 mmol), 70% aq soln of t-BuOOH (0.2 mmol), CH$_3$CN and 0.1N pH 3 phosphate buffer stirred at 25 °C for 14 h.[94] [b]Relative yields are referred from GC-MS % area of the peaks, without calibration.

The reactivity of **2** in different proportions of MeCN: pH 3 phosphate buffer was studied (0.5: 1.5 v/v, 1.0:1.0 v/v MeCN:pH 3 phosphate buffer), the conversion being highest in 0.5:1.5 MeCN:pH 3 phosphate buffer.
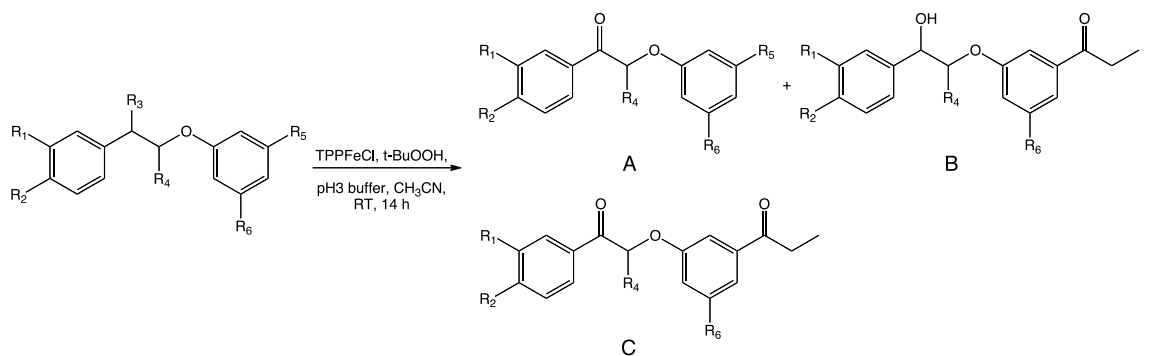
Figure 2. 4 Oxidation of the LMCs by TPPFeCl and t--BuOOH.

Table 2. 4 Oxidation of **1** - **6** with TPPFeCl/t-BuOOH.

LMCs	% smr	Yield[a] (%)		
		A	B	C
1	92	5	-	-
2	60	18	9	11
3	54	26	2	5
4	0	-	-	-
5	44	39	14	1
6	0	-	-	-

The detail procedure is given in Chapter 3 (section 3.3.1). [a]Yields are for isolated pure products.

We observed that the conversion was significantly reduced when the MeCN/phosphate buffer liquid phase was replaced by CH_2Cl_2. Similarly, when the TPPFeCl oxidation reaction was carried out with *m*-CPBA in CH_2Cl_2, an unselective fragmented product was obtained. In situations where there is an unprotected phenolic hydroxyl, polymerization (presumably phenolic oxidative coupling) results in insoluble, chromatographically immobile material. The current data clearly demonstrated that TPPFeCl/t-BuOOH oxidation system works selectively for oxidation of hydroxyl groups and hydroxylation of benzylic methylene groups in lignin model compounds. However, with increase in the concentration of t-BuOOH, and when the reaction is carried in CH_2Cl_2, the oxidation reaction is not particularly selective.

2.2   Oxidation of benzylic hydroxyl groups into ketone

Dehydrogenation (oxidation) of alcohol is the important transformation of the functional group in organic chemistry. Some of the famous conventional oxidation of alcohol reactions are Jones oxidation, Dess-martin oxidation, Swern oxidation, Corey-Kim oxidation, Oppenauer oxidation, etc. In all these reactions, a stoichiometric amount of oxidant used generates huge amount toxic waste. Recently, many researchers have published the selective greener oxidation process using molecular oxygen. We opted for a catalytic approach to the oxidation of benzylic hydroxyl groups in lignin model compounds, using molecular oxygen as the oxidant. Oxidation processes that employ dioxygen are highly desirable because O_2 is inexpensive, and no toxic byproducts are generated from the oxidizing agent itself. Although dioxygen being powerful oxidant, it is kinetically unyielding.

The multiplicity of electronic state is determined from spin quantum number **S** (+1/2 or -1/2), number of unpaired electrons.

$$\text{Multiplicity of state} = 2S + 1$$

In case of singlet diradicals, pair of electrons has spin state +1/2 and -1/2. Therefore, the multiplicity of the state will be (2*0 + 1) singlet. Likewise, in free radical R˙, one unpair electron (2*1/2 + 1) results into doublet state. On this term oxygen ground state has two unpaired electron (2*1 + 1), which results in triplet ground state.

Molecular oxygen exists in a triplet diradical ground state, whereas most of organic compounds present as a single ground state. Due to this reason, organic compounds do not react with molecular oxygen under normal reaction condition. However, oxygen reacts with doublet state radicals to form new radical.

Oxidation State
Assignment

Potential Energy (Kcal)

$^1\Sigma^+_g$

31.5

$^1\Delta_g$

22.5

$^3\Sigma^-_g$

0.0
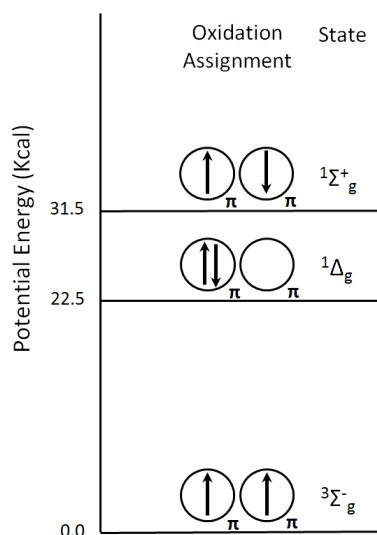
Figure 2. 5 Electronic configuration of 2pπ orbitals in molecular oxygen and corresponding potential energy.

Figure 2.5 represents potential energy of triplet oxygen $^3\Sigma^-_g$ ground state, the singlet oxygen $^1\Delta_g$ excited state, and the singlet oxygen $^1\Sigma^+_g$ excited state.[95] Triplet state oxygen is 22.5 Kcal more stable then singlet oxygen. Singlet oxygen is commonly prepared by photosensitizer pigment, and its life span is over one hour at room temperature because transition nature from the singlet to triplet transition is spin forbidden.[95] The excitation of ground state oxygen to singlet state is strictly spin forbidden under normal conditions. In order to put on use oxygen as an oxidant in organic reaction, it is important to overcome the kinetic barriers by activating the molecular oxygen. The transition metal complexes is well-known imperative activating agent. In biological system transition metal complexes bind to molecular oxygen reversibly. The transition metal formed stable reversible and irreversible adduct with oxygen due to spin orbital coupling. The transition metal-oxygen adduct can potentially oxidized organic compounds, owing an economical green oxidation process.[96] Aerobic oxidation of benzylic and allylic alcohol using transition metal is well studied. Most widely used transition metal complexes as oxidation mediators are $PdCl_2$, $Pd(OAc)_2$, Pd/C, RuO_2, MnO_2, etc.[97-102] In the literature, a number of oxidation processes promise selective oxidation of benzylic alcohol to ketones, but many have certain drawbacks, such as requiring high-pressure conditions or the use of expensive transition

metal catalysts.[103,104] Therefore, the challenge was to screen for an effective catalyst system that is economical, selective, and which operates under mild reaction conditions.

2.2.1 Oxidation by 2,3-Dichloro-5,6-dicyano-1,4-benzoquinone(DDQ)

Quinone commonly found in biological systems plays an important role as an oxygen activator in metabolic processes, enzymes, redox proteins and photosynthesis. Quinone is well known for redox reaction because of high reduction potential and electron transfer rates.[105] It plays the important role in biological oxidation reaction. The oxidation study proves that introducing electron withdrawing substituent increased one-electron reduction potentials and hydrogen atom transfer ability of the quinones and thus promotes the oxidation.[106,107] Among all synthetic quinone, 2,3-Dichloro-5,6-dicyano-1,4-benzoquinone (DDQ) is most effective.[108] DDQ being powerful oxidant used as hydrogen acceptor in oxidation of benzylic, allylic alcohol and ether.[109,110] The electrochemical redox equilibrium study between DDQ/DDQ-H_2 suggest that electron and proton transfer reaction is depends upon pH of the reaction medium. In acidic medium, reduction occurs via two electron two proton transfer route.[111]

$$DDQ + 2e + 2H^+ \rightleftharpoons DDQ\text{-}H_2$$
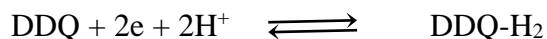
Various oxidation reaction using DDQ is reported, in most of the reaction DDQ is used in stoichiometric amount, as DDQ is get reduce to DDQ-H_2.[110,112-117] In order to regenerate DDQ, many researcher used co-catalyst such as $FeCl_3$,[118] $Mn(OAc)_3$,[104] and also by electrochemically.[119] The transition metal co-catalyst generates undesirable toxic waste, which in not acceptable from environment point of view. Since then, various organic catalyst such as N-hydroxyphthalimide and t-butyl nitrite have been reported, however high oxygen pressure is required to regenerate the catalysts.[103] Recently, use of sodium nitrite ($NaNO_2$) seems to show promising results, as reaction work under normal atmosphere pressure and temperature.

Synthesis of nitric oxide from sodium nitrite is reported in 1925. According to author, sodium nitrite($NaNO_2$) reacts with acidic to produce unstable nitrous acid (HNO_2), further HNO_2 quickly decomposed to nitric oxide and nitric acid.[120] The nitric oxide is formerly

27

autooxidized to nitrogen dioxide ($NO_2^\bullet$) in O_2 atmosphere. The autooxidation of nitric oxide is known, also it is experimental proved that reaction proceed via $ONOO^\bullet$ intermediate.[121]

(1) $3NaNO_2 + 3H^+ \rightarrow 3HNO_2 \rightarrow HNO_3 + 2NO^\bullet + H_2O$

(2) $2NO^\bullet + O_2 \rightarrow 2NO_2^\bullet$
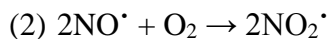
$NO_2^\bullet$ being radical reacts with another radical species. Reaction between nitrogen dioxide and phenol is well studied in past. As reported, $NO_2^\bullet$ abstract hydride from phenol to generate nitrous acid and phenoxyl radical. And in the successive step nitrous acid disproportionate into H_2O and nitrogen oxide ($NO^\bullet$).[122] The cycle between $NO^\bullet/NO_2^\bullet$ sustain as long as atmospheric O_2 is available. Because of this catalytic amount of $NaNO_2$ is sufficient to regenerate DDQ from DDO-H_2.

In 2012, Wang et al. published a method based on the use of DDQ/NaNO$_2$ for the selective oxidation of benzylic hydroxyl groups under mild conditions (Figure 2.7 and Table 2.5).[123]
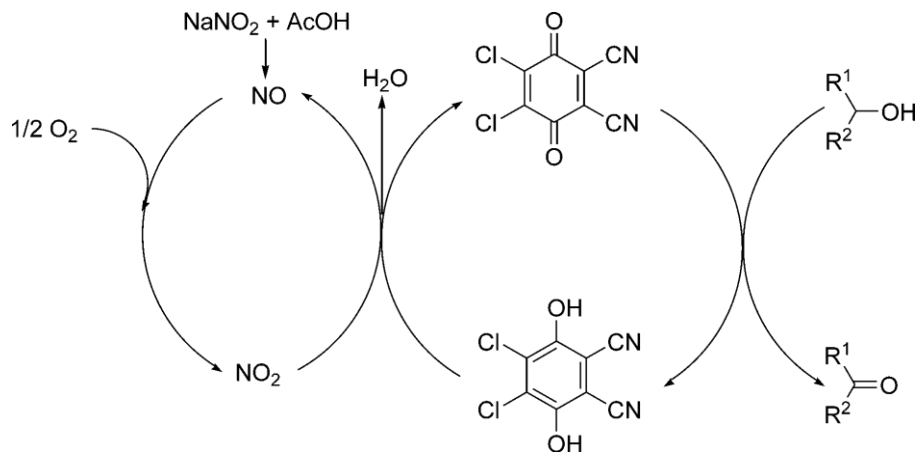
Figure 2. 6 Mechanism for aerobic oxidation of alcohol by DDQ/NaNO$_2$.

In cycle 1, DDQ oxidizes the alcohol to a ketone and gets reduced to hydroquinone - a redox reaction comprised of two protons and two electrons. The oxidation is initiated by one electron oxidation of alcohol to form radical cation. In cycle 2, NaNO$_2$ is decomposed to $NO^\bullet$, and then O_2 oxidized to $NO_2^\bullet$. The $NO_2^\bullet$ plays important role in regenerating the catalyst and both the catalytic cycle last as long as sufficient O_2 is available.

To optimize the oxidation of LMC 3 with DDQ/NaNO$_2$ oxidation system, we varying the

reaction parameters and determined the conversion and yield of oxidized product. The detail amount of catalyst, co-catalyst and reaction parameters is given in table 2.5. Typical experimental procedure for selective oxidation of LMC 3 consisting of 50 mg of LMC **3** (0.14 mmol), DDQ and $NaNO_2$ in the presence of 1.8 ml CH_2Cl_2, 0.2 ml acetic acid, under an O_2 atmosphere (1 atm) for 19 hrs.[124]   The organic phase was washed with water, combined organic layers were dried over $MgSO_4$ and concentrated in a vacuum. The products were isolated easily from the other byproducts using a preparative TLC plate.
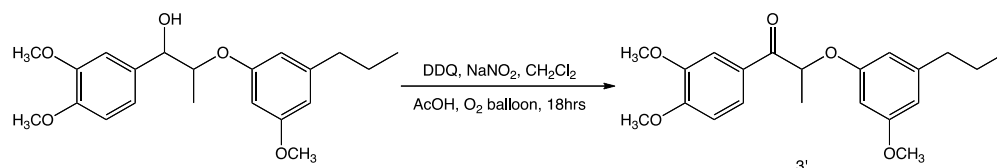
Figure 2. 7 Oxidation of benzylic hydroxyl groups in LMC **3** by DDQ and $NaNO_2$.

Table 2. 5 Catalytic aerobic oxidation of **3** with DDQ/$NaNO_2$.

Entry	DDQ eq	$NaNO_2$ eq	Temp	% smr	Yields[a] (%)	
					A	B
1	0.01	0.1	RT	76	23	
2	0.1	1	RT	32	43	-
3	1	10	RT	0	69	-
4	0.1	1	55°C	72	22	-
5	0.1	1	RT(sonication)	54	33	-

The detail procedure is given in Chapter 3 (Section 3.3.2). [a]Yields are for isolated pure products.

In this study, we found that upon increasing the amount of catalysts, we obtained acceptable yields after 19 h; however, mass balances were poor, suggesting the formation of low molecular weight, water-soluble compounds or chromatographically immobile material. In an attempt to increase the rate, the reaction was carried at 55 ºC, however, conversion declines. We also found that when reaction was carried out in a sonicating bath, the level of conversion does not increase. When 10 equivalent of $NaNO_2$ was used instead

of 1 equivalent the conversion was negligible. In another reaction, N-hydroxyphthalimide (NHPI) mediator (co-catalyst) was added into the reaction mixture, however NHPI did not increase the rate of the reaction. In an attempted to increases the conversion of compound **3**, different solvent were tried including benzene and dimethylolpropionic acid (DMPA), but the conversion was negligible. Likewise, AcOH and CH_2Cl_2 in different proportion were tried, but unfortunately the conversion didn't improved.
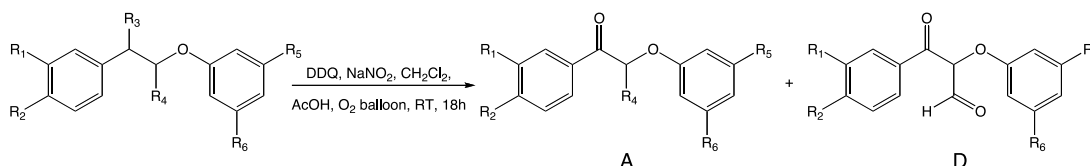
Figure 2. 8 Oxidation of benzylic hydroxyl groups in LMCs by DDQ and $NaNO_2$.

Table 2. 6 Catalytic aerobic oxidation of **1 - 6** with DDQ/$NaNO_2$.

Entry	LMCs	DDQ eq	$NaNO_2$ eq	% smr	% Yields[a]	
					A	D
6	1	0.01	0.1	0	0	-
7	2	0.01	0.1	0	0	-
8	3	0.01	0.1	76	23	-
9	3[c]	0.1	1	35	63	-
10	4	0.01	0.1	48	28	
11	4	0.1	1	0	60	-
12	5	0.01	0.1	59	33	-
13	6	0.01	0.1	40	29	5

The detail procedure is given in Chapter 3 (Section 3.3.2). [a]Yields are for isolated pure products, [c]reaction mixture was stirred at room temperature for 44 h.

As shown in Table 2.6, **1** and **2** remain unchanged under these reaction conditions. In general, when DDQ is added to the substrate dissolved in CH_2Cl_2, the solution turns blue due to formation of charge transfer complexes between the substrate and DDQ.[125,126] In our study, we found that when DDQ was added to solutions of **1** or **2**, the color did not change. These results suggest that electron transfer occurs when electron donating groups (like methoxy groups) are attached to benzene rings, but not in situations where the aromatic

ring is not electron rich. We found that with compounds **3** - **6** this oxidation process works well but the rate of the reaction was very slow, with conversions being typically 40 to 60 % after 19 h. When reaction time was increased from 19 h to 44 h conversion was even better. The study also demonstrated that in the absence of O_2 or in the absence of $NaNO_2$ oxidation reaction does not occur.[126]

2.2.2 Oxidation by (2,2,6,6-Tetramethylpiperidin-1-yl)oxyl (TEMPO)

Another interesting transition metal free aerobic oxidation process known is by using stable nitroxyl free radical. Nitroxyls radical (amine-*N*-oxide radicals) has stable resonance structure as shown below. Sterically bulk four methyl group in molecular structure of (2,2,6,6-tetramethylpiperidin-1-oxy) TEMPO, increases the stability by inhibiting dimerization via O-O, N-O or N-N bonds.
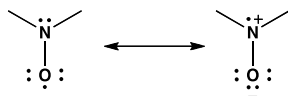
TEMPO is a commercially available stable nitroxyl radical which has commonly application in free radical polymerization, electronic paramagnetic resonance spectroscopy (EPR), polymerization inhibitor and oxidation of alcohols into the corresponding aldehydes or ketones.[127-130] TEMPO is reasonably inexpensive and has industrial applications. In order to eradicate the catalyst from the reaction mixture the polymer support TEMPO catalyst as well as organosilane supported heterogeneous catalyst is sold by some specialty chemical companies.[131]

In oxidation process, TEMPO is first converted to active oxidant, N-oxoammonium cation. N-oxoammonium salt is formed by one electron oxidation of TEMPO via various oxidant including N-chlorosuccinimide,[132] bromine or chlorine,[133] m-CPBA,[127] Fe(III) mediated $K_3Fe(CN)_{6,}$[134] electrochemical oxidation[135] and sodium hypochlorite.[136]
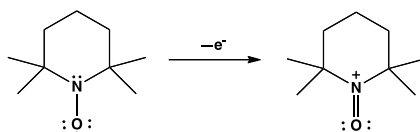
According to the literature, the TEMPO can selectivity oxidized primary or secondary alcohols under certain reaction conditions. Some researchers have found that primary alcohols were selectively oxidized over secondary, while other found the opposite.[134,137,138] Also, allylic and benzyl alcohols oxidation rate is higher and selective compare to usual alcohols.

N-oxoammonium salts are electrophile at nitrogen and/or at oxygen atom position. The mechanism of the oxidation reaction is highly dependent upon the pH of the reaction medium. In basic medium, the reaction proceeds via a bimolecular cyclic transition state and selectivity of the reaction is governed by steric factors. As shown in figure 2.9, the oxygen anion abstracts the Cα-hydrogen of the alcohols to give a ketone derivative and N-hydroxyamine. And in acidic medium, reaction does not occur via cyclic transition state therefore oxidation rate of secondary alcohol is greater.[139]

Hence, in acidic medium secondary alcohol is oxidized favorably whereas in basic medium primary alcohol is preferentially oxidized to ketone.
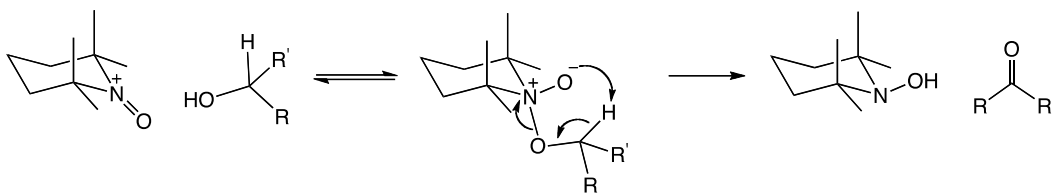
Figure 2. 9 Plausible mechanism for oxidation of alcohol under basic medium.
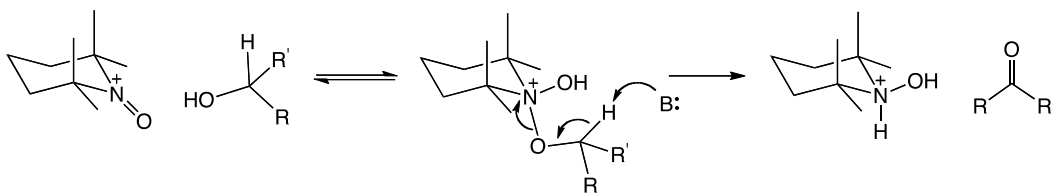
Figure 2. 10 Plausible mechanism for oxidation of alcohol under acidic medium.

TEMPOH undergoes one electron oxidation in an O_2 atmosphere to regenerate the catalyst (TEMPO).[140]
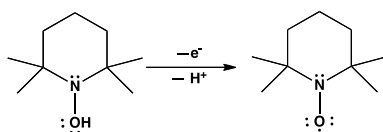
In this oxidation process TEMPO is used in catalytic amounts. As mentioned above, TEMPO is first converted to the active catalyst, an N-oxoammonium salts. At the end of the catalytic cycle, the reduced form of TEMPO is again oxidized by molecular oxygen, such that toxic waste is not generated.
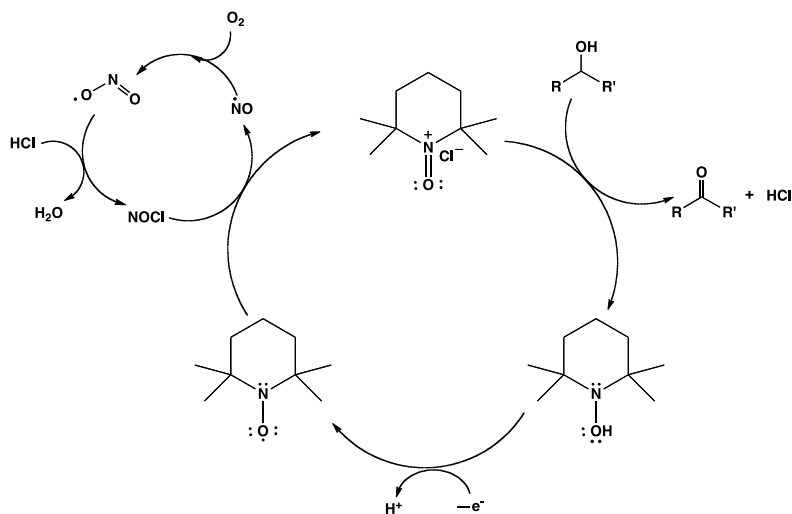
Figure 2. 11 Mechanism for aerobic oxidation of alcohol by TEMPO/NaNO$_2$.

In cycle 1, nitrosyl chloride is produced by three-step process. In first step, sodium nitrite reacts with acid to form nitric oxide, and in next step nitric oxide combine with oxygen to form nitrogen dioxide. And in last step nitrosyl chloride is formed from nitrogen dioxide and chloride. In cycle 2, TEMPO undergoes one-electron oxidation to form active oxidant N-oxoammonium cation, which oxidizes the alcohol and itself gets reduced to N-hydroxylamine. Oxygen then oxidizes the hydroxylamine to regenerated TEMPO.

We initially focused on the oxidation of benzylic hydroxyl groups using two different TEMPO-based systems that were developed by Hu and coworkers.[141,142] In reactions using TEMPO/Br$_2$/NaNO$_2$, bromination of the highly electron-rich aromatic ring occurred. The same result occurred using a TEMPO/1,3-dibromo-5,5-dimethylhydantoin/NaNO$_2$ system. We that investigated the TEMPO/CAN oxidation system developed by Kim and Jung,[143] but we found that the conversion was quite low. The reaction was carried out by treating 50 mg of substrate **2-3** with TEMPO (0.2eq) and CAN (0.1 eq) in the presence of 0.4 ml MeCN, 0.2 ml acetic acid, O$_2$ balloon at 90°C for 15 hrs.
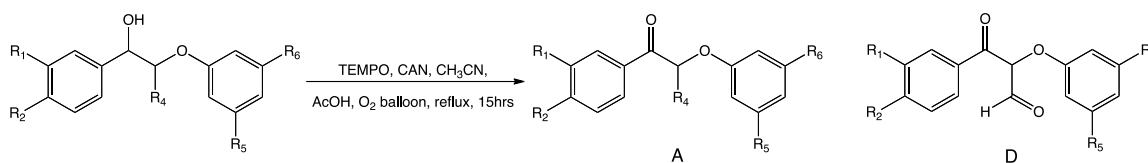
Figure 2. 12 Oxidation of the benzylic hydroxyl group in LMCs by TEMPO/CAN.

Table 2. 7 Catalytic aerobic oxidation of **2 - 3** with TEMPO/CAN.

LMCs	% Relative smr	Relative Yield[b] (%)	
		A	B
2	20	20	-
3	17	16	-

[b]Relative yields are referred from GC-MS % area of the peaks, without calibration.

Another interesting aerobic oxidation system using TEMPO, $NaNO_2$, HCl and NaCl under mild conditions was published in 2008 by Liang et al. (Figure 2.12 and Table 2.7).[144]

This oxidation reaction using TEMPO was carried by treating 50 mg substrate **1 - 6** with TEMPO (0.15eq), $NaNO_2$ (0.25eq), 36% aq HCl (0.5eq) and NaCl (0.5eq) in the presence of O_2.[15]
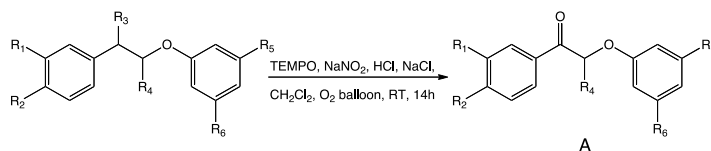
Figure 2. 13 Oxidation of the benzylic hydroxyl group in LMCs by TEMPO/$NaNO_2$.

Table 2. 8 Catalytic aerobic oxidation of **1 - 6** with TEMPO/NaNO$_2$.

LMCs	% smr	A (% yield^a)
1	100	-
2	0	100
3	0	81
4	0	-
5	0	80
6	0	-

The detail procedure is given in Chapter 3 (sub-section 3.3). ^{a}Yields are for isolated pure products.

Although encouraging results were obtained for compounds **2**, **3** and **5** under these conditions, **4** and **6**, compounds that contain free phenolic hydroxyl groups, were converted into insoluble material (presumably polymeric material). In an effort to prevent polymerization, we examined the selective protection of the phenolic hydroxyl group using benzyl bromide. Furthermore, compound **5** has hydroxyl group at Cα and Cγ carbon, but under this reaction conditions on Cα hydroxyl group oxidized to ketone. This results suggest that secondary alcohol preferentially oxidized over primary alcohol. The results were consistence with the relative oxidation rates of different hydroxyl mentioned in literature.

2.3   Protection of phenolic hydroxyl group
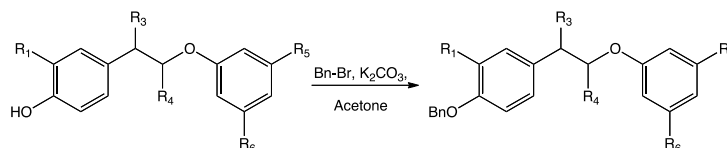
Figure 2. 14 Protection of phenolic hydroxyl groups of LMC **4, 6** by benzyl bromide and K$_2$CO$_3$. Note: benzyl protected lignin model compounds are denoted as **4 - P** and **6 - P**.

The optimization of the reaction conditions between benzyl bromide and substrate is as followed. 50 mg of substrate **4 or 6** (1 eq), benzyl bromide (2 eq) and K$_2$CO$_3$ (1 eq) was heated at reflux at 65°C for 5 hrs in the presence of 1.0 ml acetone. The mixture was concentrated in vacuum. The residue was diluted with water (10 mL) and extracted with

EtOAc (3 × 10 mL). The organic layer was washed with water, and then evaporated to dryness. The residue was subjected to column chromatography on silica gel (EtOAc: Hexane 1:9) to yield 100% product **(4' - P, 6' - P)** and selectivity. These reactions resulted in nearly quantitative yields and complete selectivity for reaction at phenolic hydroxyl group.

2.4   Baeyer Villiger Oxidation of ketone

Baeyer Villiger oxidation (BVO) is one of the most important reactions in organic chemistry. Since the discovery of the reaction in 1899, it has become a widely used method to convert a ketone into its corresponding ester. The reaction involves insertion of an oxygen atom between a carbonyl carbon and one of the alkyl/ aryl groups. Thus, the reaction is also known as the Baeyer-Villiger rearrangement. The relative migratory ability of substituent attached to the carbonyl carbon depends on the substituent ability to form more stable carbocation. The migration order of substituents is tert. alkyl > cyclohexyl > sec. alkyl > phenyl > prim. alkyl > CH_3.[145,146] Also, a phenyl group with an electron-donating substituent has better migration aptitude compared to non-substituted phenyl group or a phenyl group with an electron accepting substitute.[147] The ester that is formed in a BVO reaction is hydrolysed to the corresponding carboxylic acid and alcohol/ phenol *in situ* or as a separate step. Most commonly used oxidants are m-chloroperbenzoic acid (m-CPBA), trifluoroperacetic acid (TFPAA), peroxybenzoic acid and hydrogen peroxide(H_2O_2).[148] The peroxy acids are very effective oxidants compared to H_2O_2. However peroxy acids generate an equivalent amount of carboxylic acid waste. H_2O_2 eternally has an advantage over peroxy acids because H_2O_2 is an extremely clean oxidant and aqueous H_2O_2 is available at fairly cheap price. Further, water present in the reaction medium hydrolyses the ester to carboxylic acid and alcohol/phenol. In spite of this advantage, H_2O_2 is the weakest oxidant.[148] In general, to increase the oxidant efficiency, reaction has to be catalyst by Bronsted or Lewis acid catalyst. The carboxylic acid and H_2O_2 is another interesting way to generates peracid *in-situ*.[149] We performed BVO using formic acid/ aq H_2O_2 and using acetic acid/ aq H_2O_2 mixture, these results suggest that

formic acid/H_2O_2 oxidation mixture results in much better conversion. In these process, formic peracid reacts with the ketone to produce the corresponding ester, H_2O_2 functioning as an oxidant, whereas the formic acid acts as the catalyst.[149]

It would be more valuable to find ways to enhance the conversion efficiency. With the aim of optimizing the reaction conditions, we performed several sets of experiments. To simplify these experiments, we first studied the oxidation of 4-methyl acetophenone as a simple model ketone.
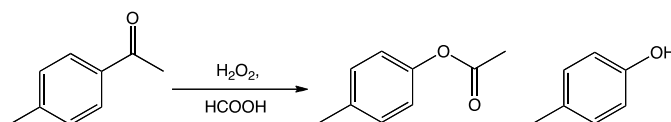
Figure 2. 15 Baeyer-Villiger oxidation of (4-methylphenyl) acetate by H_2O_2 and HCOOH.

To study the conversion of BVO reaction as a function of time, reactions were carried by treating 100 mg 4-methyl acetophenone with 30% H_2O_2 (10 eq), HCOOH (10 eq) at 20 °C from 1 to 24 hrs.
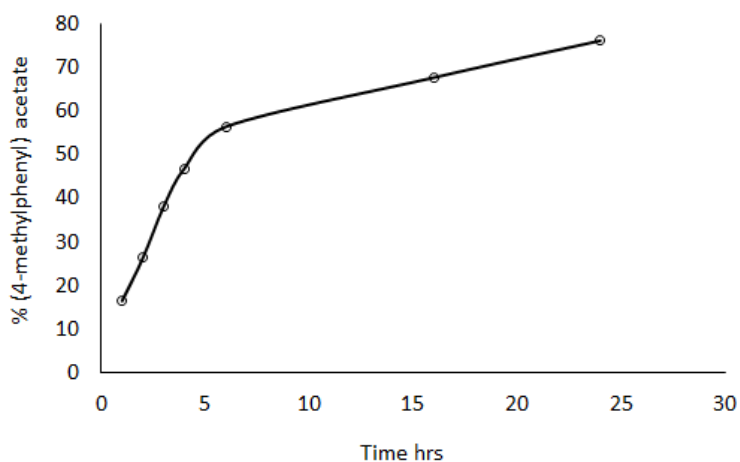
Figure 2. 16 Plot of % of (4-methylphenyl) acetate formed after BVO as a function of time. ([b]Relative % yields are referred from GC-MS % area of the peaks, without calibration).

As shown in figure 2.16, the conversion steady increases with time. This suggest that H_2O_2 does not completely decompose under these reaction conditions even after 24 hrs.
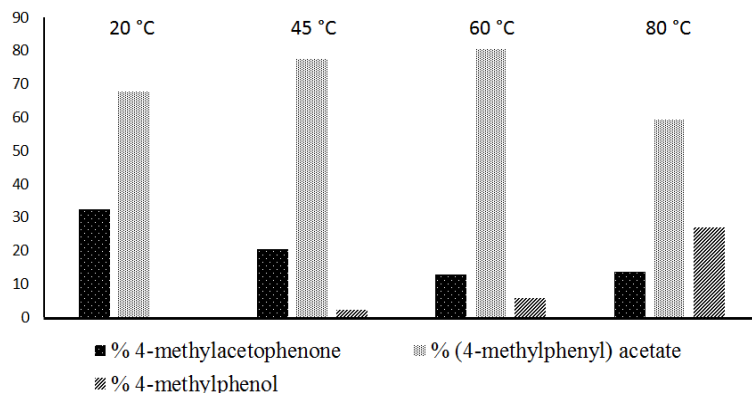
Figure 2. 17 Illustrate % of 4-methylacetophenone, % (4-methylphenyl) acetate and % 4-methlyphenol after BVO of 4-methylacetonephenone at four different temperature. (^{b}Relative % yields are referred from GC-MS % area of the peaks, without calibration).

The influence of reaction temperature on the conversion of the reaction is shown in figure 2.17. The results suggest that conversion significantly increase as the temperature is increased to 45 °C from 20 °C. However, the conversion slight drop as reaction was performed at 80 °C. These results illustrate that reaction temperature between 45 °C to 60 °C seems to be ideal for BVO reaction to achieve the best conversion. We also carried out this reaction using different amounts of H_2O_2/HCOOH.
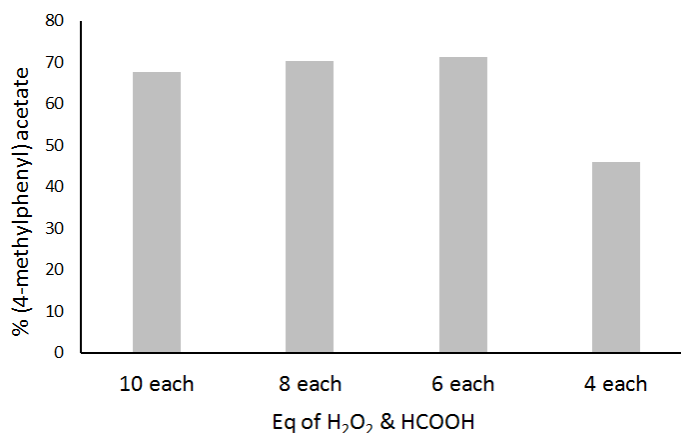
Figure 2. 18 Illustrate % of (4-methylphenyl)acetate after BVO using different equivalent of H_2O_2/HCOOH

The results in figure 2.18, suggest that 6 to 8 equivalents each of formic acid and H_2O_2 give maximum conversion. By taking consideration of several reactions factors, our optimized reaction parameters are 50 mg substrate (**2' - 6'**) with 30% H_2O_2 (8 eq), HCOOH

38

(8 eq) and 1, 2–dichloroethane (4 eq) at 50 °C for 24 h. Based on model studies and calculations Mora-Diez, et al. reports the effect of the solvent on BVO reaction mechanism.[150] According to their study, the reaction proceeds via a concerted non-ionic pathway, which is the lowest energy pathway in a nonpolar solvent like 1, 2-dichloroethane.[151]
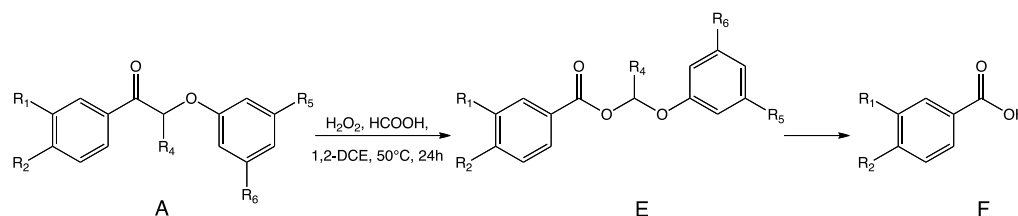
Figure 2. 19 Baeyer-Villiger oxidation of lignin model compounds by H_2O_2 and HCOOH

Table 2. 9 Baeyer-Villiger oxidation of **2', 3', 4'- P, 5', 6'- P** with H_2O_2/HCOOH

LMCs	% smr	E (% yield[a])	F (% yield[a])
2′	90	10	-
3′	0	-	81
4′-P	0	-	80
5′	0	-	40
6′-P	0	-	80

[a]Yields are for isolated pure products. Note: 4' - P, 6' - P: benzyl protected lignin model compounds

Following the Baeyer-Villiger oxidation of **3′**, **4′**- P, **5′**, and **6′- P** (Figure 2.19 and Table 2.9) no trace of starting material was recovered; the only product isolated was the corresponding carboxylic acid. In these reactions, the migratory aptitude of the aromatic group is not as high as the migratory aptitude of the alkoxy group, and the only products obtained were substituted benzoic acids. The phenolic fragments were not isolated.

2.5   Conclusions

We have synthesized six different lignin model compounds, which have identical functional groups and linkages that of native lignin. Each model compounds has distinct reactivity towards oxidation conditions. In this study, we demonstrate that iron porphyrin oxidation system not only oxidized benzylic hydroxyl group into ketone but also hydroxylate of benzylic methylene groups. Phenolic model compounds appear to undergo coupling reactions, affording polymeric products. Solvent and oxidant play important role in selectivity of the reaction, as when the TPPFeCl oxidation reaction was carried out with *m*-CPBA in CH_2Cl_2, an unselective fragmented product was obtained. Further, higher concentration of t-BuOOH in the reaction also results into fragmentation and decrease selectivity of the oxidation of the reaction. We have demonstrated that the DDQ/NaNO$_2$ aerobic oxidation systems are suitable for the oxidation electron rich model compounds, the LMCs 1-2 doesn't reacts. Likewise, phenolic LMCs doesn't results into complete polymerization reaction. The TEMPO/NaNO$_2$ oxidation process, works effective for non-phenolic LMCs. The TEMPO oxidation results in roughly 80% of the corresponding ketone. However, phenolic LMCs gives chromatographically immobile compounds. We found that DDQ and TEMPO oxidation process is ineffective under non-aerobic conditions. To avoid this side reaction, protection of the phenolic hydroxyl groups is an essential step. We illustrate 8 equivalent each of formic acid and hydrogen peroxide gives maximum yield. In our LMCs Baeyer-Villiger oxidation study, LMCs 3-6 oxidized ester further undergoes hydrolysis to corresponding carboxylic acid. Also, alkoxy group has higher migration aptitude compare to phenyl.

In summary, we have developed a process for selective cleavage of the Cα-Cβ linkage in lignin model compounds via Baeyer-Villiger oxidation. We are currently studying this oxidation process in ionic liquids. Future work will also focus on the investigation of catalysts for two electron oxidation of benzylic hydroxyl groups.

41

CHAPTER 3. EXPERIMENTAL PROCEDURE AND DATA

3.1   Synthesis and characterization of lignin model compounds (LMCs)

3.1.1 Synthesis of 1-(Phenethyloxy)benzene (1)[152]
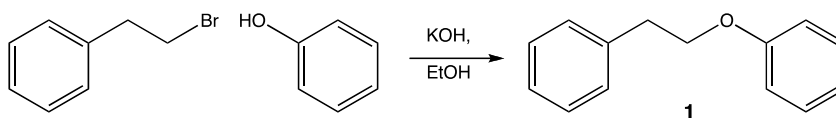
A mixture of KOH (0.6 g, 10.7 mmol) and phenol (2 g, 21.3 mmol) was dissolved in
ethanol (3.4 mL) by stirring at 45 °C. 1-(2-bromoethyl)benzene (1.98 g, 10.7 mmol) was
added, and the resulting mixture was heated at reflux for 24 h. The reaction mixture was
then concentrated in vacuum. The residue was diluted with water (100 mL) and extracted
with CH_2Cl_2 (3 × 50 mL). The organic layer was washed with aqueous 2N NaOH and
with water and then evaporated to dryness. The residue was subjected to column
chromatography on silica gel (hexane) to yield 1-(phenethyloxy)benzene (1.4 g, 66%). ^{1}H
NMR (400 MHz, CDCl$_3$): δ 7.43 (m, 7H), δ 7.11 (m, 3H), δ 4.33 (t, J=7.24 Hz, 2H), δ
3.27 (t, J=7.26 Hz, 2H). ^{13}C NMR (400 MHz, CDCl$_3$): δ 158.9, 138.4, 129.6, 129.1,
128.6, 126.6, 120.8, 114.7, 68.6, 35.9. GC-MS m/z (relative intensity): 198 (M$^+$, 32), 105
(100), 91 (10), 77 (34), 65 (12), 51(13).

3.1.2 Synthesis of 2-(3-propylphenoxy)-1-phenylethanol (2)[153]

Step 1- Synthesis of 2-(3-propylphenoxy)-1-phenylethanone (**2'**)
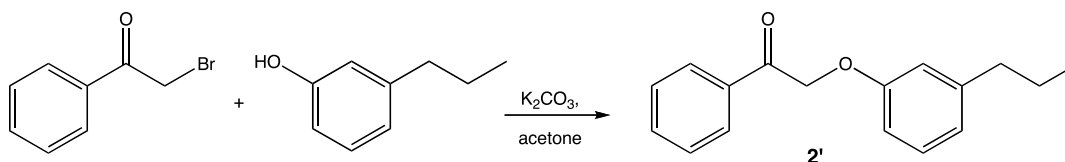
2-Bromoacetophenone (2 g, 10.05 mmol) was added to a solution of 3-propylphenol (1.71
g, 12.56 mmol) and potassium carbonate (1.73 g, 12.56 mmol) in acetone (28 mL). The
reaction mixture was heated at reflux for 5 h and was then concentrated under vacuum. The

residue was diluted with water (100 mL) and extracted with CH_2Cl_2 (3 × 50 mL). The organic layer was washed with 2N NaOH and with water and then evaporated to dryness. The residue was subjected to column chromatography on silica gel (EtOAc:hexane 1:9) to yield 2-(3-propylphenoxy)-1-phenylethanone (70%) as white crystals. ^{1}H NMR (400 MHz, CDCl₃): δ 8.02 (d, J=7.82 Hz, 2H), δ 7.61 (t, J=7.43 Hz, 1H), δ 7.49 (t, J=7.63 Hz, 2H), δ 7.20 (t, J=8.12 Hz, 1H), δ 6.83 (d, J=5.87 Hz, 2H), δ 6.77 (d, J=8.38 Hz, 1H), δ 5.24 (s, 2H), δ 2.57 (t, J=7.63 Hz, 2H), δ 1.65 (m, J=14.86 ,7.43 Hz, 2H), δ 0.953 (t, J= 7.43 Hz, 3H). GC-MS m/z (relative intensity): 254 (M⁺, 100), 236 (6), 207 (14), 105 (100), 91 (38), 77 (70), 65 (12), 51(17).

Step 2 - Reduction of 2-(3-propylphenoxy)-1-phenylethanone[154]
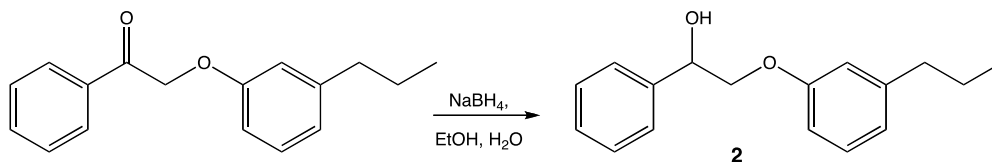
Sodium borohydride (0.133 g, 3.5 mmol) was added to a solution of 2-(3-propylphenoxy)-1-phenylethanone (1.778 g, 7.0 mmol) in ethanol (45 mL) and water (8 mL). The reaction mixture was stirred for 3 h at room temperature. The mixture was quenched with saturated aqueous NH_4Cl (15 mL) and concentrated under vacuum. The residue was diluted with water (100 mL) and extracted with CH_2Cl_2 (2 × 50 mL). The organic layer was washed with water and then evaporated to dryness. The residue was subjected to column chromatography on silica gel (EtOAc:hexane 1:9) to yield 2-(3-propylphenoxy)-1-phenylethanol (95%). ^{1}H NMR (400 MHz, CDCl₃): δ 7.41 (m, 5H), δ 7.2 (t, J= 8.02 Hz, 1H), δ 6.7 (m, 3H), δ 5.14-5.12 (t, J= 2.74 Hz, 1H), δ 4.12 (dd, J= 3.13 Hz, 1H), δ 4.01 (t, J= 9.38 Hz, 1H), δ2.56 (t, J= 7.43 Hz, 2H), δ 1.64 (tq, J=14.86, 7.43 Hz, 2H), δ 0.94 (t, J= 7.43, 3H). ^{13}C NMR (400 MHz, CDCl₃): δ 158.6, 144.7, 139.9, 129.4, 128.8, 128.4, 126.5, 121.8, 115.1, 111.9, 73.5, 72.8, 38.3, 24.6, 14.0. GC-MS m/z (relative intensity): 256 (M⁺, 18), 238 (10), 150 (70), 136 (52), 122 (29), 107(100), 91 (57), 79 (71), 65 (13), 51 (15).

3.1.3 Synthesis of 2-(3-methoxy-5-propylphenoxy)-1-(3,4-dimethoxyphenyl) propan-1-ol (3)[155]

Step 1- Synthesis of 1-(3,5-dimethoxyphenyl)propan-1-one (7)[155]
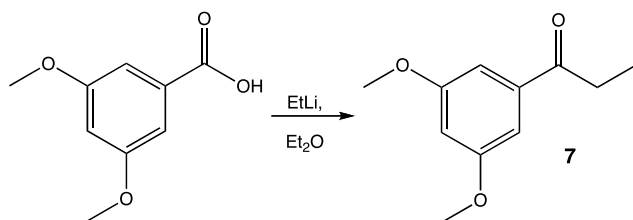
A solution of 3,5-dimethoxybenzoic acid (11 g, 60.44 mmol) in dry diethyl ether (86 mL) was stirred at -78 °C under N_2 for 5 min. 0.5 M ethyl lithium in benzene/cyclohexane 9:1 (333 mL was, 166.21 mmol) was added over 1 h, the reaction mixture was stirred at -78 °C for a further 1 h and then stirred overnight at room temperature. The reaction mixture was poured onto 250 g ice and 250 mL of 1 M HCl. The product was extracted with EtOAc (3 × 100 mL). The organic layer was washed with saturated $NaHCO_3$ and with the water and concentrated under vacuum. The residue was subjected to column chromatography on silica gel (EtOAc:hexane 1:9) to yield 1-(3,5-dimethoxyphenyl)propan-1-one (75%). ^{1}H NMR (400 MHz, CDCl$_3$): δ 7.0 (d, J=2.34 Hz, 2H), δ 6.54 (t, J=2.34 Hz, 1H), δ 3.74 (s, 3H), δ 3.73 (s, 3H), δ 2.86 (q, J=7.43 Hz, 2H), δ 1.12 (t, J=7.23 Hz, 3H). GC-MS m/z (relative intensity): 194 (M$^+$, 72), 165 (100), 137 (45), 122 (39), 107(17), 92 (5), 77(12), 69 (6), 63 (12), 57 (3), 51 (6).

Step 2 - Synthesis of 1,3-dimethoxy-5-propylbenzene (8)[155]
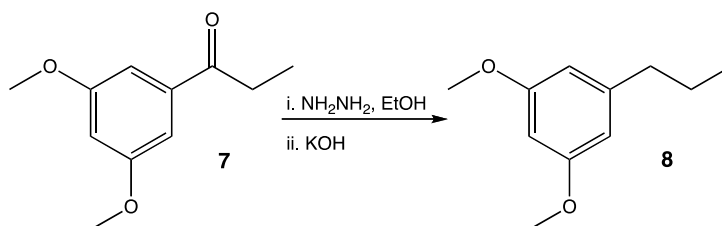
To a solution of 1-(3,5-dimethoxyphenyl)propan-1-one (6.5 g, 33.51 mmol) in 52 mL of absolute ethanol was added 51% hydrazine hydrate solution (5.256 g, 83.76 mmol), after which the mixture was heated to reflux for 6 h. The reaction mixture was concentrated under vacuum, KOH (11.2 g) was added, and the mixture was stirred at 180 °C for 1 h. The residue was diluted with water (100 mL) and the product was extracted into CH$_2$Cl$_2$ (2 × 50 mL). The organic layer was washed with water and concentrated under vacuum. The residue was subjected to column chromatography on silica gel (EtOAc:hexane 1:18) to

yield 1,3-dimethoxy-5-propylbenzene quantitatively. ^{1}H NMR (400 MHz, CDCl$_3$): δ 6.44 (s, 1H), δ 6.43 (s, 1H), δ 6.39 (dd, J=2.34, 1.96 Hz, 1H), δ 3. 83 (s, 3H), δ 3.83 (s, 3H), δ 2.61 (t, J=7.82 Hz, 2H), δ 1.73 (tq, J=7.43, 7.43 Hz, 2H), δ 1.04 (t, J=7.43 Hz, 3H). GC-MS *m*/*z* (relative intensity): 180 (M$^+$, 42), 165 (15), 152 (100), 137 (5), 121 (9), 109(5), 91 (14), 77(12), 65 (8), 51 (5).

Step 3 - Synthesis of 3-methoxy-5-propylphenol (9)[156]
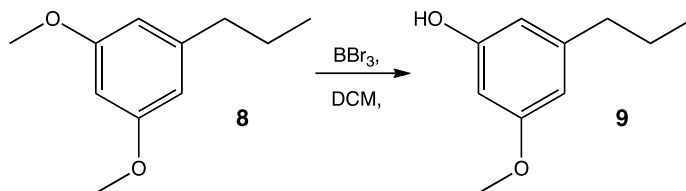
A solution of 1,3-dimethoxy-5-propylbenzene (5.5 g, 30.55mmol) in dry dichloromethane was stirred at -10 °C under N$_2$. 1 M BBr$_3$ in CH$_2$Cl$_2$ (30.55 mL, 30.55 mmol) was added over 15 min, the reaction mixture was stirred at -10 °C for 1 h and then stirred overnight at room temperature. The reaction mixture was again cooled to -10 °C, quenched with 1M HCl and the product was extracted with CH$_2$Cl$_2$ (3 × 50 mL). The organic layer was washed with water and concentrated under vacuum. The residue was subjected to column chromatography on silica gel (EtOAc:hexane 1:9) to yield 3-methoxy-5-propylphenol (80%). ^{1}H NMR (400 MHz, CDCl$_3$): δ 6.40 (dd, J=1.96, 1.56 Hz, 1H), δ 6.36 (dd, J=1.95, 1.2 Hz, 1H), δ 6.33 (dd, J=2.35, 2.34 Hz, 1H), δ 3.77 (s, 3H), δ 2.51 (t, J=7.84, 2H), δ 1.62 (tq, J=7.82, 7.43, 6.633 Hz, 2H), δ 0.96 (t, J=7.23 Hz, 3H). GC-MS *m*/*z* (relative intensity): 166 (M$^+$, 46), 151 (18), 138 (100), 123 (4.5), 107 (9), 94(6), 77(12), 65 (5.5), 51 (4).

Step 4 - Synthesis of 1-(3,4-dimethoxyphenyl)propan-1-one (10)[155]
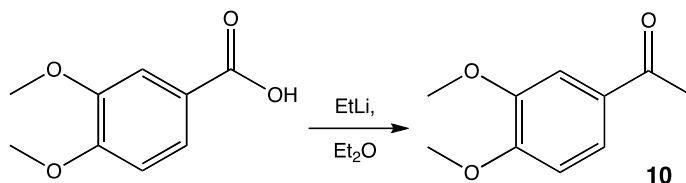
A solution of 3,4-dimethoxybenzoic acid (4 g, 21.97 mmol) in dry diethyl ether (86 mL) was stirred at -78 °C under N$_2$ for 5 min. 0.5 M ethyl lithium in benzene/cyclohexane 9:1 (121 mL, 60.42 mmol) was added over 1 h , the reaction mixture was stirred at -78 °C for a further 1 h and then stirred overnight at room temperature. The reaction mixture was

poured onto 100 g ice and 100 mL of 1 M HCl. The product was extracted with EtOAc (3 × 50 mL). The organic layer was washed with saturated $NaHCO_3$ and with water and concentrated under vacuum. The residue was subjected to column chromatography on silica gel (EtOAc:hexane 1:9) to yield 1-(3,4-dimethoxyphenyl)propan-1-one (73%). ^{1}H NMR (400 MHz, CDCl$_3$): δ 7.6 (dd, J=1.96 Hz, 1H), δ 7.55 (d, J=1.96 Hz, 1H), δ 6.89 (d, J=8.41 Hz, 1H), δ 3.95 (s, 3H), δ 3.94 (s, 3H), δ 2.97 (q, J=7.34 Hz, 2H), δ 1.22 (t, J=7.34 Hz, 3H). GC-MS m/z (relative intensity): 194 (M$^+$, 26), 165 (100), 137 (11), 122 (7), 107(5), 92 (4.5), 79(14), 63 (3.5), 51 (6).

Step 5 - Synthesis of 2-bromo-1-(3,4-dimethoxyphenyl)propan-1-one (11)
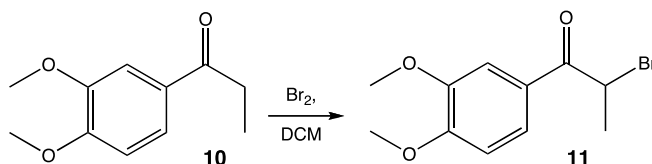
To a solution of 1-(3,4-dimethoxyphenyl)propan-1-one (1.5 g, 7.73 mmol) in dry dichloromethane (30 mL) at 0 °C, Br$_2$ (0.4 mL, 7.73 mmol) was added dropwise over 15 min. The resulting mixture was stirred at room temperature for 2 h. The organic phase was washed with successively 1 M NaHCO$_3$, 1 M Na$_2$S$_2$O$_3$ and twice with water. The combined organic layers were dried over MgSO$_4$ and concentrated under vacuum. The residue was subjected to column chromatography on silica gel (EtOAc:hexane 1:3) to yield 2-bromo-1-(3,4-dimethoxyphenyl)propan-1-one quantitatively. ^{1}H NMR (400 MHz, CDCl$_3$): δ 7.62 (dd, J=2.05 Hz, 1H), δ 7.54 (d, J=2.05 Hz, 1H), δ 6.87 (d, J=8.49 Hz, 1H), δ 5.26 (q, J=6.73 Hz, 1H), δ 3.92 (s, 3H), δ 3.90 (s, 3H), δ 1.85 (d, J=6.73 Hz, 3H). GC-MS m/z (relative intensity): 274 (M$^+$, 9), 272(M$^+$, 9), 65 (100), 137 (8), 122 (4.5), 107(4), 92 (3), 79(10), 63 (2.5), 51 (4.5).

Step 6 – Synthesis of 2-(3-methoxy-5-propylphenoxy)-1-(3,4-dimethoxyphenyl)propan-1-one (3')[157]

46
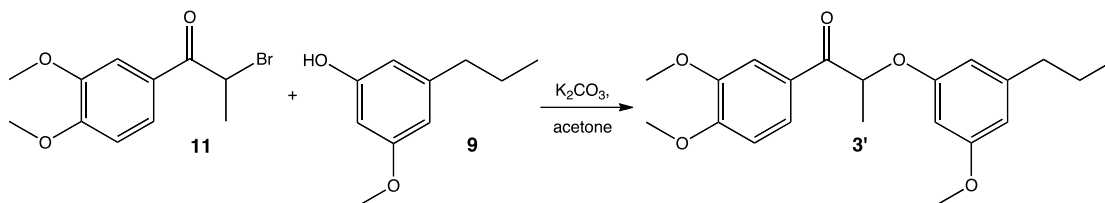
3-methoxy-5-propylphenol (1.00 g, 6.05 mmol) and potassium carbonate (0.84 g, 6.05 mmol) were stirred in acetone (18.5 mL). 2-bromo-1-(3,4-dimethoxyphenyl)propan-1-one (1.5 g, 5.5 mmol) was added to the reaction mixture which was refluxed for 5 h. The reaction mixture was then concentrated under vacuum. The residue was diluted with water (50 mL) and extracted with EtOAc (3 × 25 mL). The organic layer was washed with 2N NaOH and then with water. The residue was subjected to column chromatography on silica gel (EtOAc:hexane 1:3) to yield 2-(3-methoxy-5-propylphenoxy)-1-(3,4-dimethoxyphenyl)propan-1-one quantitatively. ^{1}H NMR (400 MHz, CDCl$_3$): δ 7.77 (dd, J=8.4, 1.95, 1H), δ 7.59 (d, J=1.95 Hz, 1H), δ 6.86 (d, J=8.41 Hz, 1H), δ 6.29 (d, J=2.15 Hz, 2H), δ 6.25 (dd, J=2.34, 2.15 Hz, 1H), δ 5.39 (q, J=6.84 Hz, 1H), δ 3.89 (s, 3H), δ 3.85 (s, 3H), δ 3.66 (s, 3H), δ 2.43 (t, J=7.53 Hz, 2H), δ1.67 (d, J=6.84 Hz, 3H), 1.53 (tq, J=7.62, 7.43 Hz, 2H), δ 0.85 (t, J=7.34 Hz, 3H). GC-MS m/z (relative intensity): 358 (M$^+$, 27), 340 (20), 311 (5), 193 (14), 165(100), 151(5.5), 137(5), 121(5.5), 105(2.5), 91 (6), 77(7), 65 (2), 51 (2).

Step 7 – Synthesis of 2-(3-methoxy-5-propylphenoxy)-1-(3,4-dimethoxyphenyl)propan-1-ol (3)[91]
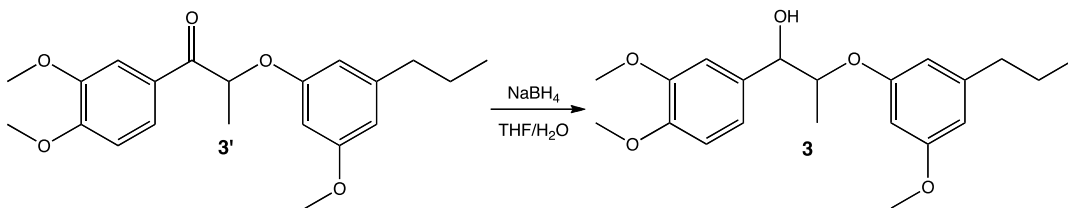
Sodium borohydride (0.38 g, 10.06 mmol) was added to a solution of 2-(3-methoxy-5-propylphenoxy)-1-(3,4-dimethoxyphenyl)propan-1-one (1.8 g, 5.03 mmol) in THF (13.6 mL) and water (4.5 mL). The reaction mixture was stirred for 4 h at room temperature. The mixture was quenched with saturated aqueous NH$_4$Cl (10 mL) and was concentrated under vacuum. The residue was diluted with water (50 mL) and extracted with EtOAc (2 × 50 mL). The organic layer was washed with water and then evaporated to dryness. The residue was subjected to column chromatography on silica gel (EtOAc:hexane 1:3) to yield 2-(3-methoxy-5-propylphenoxy)-1-(3,4-dimethoxyphenyl)propan-1-ol quantitatively. ^{1}H NMR (400 MHz, CDCl$_3$, mixture of diastereomers): δ 6.95 (m, 2H), δ 6.84 (d, J=8.21 Hz, 1H), δ 6.35 (m, 3H), δ 4.94 (d, 3.52 Hz, 0.25H), δ 4.62 (d, 7.43 Hz, 0.75H), δ 4.5 (qd, J=6.26,

3.91 Hz, 0.25H), 4.34 (qd, J=12. 12, 6.26 Hz, 0.75 H), δ 3.85 (d, 3H), δ 3.84 (d, 3H), δ 3.74 (d, 3H), δ 3.13 (s, 1H), 2.51 (m, 2H), δ 1.625(m, 2H), δ 1.2 (d, 6.25 Hz, 0.75H), δ 1.11 (d, 5.87 Hz, 2.25H), δ 0.94 (m, 3H). ^{13}C NMR (400 MHz, CDCl$_3$, mixture of diastereomers): δ 160.82, 160.8, 158.8, 158.6, 149.1, 149.03, 149.0, 148.5, 145.4, 145.3, 133.0, 132.6, 120.0, 118.7, 111.0, 110.2, 109.7, 108.80, 108.77, 107.2, 107.1, 100.0, 99.9, 78.9, 78.0, 77.9, 75.0, 56.0, 55.3, 38.4, 24.5, 24.4, 16.0, 14.0, 13.3. GC-MS *m/z* (relative intensity): Major diastereomer: 360 (M$^+$, 3), 342 (100), 327 (20), 313(10), 299(20), 284(10), 268(6), 253(6), 239(5), 225(5), 207(13), 194 (68), 178(36), 167(94), 150(36), 139(40), 121(13), 115(17), 107(17), 91 (28), 77(23), 65 (11), 51 (9). Minor diastereomer: 360 (M$^+$, 1), 342 (63), 327 (14), 313(8), 299(16), 284(8), 268(6), 253(6), 239(5), 225(5), 207(23), 194 (77), 178(32), 167(100), 150(27), 139(40), 121(13), 115(14), 107(17), 91 (32), 77(23), 65 (11), 51 (9).

3.1.4 Synthesis of 4-(2-(3-methoxy-5-propylphenoxy)-1-hydroxypropyl)-2-methoxyphenol (4)

Step 1 – Synthesis of 2-methoxy-4-prop-1-enyl)phenyl acetate (12)

Acyl chloride (2.69 mL, 33.53 mmol) was added to a solution 2-methoxy-4-(prop-1-enyl)phenol (5 g, 30.49 mmol) and pyridine (2.70 mL, 33.53 mmol) in dichloromethane (100 mL). The mixture was stirred at room temperature for 30 minutes. The reaction mixture was then carefully poured into water. The product was extracted with Et$_2$O (2 × 50 mL). The organic layer was washed with 0.05N HCl and with water and was concentrated under vacuum. The residue was sufficiently pure to be used in the following step. ^{1}H NMR (400 MHz, CDCl$_3$, mixture of E-Z isomers): δ 6.93 (m, 3H), δ 6.35 (m, 1H), δ 6.16 (m, 0.6), δ 5.77 (m, 0.4 H), δ 3.81 (d, 3H), δ 2.29 (d, 3H), δ 1.88 (m, 3H). GC-MS *m/z* (relative intensity, major isomer): 206 (M$^+$, 9.5), 164 (100), 149 (22), 131 (13), 121(8), 103(12), 91(18), 77(12), 65(6), 55 (5), 51(5).

<u>Step 2</u> – Synthesis of 4-(2-iodopropanoyl)-2-methoxyphenyl acetate (13)[158]
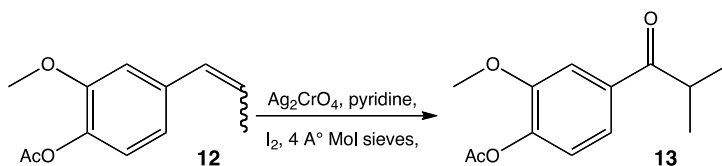
Iodine (6.43 g, 25.34 mmol), silver chromate (6.16 g, 18.58 mmol), 4 Å molecular sieves (5.25 g) and pyridine (0.67 g, 8.45 mmol) were stirred in dichloromethane (50 mL) at 0 °C for 10 min. 2-methoxy-4-prop-1-enyl)phenyl acetate (3.48 g, 16.89 mmol) was dissolved in dichloromethane (10 mL) and was slowly added to above reaction mixture. The reaction mixture was stirred at 0 °C for 20 min and then at room temperature for 1 h. The reaction mixture was then filtered. The filtrate was washed successively with 5% sodium thiosulfate, saturated NaCl, and twice with water. The filtrate was dried over $MgSO_4$ and concentrated under vacuum. The residue was subjected to column chromatography on silica gel (hexane:CH_2Cl_2 1:2) to yield 4-(2-iodopropanoyl)-2-methoxyphenyl acetate in 55% yield. ^{1}H NMR (400 MHz, CDCl$_3$): δ 7.66 (d, J=1.95 Hz, 1H), δ 7.6 (dd, J=8.21, 1.96 Hz, 1H), δ 7.12 (d, 8.21 Hz, 1H), δ 5.46 (q, J= 6.65 Hz, 1H), δ 3.9 (s, 3H), δ 2.34 (s, 3H), δ 2.1 (d, J=6.65 Hz, 3H). GC-MS m/z (relative intensity): 348 (M$^+$, 2), 306 (55), 180 (4), 151 (100), 119(7.5), 108(3), 91(9), 79(5), 65(2), 51(5).

<u>Step 3</u> – Synthesis of 2-(3-methoxy-5-propylphenoxy)-1-(4-hydroxy-3-methoxyphenyl)propan-1-one (4')[159]
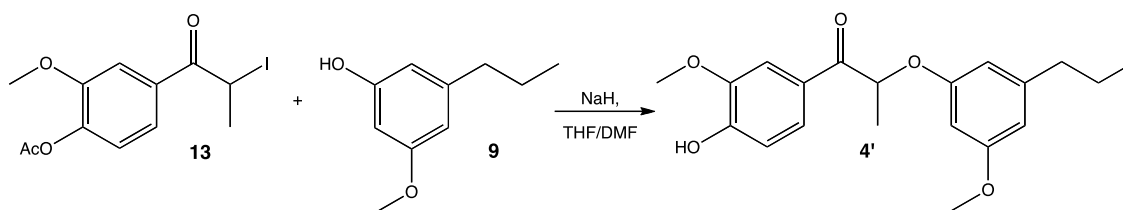
60 % NaH (dispersion in mineral oil) (0.12 g, 3 mmol), freshly prepared 4-(2-iodopropanoyl)-2-methoxyphenyl acetate (1.04 g, 3 mmol) and 3-methoxy-5-propylphenol (0.52 g, 3.15 mmol) were placed in 3 individual one-neck round bottom flasks. The flasks were degassed with N_2 for 15 minutes. 1 ml THF and 4 ml DMF were added to the individual flasks. The solution of NaH in THF/DMF was cooled to 0 °C, after which the solution of 3-methoxy-5-propylphenol was added. The mixture was stirred at room temperature for 1 h, then cool to 0 °C again. The 4-(2-iodopropanoyl)-2-methoxyphenyl

49

acetate solution was added and the resulting mixture was stirred at room temperature for 3 h. The reaction was poured onto 100 ml ice water. The resulting aqueous layer was purified and extracted with EtOAc (50 mL). The EtOAc extract was washed with water, dried (MgSO$_4$), and concentrated under vacuum. The residue was subjected to column chromatography on silica gel (EtOAc:hexane 1:3) to yield 2-(3-methoxy-5-propylphenoxy)-1-(4-hydroxy-3-methoxyphenyl)propan-1-one (48%). ^{1}H NMR (400 MHz, CDCl$_3$): δ 7.71 (dd, , J=8.6, 1.95, 1H), 7.59 (d, J=1.56 Hz, 1H), δ 6.92 (d, J=8.21 Hz, 1H), δ 6.29 (t, J=1.95 Hz, 2H), δ 6.24 (t, J=1.95 Hz, 1H), δ 5.38 (q, J=6.65 Hz, 1H), δ 3.9 (s, 3H), δ 3.69 (s, 3H), δ 2.43 (t, J=7.53 Hz, 2H), δ1.67 (d, J=6.84 Hz, 3H), 1.53 (tq, J=7.62, 7.43 Hz, 2H), δ 0.85 (t, J=7.34 Hz, 3H). GC-MS m/z (relative intensity): 344 (M$^+$, 32), 326 (3), 207 (4), 193(37), 151 (100), 138(4), 123(8), 108(3), 91(8), 77(4), 65(2.5), 51(1).

Step 4 – Synthesis of 4-(2-(3-methoxy-5-propylphenoxy)-1-hydroxypropyl)-2-methoxyphenol (4)[91]
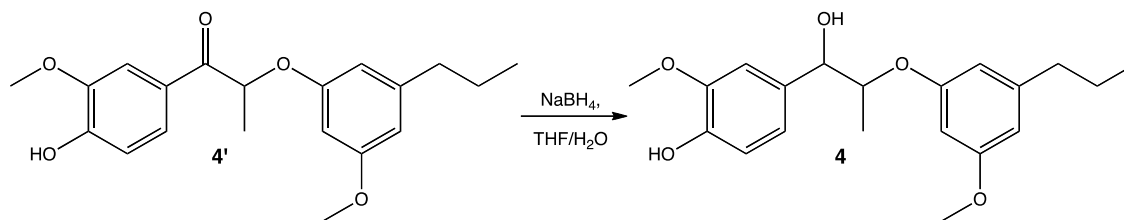
2-(3-methoxy-5-propylphenoxy)-1-(4-hydroxy-3-methoxyphenyl)propan-1-one (0.69g, 2.0 mmol) was stirred in THF (9.3 mL) and water (4.7 mL) at room temperature. Sodium borohydride (0.3g, 8 mmol) was added over 3 h and the solution was further stirred for 1 h at room temperature. The mixture was quenched with saturated aqueous NH$_4$Cl (5 mL) and concentrated under vacuum. The residue was diluted with water (100 mL) and extracted with EtOAc (3 × 50 mL). The residue was subjected to column chromatography on silica gel (EtOAc:hexane 1:3) to yield 4-(2-(3-methoxy-5-propylphenoxy)-1-hydroxypropyl)-2-methoxyphenol (80%). ^{1}H NMR (400 MHz, CDCl$_3$, mixture of diastereomers): δ 6.98 (dd, 1H), 6.88 (m, 2H), δ 6.36 (m, 3H), δ 5.64 (d, 1H), δ 4.96 (t, 0.25H), δ 4.61 (dd, 0.75H), δ 4.5 (m, 0.25H), δ 4.36 (m, 0.75H), δ 3.91 (d, 3H), δ 3.77 (d, 3H), δ 3.06 (s, 1H), δ 2.53 (m, 2H), δ 1.62 (m, 2H), δ 1.19 (d, 0.75H), δ 1.12 (d, 2.25H), δ 0.95 (m, 3H). ^{13}C NMR (400 MHz, CDCl$_3$, mixture of diastereomers): δ 160.91, 160.89, 158.8, 158.6, 146.8, 145.8, 145.5, 145.5, 145.2, 132.3, 131.9, 120.8, 119.5, 114.4, 114.3, 109.6, 109.1, 108.91, 108.86,

50

107.4, 107.3, 100.07, 100.0, 79.1, 78.2, 78.1, 75.2, 56.2, 55.5, 38.5, 24.54, 24.52, 16.06, 14.05, 13.3. GC-MS m/z (relative intensity): major diastereomer: 346 (M^+, 3.5), 328 (100), 313 (15), 229(12), 285(15), 270(8), 253(6), 204(10), 194(60), 180(22), 166(32), 153(100), 138(36), 131(8), 121(16), 115(10), 109(10), 103(10), 91(22), 77(18), 65(12), 51(6). Minor diastereomer: 346 (M^+, 0), 328 (100), 313 (15), 229(10), 285(16), 270(9), 253(5), 207(10), 194(41), 180(29), 166(32), 153(78), 138(43), 131(8), 121(16), 115(10), 107(10), 91(19), 77(17), 65(14), 51(8).

3.1.5 Synthesis ethyl 2-(3-methoxy-5-propylphenoxy)-3-(3,4-dimethoxyphenyl)propane-1,3-diol (5)

<u>Step 1</u> – Synthesis of ethyl 3-(3,4-dimethoxyphenyl)-3-oxopropanoate (14)[160]

14
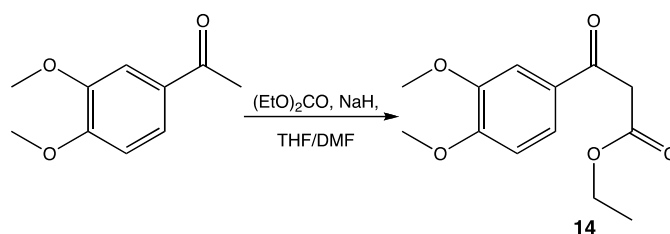
A solution of 3,4-dimethoxyacetophenone (5 g, 27.78 mmol) and 60% NaH (dispersion in mineral oil) (3.33 g, 83.5 mmol) in dry THF under N_2 was stirred for 10 minutes at ambient temperature. Diethylcarbonate (6.73 mL, 55.56 mmol) was added dropwise over 10 min, and the mixture was then refluxed at 80 °C for 5 h. The reaction was poured onto 50 g ice and 50 mL of 1 M HCl. The resulting aqueous layer was extracted with diethyl ether (3 x 100 mL). The combined diethyl ether layers were washed with saturated NaHCO₃, dried (MgSO₄), and concentrated under vacuum. The residue was subjected to column chromatography on silica gel (EtOAc:hexane 3:7) to yield ethyl 3-(3,4-dimethoxyphenyl)-3-oxopropanoate (70%). ^{1}H NMR (400 MHz, CDCl₃): δ 7.53 (dd, J=2.05 Hz, 1H), δ 7.5 (d, J=2.05 Hz, 1H), δ 6.88 (d, J=8.49 Hz, 1H), δ 4.19 (q, 7.17 Hz, 2H), δ 3.94 (s, 2H), δ 3.92 (s, 3H), δ 3.90 (s, 3H), δ 1.24 (t, J=7.18 Hz, 3H).

Step 2 – Synthesis of ethyl 2-bromo-3-(3,4-dimethoxyphenyl)-3-oxopropanoate (15)[161]
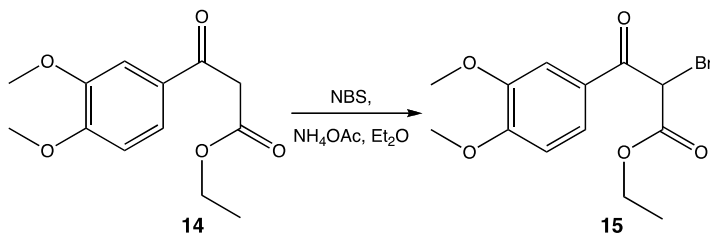
A solution of 3-(3,4-dimethoxyphenyl)-3-oxopropanoate (1.5 g, 5.95 mmol) in dry Et$_2$O (10 mL) was treated with N-bromosuccinimide (1.06 g, 5.95 mmol) and ammonium acetate (0.046 g, 0.595 mmol). The mixture was stirred at room temperature for 30 min, after which it was filtered. The filtrate was washed with water, dried (MgSO$_4$) and concentrated under vacuum. The residue was subjected to column chromatography on silica gel (EtOAc:hexane 3:7) to yield of 95% ethyl 2-bromo-3-(3,4-dimethoxyphenyl)-3-oxopropanoate. ^{1}H NMR (400 MHz, CDCl$_3$): δ 7.6 (dd, J=2.05 Hz, 1H), δ 7.52 (d, J=2.05 Hz, 1H), δ 6.89 (d, J=8.49 Hz, 1H), δ 5.636 (s, 1H), δ 4.25 (q, 7.02 Hz, 2H), δ 3.94 (s, 3H), δ 3.91 (s, 3H), δ 1.23 (t, 7.32 Hz, 3H). GC-MS m/z (relative intensity): 332 (M$^+$, 7.5), 330(7.5), 252 (2), 165 (100), 151(6.5), 137 (6), 122(3.5), 107(4), 92(4), 79(8), 63(3), 51(3.5).

Step 3 – Synthesis of ethyl 2-(3-methoxy-5-propylphenoxy)-3-(3,4-dimethoxyphenyl)-3-oxopropanoate (5')[159]
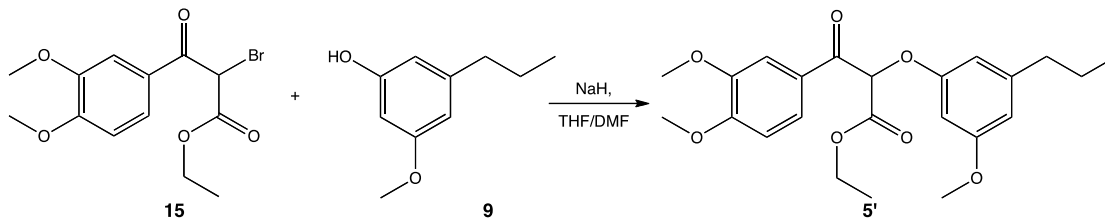
60 % NaH (dispersion in mineral oil) (0.24 g, 6 mmol), ethyl 2-bromo-3-(3, 4-dimethoxyphenyl)-3-oxopropanoate (2 g, 6 mmol) and 3-methoxy-5-propylphenol (1.2 g, 7.23 mmol) were placed in 3 individual one-neck round bottom flasks. The flasks were purged with N$_2$ for 15 min, after which 2 ml THF and 7.6 ml DMF were added to the individual flasks. The solution of NaH in THF/DMF was cooled to 0 °C and the solution of 3-methoxy-5-propylphenol was added. The mixture was stirred at room temperature for

1 h and then cooled to 0 °C again. The ethyl 2-bromo-3-(3, 4-dimethoxyphenyl)-3-oxopropanoate solution was added and the resulting mixture was stirred at room temperature for 8 h. The reaction mixture was then poured onto 100 ml ice water. The resulting aqueous layer was extracted with EtOAc (50 mL). The EtOAc extract was washed with water, dried (MgSO$_4$), and concentrated under vacuum. The residue was subjected to column chromatography on silica gel (EtOAc:hexane 3:7) to yield ethyl 2-(3-methoxy-5-propylphenoxy)-3-(3,4-dimethoxyphenyl)-3-oxopropanoate (81%) . ^{1}H NMR (400 MHz, CDCl$_3$): δ 7.85 (dd, J=1.95 Hz, 1H), δ 7.65 (d, J=1.96 Hz, 1H), δ 6.90 (d, J=8.6 Hz, 1H), δ 6.43 (m, 3H), δ 5.83, (s, 1H), δ 4.3 (q, J=7.03 Hz, 2H),), δ 3.91 (s, 3H), δ 3.90 (s, 3H), δ 3.73 (s, 3H), δ 2.51 (t, J=7.04 Hz, 2H), δ 1.60 (tq, J= 7.63 Hz, 2H), δ 1.25 (t, J= 7.24 Hz, 3H), δ 0.92 (t, J= 7.24 Hz, 3H).

Step 4 – Synthesis of 2-(3-methoxy-5-propylphenoxy)-1-(3,4-dimethoxyphenyl)propane-1,3-diol (5)[91]
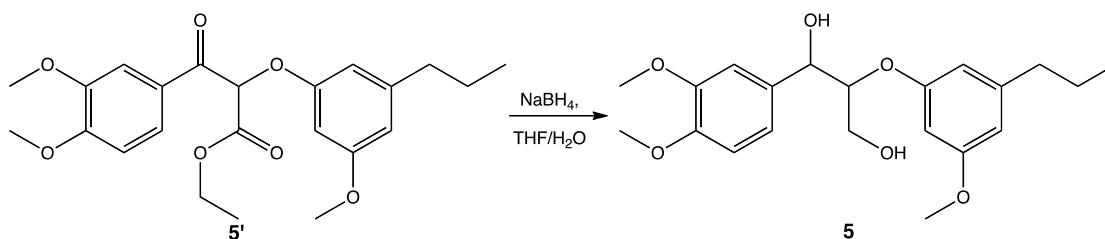
Ethyl 2-(3-methoxy-5-propylphenoxy)-3-(3,4-dimethoxyphenyl)-3-oxopropanoate (1.8 g, 4.327 mmol) was stirred in THF (37.5 mL) and H$_2$O (12.5 mL) at room temperature. Sodium borohydride (1.64 g, 43.27 mmol) was added over 3 h and the solution was further stirred for 24 h at room temperature. The mixture was quenched with saturated aqueous NH$_4$Cl (15 mL) and concentrated under vacuum. The residue was diluted with water (100 mL) and extracted with EtOAc (3 × 50 mL). After removal of solvent under vacuum, the residue was subjected to column chromatography on silica gel (EtOAc:hexane 1:1) to yield 2-(3-methoxy-5-propylphenoxy)-1-(3, 4-dimethoxyphenyl)propane-1,3-diol (68%). ^{1}H NMR (400 MHz, CDCl$_3$ with one drop of D$_2$O, mixture of diastereomers): δ 6.94 (m, 2H), δ 6.81 (m, 1H), δ 6.31 (m, 3H), δ 4.97 (m, 1H), δ 4.37-4.15 (m, 1H), δ 3.94-3.2 (m, 2H), δ 3.84 (t, 6H), δ 3.71 (d, 3H), δ 2.47 (m, 2H), δ 1.58 (m, 2H), δ 0.92 (m, 3H). ^{13}C NMR (400 MHz, CDCl$_3$, mixture of diastereomers): δ 160.8, 160.7, 159.2, 158.8, 149.2, 149, 148.7, 145.6, 145.4, 133.3, 132.5, 119.4, 118.8, 111.1, 110.1, 109.6, 109.1, 109, 107.8,

107.8, 100.32, 100.26, 82.9, 82, 74.1, 73.7, 61.7, 61.3, 56.01, 55.99, 55.4, 55.3, 38.41, 38.38, 24.44, 24.40, 13.97, 13.96. GC-MS *m/z* (relative intensity): Major diastereomer: 376 (M$^+$, 0.5), 358(1.5) 328 (10), 192 (100), 167(30), 151(12.5), 139(30), 121(12), 108(8), 91(15), 77(15), 65(7), 51(5.5). Minor diastereomer: 376 (M$^+$, 0.3), 358(1.1) 328 (7), 210(7), 192 (100), 167(30), 151(11), 139(30), 121(10), 108(8), 91(11), 77(14), 65(7), 51(5.5).

3.1.6 Synthesis of 4-(2-(3-methoxy-5-propylphenoxy)-1,3-dihydroxypropyl)-2-methoxyphenol (6)

Step 1 − Synthesis of ethyl 3-(4-hydroxy-3-methoxyphenyl)-3-oxopropanoate (16)[160]
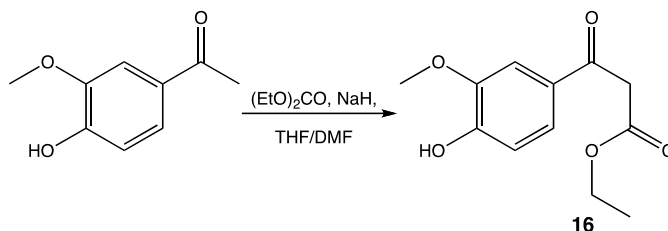
A solution of 4-hydroxy-3-methoxyacetophenone (5 g, 30.12 mmol) and 60 % NaH (dispersion in mineral oil) (4.22 g, 105.5 mmol) in dry THF under N$_2$ was stirred for 10 minutes at ambient temperature. Diethylcarbonate (21.90 mL, 180.75 mmol) was added dropwise over 10 min, and the mixture was refluxed at 80 °C for 5 h. The reaction mixture was poured onto 50 g ice and 50 mL of 1M HCl. The resulting aqueous layer was extracted with diethyl ether (50 mL). The combined diethyl ether layers were washed with saturated NaHCO$_3$, dried (MgSO$_4$), and concentrated under vacuum. The residue was subjected to column chromatography on silica gel (EtOAc: hexane 4:6) to yield ethyl 3-(4-hydroxy-3-methoxyphenyl)-3-oxopropanoate (70%). ^{1}H NMR (400 MHz, CDCl$_3$): δ 7.52 (d, J=1.95 Hz, 1H), δ 7.48 (dd, J=8.21, 1.96 Hz, 1H), δ 6.93 (d, J=8.22, 1H), δ 6.34 (s, 1H), δ 4.19 (q, 7.04 Hz, 2H), δ 3.928 (s, 2H), δ 3.917 (s, 3H), δ 1.24 (t, 7.23 Hz, 3H).

Step 2 − Synthesis of ethyl 2-bromo-3-(4-hydroxy-3-methoxyphenyl)-3-oxopropanoate (17)

16 → **17**
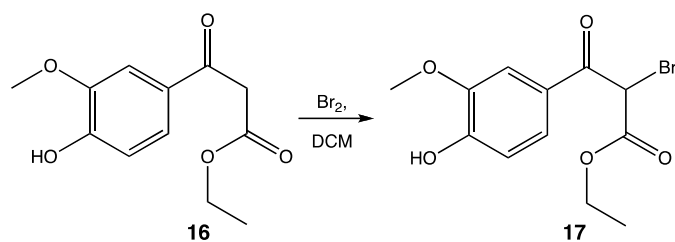
To a solution of ethyl 3-(4-hydroxy-3-methoxyphenyl)-3-oxopropanoate (5.43 g, 22.82 mmol) in dry dichloromethane (110 mL) at 0 °C, Br$_2$ (1.18 mL, 22.83 mmol) was added dropwise over 15 min. The resulting reaction mixture was stirred at room temperature for 2 h. The organic phase was washed successively with 1M NaHCO$_3$, 1M Na$_2$S$_2$O$_3$ and twice with water. The combined organic layers were dried over MgSO$_4$ and concentrated under vacuum. The residue was subjected to column chromatography on silica gel (EtOAc:hexane 3:7) to yield ethyl 2-bromo-3-(4-hydroxy-3-methoxyphenyl)-3-oxopropanoate (71%). ^{1}H NMR (400 MHz, CDCl$_3$): δ 7.56 (dd, J=8.43, J=1.95, 1H), δ 7.55 (d, J=1.95 Hz, 1H), δ 6.95 (dd, J=7.43, 0.78 Hz, 1H), δ 6.33 (s, 1H), δ 5.64 (s,1H), δ 4.27 (q, 7.23 Hz, 2H), δ 3.94 (s, 3H), δ 1.248 (t, 7.03 Hz, 3H). GC-MS *m/z* (relative intensity): 318 (M$^+$, 6.4), 316(6.4), 215(1.5), 151 (100), 137 (6), 123(8.5), 108(4.5), 93(4), 77(2.5), 65(5), 52(4.5).

Step 3 – Synthesis of ethyl 2-(3-methoxy-5-propylphenol)-3-(4-hydroxy-3-methoxyphenyl)-3-oxopropanoate (6')[159]

17 + **9** → **6'**
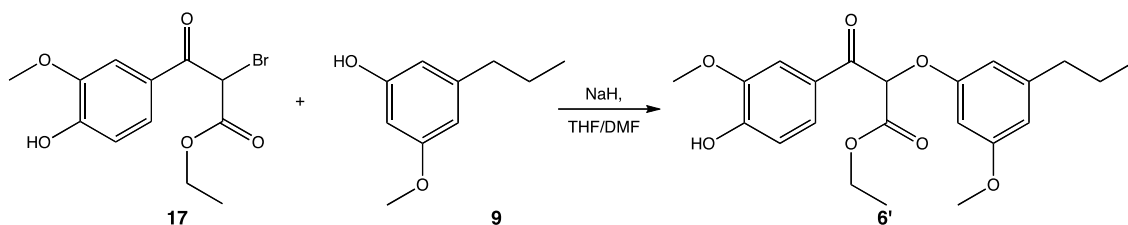
60 % NaH dispersed in mineral oil (0.3108 g, 7.77 mmol), ethyl 2-bromo-3-(4-hydroxy-3-methoxyphenyl)-3-oxopropanoate (0.98 g, 3.11 mmol) and 3-methoxy-5-propylphenol (1.29 g, 7.77 mmol) were placed in 3 individual one-neck round bottom flasks. The flasks were purged with N$_2$ for 15 min after which 1.6 ml THF and 5.6 ml DMF were added to each flask. The solution of NaH in THF/DMF was cooled to 0 °C and the solution of 3-methoxy-5-propylphenol was added. The mixture was stirred at room temperature for 1 h and then cooled to 0 °C again. The ethyl 2-bromo-3-(3, 4-dimethoxyphenyl)-3-

oxopropanoate solution was added, and the resulting mixture was stirred at room temperature for 8 h. The mixture was then poured onto 100 ml ice-water. The resulting aqueous layer was extracted with EtOAc (50 mL). The EtOAc extract was washed with water, dried (MgSO₄), and concentrated under vacuum. The residue was subjected to column chromatography on silica gel (EtOAc:hexane 3:7) to yield ethyl 2-(3-methoxy-5-propylphenol)-3-(4-hydroxy-3-methoxyphenyl)-3-oxopropanoate(30%) . ^{1}H NMR (400 MHz, CDCl₃): δ 7.63 (m, 2H), δ 6.95 (m, 1H), δ 6.37 (m, 2H), δ 6.12 (m, 1H), δ 5.7, 5.178 (s, 1H), δ 4.29 (m, 2H), δ 3.94 (d, 3H), δ 3.73 (d, 3H), δ 2.5 (t, 2H), δ 1.58 (m, 2H), δ 1.23 (t, J= 7.24 Hz, 3H), δ 0.90 (m, 3H).

Step 4 – Synthesis of 4-(2-(3-methoxy-5-propylphenoxy)-1,3-dihydroxypropyl)-2-methoxyphenol (6)[91]
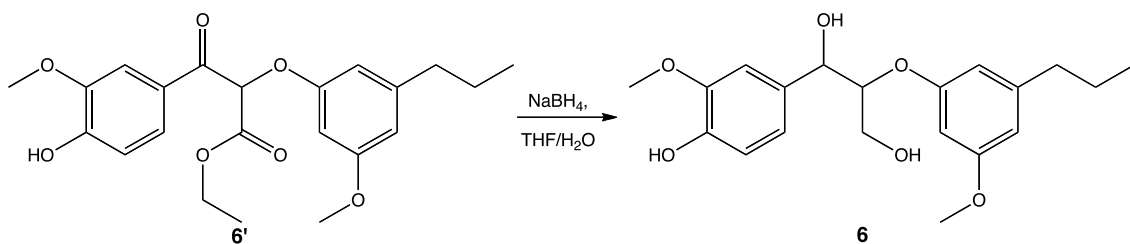
Ethyl 2-(3-methoxy-5-propylphenol)-3-(4-hydroxy-3-methoxyphenyl)-3-oxopropanoate (1.25 g, 3.11 mmol) was stirred in THF (37.5 mL) and H₂O (3.75 mL) at room temperature. Sodium borohydride (1.18 g, 31.1 mmol) was added over 3 h and the solution was further stirred for 24 h at room temperature. The reaction mixture was treated with a saturated solution of ammonium chloride, after which volatile material was removed under vacuum. The residue was diluted with water (100 mL) and extracted with dichloromethane (3 × 50 mL). After evaporation of the solvent, the residue was subjected to column chromatography on silica gel (EtOAc:hexane 1:1) to yield of 4-(2-(3-methoxy-5-propylphenoxy)-1,3-dihydroxypropyl)-2-methoxyphenol (36%). ^{1}H NMR (400 MHz, CDCl₃ with drop of D₂O, mixture of diastereomers): δ 6.92 (m, 3H), δ 6.32 (m, 3H), δ 5.79 (s, 1H), δ 4.97 (m, 1H), δ 4.35 (m, 1H), δ 3.96-3.55 (m, 2H), δ 3.85 (d, 3H), δ 3.73 (d, 3H), δ 2.48 (m, 2H), δ 1.59 (m, 2H), δ 0.92 (m, 3H). ^{13}C NMR (400 MHz, CDCl₃, mixture of diastereomers): δ 160.8, 160.7, 159.2, 158.9, 146.9, 146.8, 145.6, 145.6, 145.4, 145.3, 132.7, 131.9, 119.5, 114.54, 114.5, 109.7, 109.2, 109.1, 109.0, 107.8, 100.34, 100.25, 82.8,

82.0, 74.0, 73.7, 61.6, 61.2, 56.0, 55.4, 55.3, 38.38, 38.35, 24.41, 24.37, 13.94, 13.93. GC-MS *m/z* (relative intensity): Major diastereomer: 362 (M⁺, 0.16), 344(1.5) 314 (3.4), 192 (100), 164(32), 153(27.5), 138(18), 121(8), 105(4.5), 93(21), 77(11), 65(15), 51(4). Minor diastereomer: 362 (M⁺, 0.2), 344(0.7) 314 (1.4), 192 (100), 164(32), 153(26), 138(18), 121(8), 105(4.5), 93(19), 77(10), 65(13), 51(0.3).

3.2 Copies of ¹H and ¹³C NMR Spectra
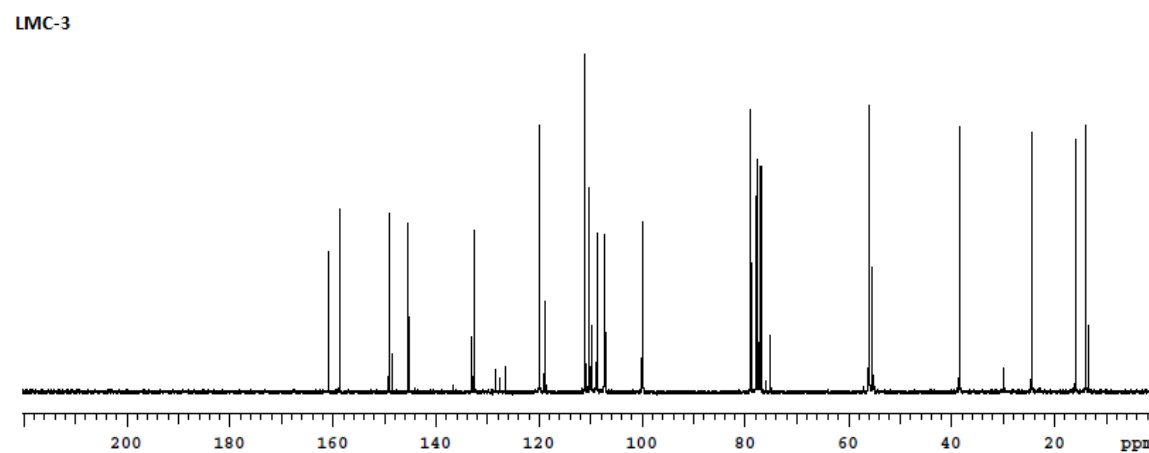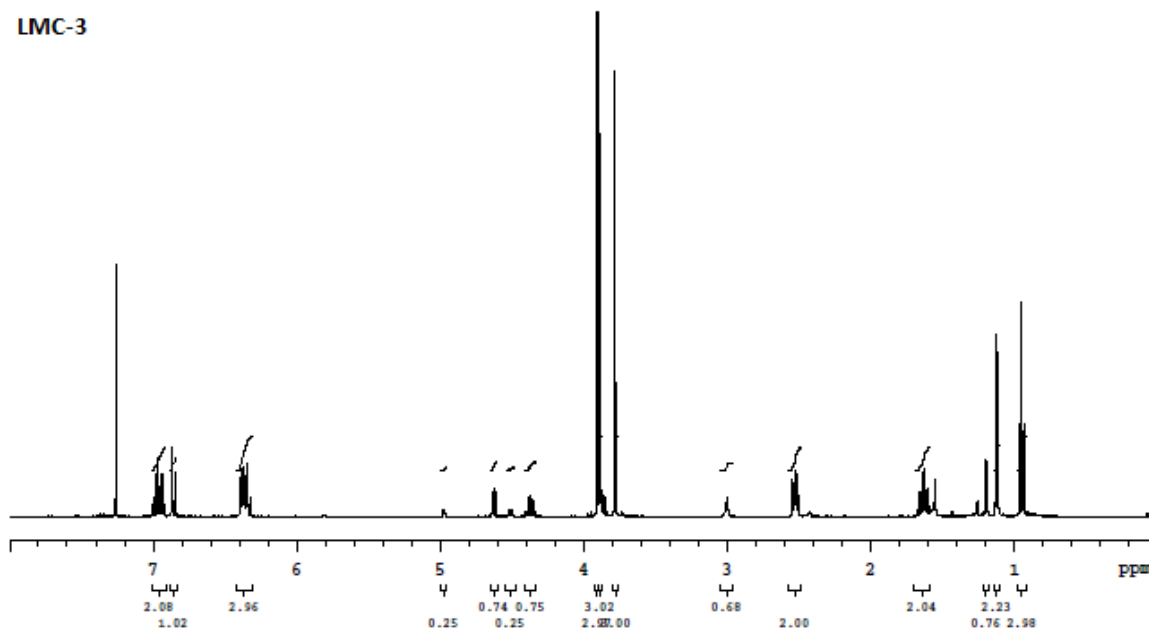
LMC-3

LMC-3

Figure 3. 1 ^{1}H NMR and ^{13}C NMR spectra of LMC **3** in CDCl$_3$
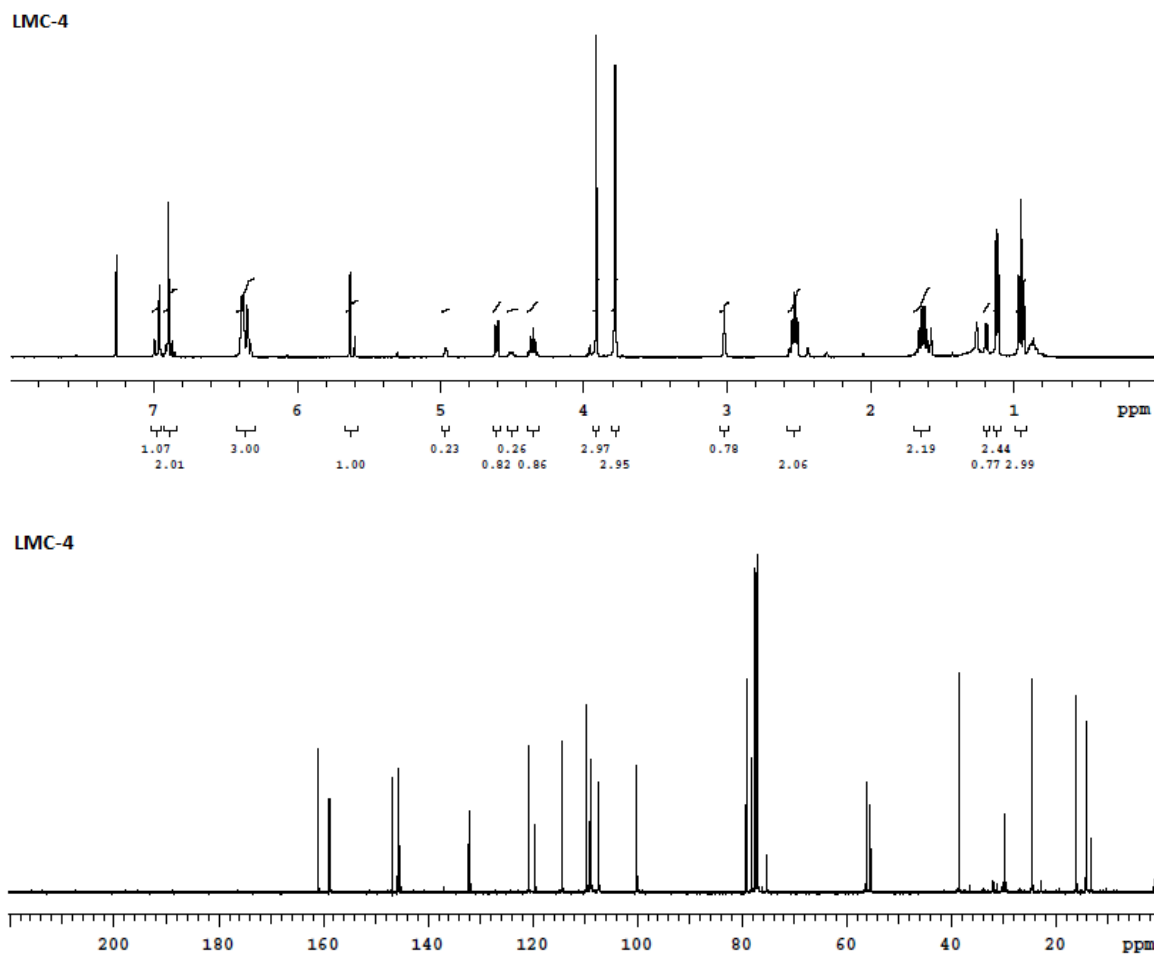
LMC-4

LMC-4

Figure 3. 2 ^{1}H NMR and ^{13}C NMR spectra of LMC **4** in CDCl$_3$
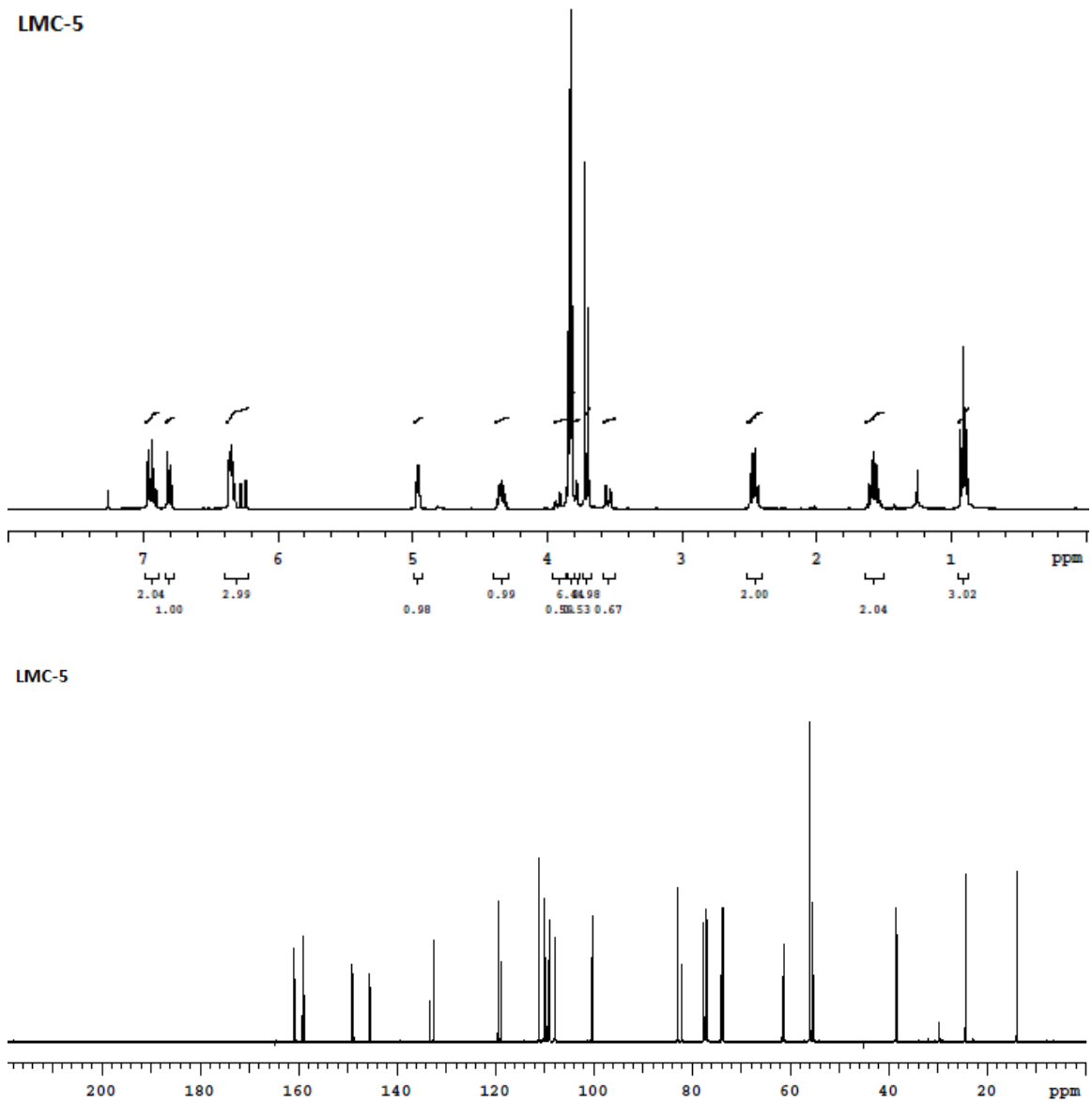
LMC-5

LMC-5

Figure 3. 3 ^{1}H NMR and ^{13}C NMR spectra of LMC **5** in CDCl$_3$
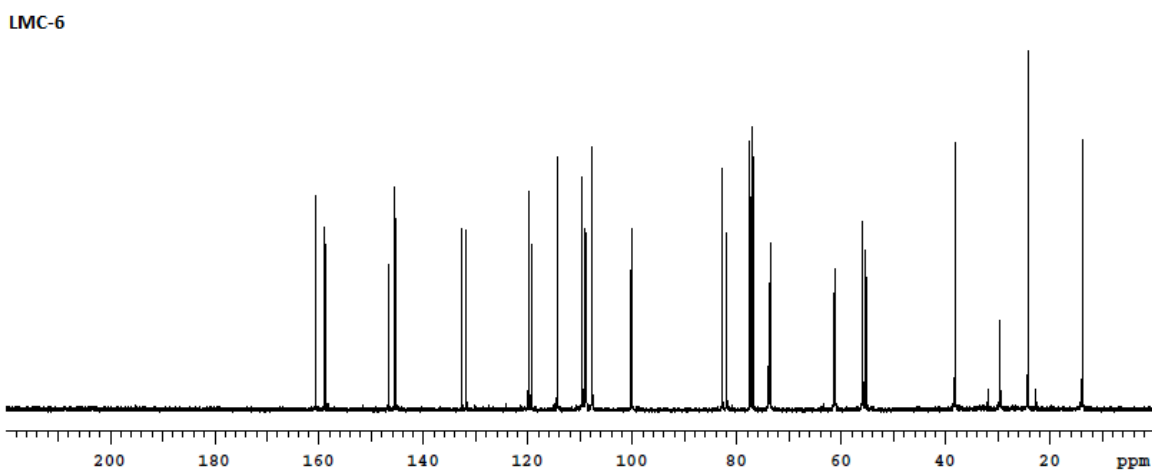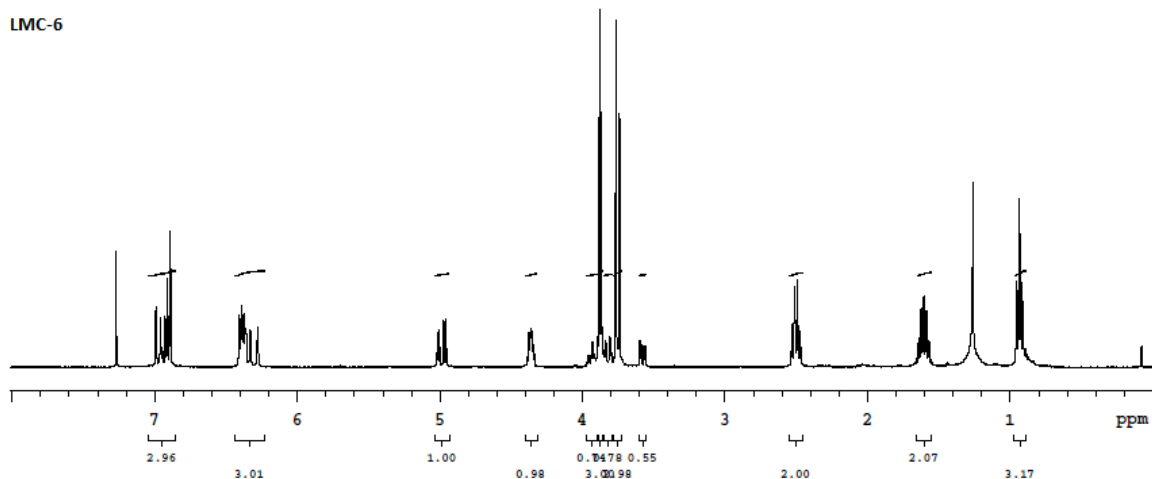
LMC-6

LMC-6

Figure 3. 4 ^{1}H NMR and ^{13}C NMR spectra of LMC **6** in CDCl$_3$

Residual grease at δ 1.26 (s), δ 0.86 (m) in ^{1}H NMR and δ 29.76 in ^{13}C NMR spectra. Solvent residual peak (CDCl$_3$) at δ 7.26 (s) in ^{1}H NMR and δ 77.23 (t) in ^{13}C NMR spectra.

3.3 Procedure for oxidation of Lignin Model Compounds

3.3.1 Hydroxylation of benzylic methylene groups in LMCs by an iron porphyrin catalyst

LMC 1 (50 mg, 0.25 mmol), TPPFeCl (1.77 mg, 0.0025 mmol), 70% aq soln of t-BuOOH (0.035 mL, 0.25 mmol), CH_3CN (0.5 mL) and 0.1N pH 3 phosphate buffer (1.5 mL) stirred at 25ºC for 14 h. The product was extracted with ethyl acetate and washed with saturated aq NaCl soln. The combined organic layers were dried over $MgSO_4$ and concentrated under vacuum. The products were isolated using a preparative TLC plate to yield of LMC 1 (92%) and 2-phenoxy-1-phenylethanone (5%).

LMC 2 (50 mg, 0.2 mmol), TPPFeCl (1.38 mg, 0.002 mmol), 70% aq soln of t-BuOOH (0.026 mL, 0.2 mmol), CH_3CN (0.5 mL) and 0.1N pH 3 phosphate buffer (1.5 mL) stirred at 25ºC for 14 h. The product was extracted with ethyl acetate and washed with saturated aq NaCl soln. The combined organic layers were dried over $MgSO_4$ and concentrated under vacuum. The products were isolated using a preparative TLC plate to yield of LMC 2 (60%), LMC 2' (18%), 1-(3-(2-hydroxy-2-phenylethoxy)phenyl)propan-1-one (9%) and 1-(3-(phenacyloxy)phenyl)-propan-1-one (11%).

LMC 3 (50 mg, 0.14 mmol), TPPFeCl (0.95 mg, 0.0014 mmol), 70% aq soln of t-BuOOH (0.018 mL, 0.13 mmol), CH_3CN (0.5 mL) and 0.1N pH 3 phosphate buffer (1.5 mL) stirred at 25ºC for 14 h. The product was extracted with ethyl acetate and washed with saturated aq NaCl soln. The combined organic layers were dried over $MgSO_4$ and concentrated under vacuum. The products were isolated using a preparative TLC plate to yield of LMC 3 (54%), LMC 3' (26%), 1-(3-(1-hydroxy-1-(3,4-dimethoxyphenyl)propan-2-yloxy)-5-methoxyphenyl)propan-1-one (2%) and 1-(3,4-dimethoxyphenyl)-2-(3-methoxy-5-propionylphenoxy)-1-propanone (5%).

LMC 4 (42 mg, 0.12 mmol), TPPFeCl (0.85 mg, 0.0012 mmol), 70% aq soln of t-BuOOH (0.017 mL, 0.12 mmol), CH_3CN (0.5 mL) and 0.1N pH 3 phosphate buffer (1.5 mL) stirred at 25ºC for 14 h. The product was extracted with ethyl acetate and washed with saturated

aq NaCl soln. The combined organic layers were dried over $MgSO_4$ and concentrated under vacuum. The products were chromatographically immobile.

LMC 5 (50 mg, 0.13 mmol), TPPFeCl (0.82 mg, 0.0012 mmol), 70% aq soln of t-BuOOH (0.017 mL, 0.12 mmol), CH_3CN (0.5 mL) and 0.1N pH 3 phosphate buffer (1.5 mL) stirred at 25ºC for 14 h. The product was extracted with ethyl acetate and washed with saturated aq NaCl soln. The combined organic layers were dried over $MgSO_4$ and concentrated under vacuum. The products were isolated using a preparative TLC plate to yield of LMC 5 (44%), LMC 5' (39%), 1-(3-(1,3-dihydroxy-1-(3,4-dimethoxyphenyl)propan-2-yloxy)-5-methoxyphenyl)propan-1-one (14%), 1-(3,4-dimethoxyphenyl)-3-hydroxy-2-(3-methoxy-5-propionylphenoxy)propan-1-one (1%).

LMC 6 (50 mg, 0.14 mmol), TPPFeCl (0.95 mg, 0.0014 mmol), 70% aq soln of t-BuOOH (0.018 mL, 0.13 mmol), CH_3CN (0.5 mL) and 0.1N pH 3 phosphate buffer (1.5 mL) stirred at 25ºC for 14 h. The product was extracted with ethyl acetate and washed with saturated aq NaCl soln. The combined organic layers were dried over $MgSO_4$ and concentrated under vacuum. The products were chromatographically immobile.

3.3.2 Oxidation of benzylic hydroxyl groups my DDQ/$NaNO_2$

1. Catalytic aerobic oxidation of 3 with DDQ (0.01 eq), $NaNO_2$ (0.1 eq) at RT

LMC 3 (50 mg, 0.14 mmol), DDQ (0.32 mg, 0.0014 mmol), $NaNO_2$ (0.96 mg, 0.014 mmol), CH_2Cl_2 (1.8 mL) and acetic acid (0.2 mL) stirred under an O_2 atmosphere (1 atm) at 25 °C for 19 h. The product was extracted with ethyl acetate and washed with saturated aq NaCl soln. The combined organic layers were dried over $MgSO_4$ and concentrated under vacuum. The products were isolated using a preparative TLC plate to yield of LMC 3 (76%) and LMC 3' (23%).

2. Catalytic aerobic oxidation of 3 with DDQ (0.1 eq), $NaNO_2$ (1 eq) at RT

LMC 3 (50 mg, 0.14 mmol), DDQ (3.2 mg, 0.014 mmol), $NaNO_2$ (9.6 mg, 0.14 mmol), CH_2Cl_2 (1.8 mL) and acetic acid (0.2 mL) stirred under an O_2 atmosphere (1 atm) at 25 °C

for 19 h. The product was extracted with ethyl acetate and washed with saturated aq NaCl soln. The combined organic layers were dried over $MgSO_4$ and concentrated under vacuum. The products were isolated using a preparative TLC plate to yield of LMC 3 (32%) and LMC 3' (43%).

3. Catalytic aerobic oxidation of 3 with DDQ (1 eq), $NaNO_2$ (10 eq) at RT

LMC 3 (50 mg, 0.14 mmol), DDQ (32 mg, 0.14 mmol), $NaNO_2$ (96 mg, 1.4 mmol), CH_2Cl_2 (1.8 mL) and acetic acid (0.2 mL) stirred under an O_2 atmosphere (1 atm) at 25 °C for 19 h. The product was extracted with ethyl acetate and washed with saturated aq NaCl soln. The combined organic layers were dried over $MgSO_4$ and concentrated under vacuum. The products were isolated using a preparative TLC plate to yield of LMC 3' (69%).

4. Catalytic aerobic oxidation of 3 with DDQ (0.1 eq), $NaNO_2$ (1 eq) at 55°C

LMC 3 (50 mg, 0.14 mmol), DDQ (3.2 mg, 0.014 mmol), $NaNO_2$ (9.6 mg, 0.14 mmol), CH_2Cl_2 (1.8 mL) and acetic acid (0.2 mL) stirred under an O_2 atmosphere (1 atm) at 55 °C for 19 h. The product was extracted with ethyl acetate and washed with saturated aq NaCl soln. The combined organic layers were dried over $MgSO_4$ and concentrated under vacuum. The products were isolated using a preparative TLC plate to yield of LMC 3 (72%) and LMC 3' (22%).

5. Catalytic aerobic oxidation of 3 with DDQ (0.1 eq), $NaNO_2$ (1 eq) sonication at RT

LMC 3 (50 mg, 0.14 mmol), DDQ (0.32 mg, 0.0014 mmol), $NaNO_2$ (0.96 mg, 0.014 mmol), CH_2Cl_2 (1.8 mL) and acetic acid (0.2 mL) sonicated under an O_2 atmosphere (1 atm) at 25 °C for 19 h. The product was extracted with ethyl acetate and washed with saturated aq NaCl soln. The combined organic layers were dried over $MgSO_4$ and concentrated under vacuum. The products were isolated using a preparative TLC plate to yield of LMC 3 (54%) and LMC 3' (33%).

6. Catalytic aerobic oxidation of 1 with DDQ (0.01 eq), $NaNO_2$ (0.1 eq)

LMC 1 (50 mg, 0.25 mmol), DDQ (0.57 mg, 0.0025 mmol), $NaNO_2$ (1.74 mg, 0.025 mmol), CH_2Cl_2 (1.8 mL) and acetic acid (0.2 mL) stirred under an O_2 atmosphere (1 atm) at 25 °C for 19 h. The product was extracted with ethyl acetate and washed with saturated

aq NaCl soln. The combined organic layers were dried over $MgSO_4$ and concentrated under vacuum. The products were isolated using a preparative TLC plate to yield of LMC 1 (100%).

7. Catalytic aerobic oxidation of 2 with DDQ (0.01 eq), $NaNO_2$ (0.1 eq)

LMC 2 (50 mg, 0.2 mmol), DDQ (0.44 mg, 0.002 mmol), $NaNO_2$ (1.35 mg, 0.02 mmol), CH_2Cl_2 (1.8 mL) and acetic acid (0.2 mL) stirred under an O_2 atmosphere (1 atm) at 25 °C for 19 h. The product was extracted with ethyl acetate and washed with saturated aq NaCl soln. The combined organic layers were dried over $MgSO_4$ and concentrated under vacuum. The products were isolated using a preparative TLC plate to yield of LMC 2 (100%).

8. Catalytic aerobic oxidation of 3 with DDQ (0.1 eq), $NaNO_2$ (1 eq) for 44 hrs.

LMC 3 (50 mg, 0.14 mmol), DDQ (0.32 mg, 0.0014 mmol), $NaNO_2$ (0.96 mg, 0.014 mmol), CH_2Cl_2 (1.8 mL) and acetic acid (0.2 mL) stirred under an O_2 atmosphere (1 atm) at 25 °C for 44 h. The product was extracted with ethyl acetate and washed with saturated aq NaCl soln. The combined organic layers were dried over $MgSO_4$ and concentrated under vacuum. The products were isolated using a preparative TLC plate to yield of LMC 3 (76%) and LMC 3' (23%).

9. Catalytic aerobic oxidation of 4 with DDQ (0.01 eq), $NaNO_2$ (0.1 eq)

LMC 4 (41 mg, 0.12 mmol), DDQ (0.27 mg, 0.0012 mmol), $NaNO_2$ (0.82 mg, 0.012 mmol), CH_2Cl_2 (1.47 mL) and acetic acid (0.16 mL) stirred under an O_2 atmosphere (1 atm) at 25 °C for 19 h. The product was extracted with ethyl acetate and washed with saturated aq NaCl soln. The combined organic layers were dried over $MgSO_4$ and concentrated under vacuum. The products were isolated using a preparative TLC plate to yield of LMC 4 (48%) and LMC 4' (28%).

10. Catalytic aerobic oxidation of 4 with DDQ (0.1 eq), $NaNO_2$ (1 eq)

LMC 4 (25 mg, 0.072 mmol), DDQ (1.64 mg, 0.0072 mmol), $NaNO_2$ (5 mg, 0.072 mmol), CH_2Cl_2 (0.9 mL) and acetic acid (0.1 mL) stirred under an O_2 atmosphere (1 atm) at 25 °C for 19 h. The product was extracted with ethyl acetate and washed with saturated aq NaCl

soln. The combined organic layers were dried over $MgSO_4$ and concentrated under vacuum. The products were isolated using a preparative TLC plate to yield of LMC 4' (60%).

11. Catalytic aerobic oxidation of 5 with DDQ (0.01 eq), $NaNO_2$ (0.1 eq)

LMC 5 (50 mg, 0.13 mmol), DDQ (0.30 mg, 0.0013 mmol), $NaNO_2$ (0.92 mg, 0.013 mmol), CH_2Cl_2 (1.8 mL) and acetic acid (0.2 mL) stirred under an O_2 atmosphere (1 atm) at 25 °C for 19 h. The product was extracted with ethyl acetate and washed with saturated aq NaCl soln. The combined organic layers were dried over $MgSO_4$ and concentrated under vacuum. The products were isolated using a preparative TLC plate to yield of LMC 5 (59%) and LMC 5' (33%).

12. Catalytic aerobic oxidation of 6 with DDQ (0.01 eq), $NaNO_2$ (0.1 eq)

LMC 6 (50 mg, 0.14 mmol), DDQ (0.31 mg, 0.0014 mmol), $NaNO_2$ (0.95 mg, 0.014 mmol), CH_2Cl_2 (1.8 mL) and acetic acid (0.2 mL) stirred under an O_2 atmosphere (1 atm) at 25 °C for 19 h. The product was extracted with ethyl acetate and washed with saturated aq NaCl soln. The combined organic layers were dried over $MgSO_4$ and concentrated under vacuum. The products were isolated using a preparative TLC plate to yield of LMC 6 (40%) and LMC 6' (29%) and 2-(3-methoxy-5-propylphenoxy)-3-(4-hydrox-3-methoxyphenyl)-3-oxopropanal (5%).

3.3.3 Oxidation of benzylic hydroxyl groups my TEMPO/$NaNO_2$

LMC 1 (50 mg, 0.25 mmol), TEMPO (5.91 mg, 0.038 mmol), $NaNO_2$ (4.36 mg, 0.063 mmol), 36% aq HCl (10.38 μL, 0.125 mmol), NaCl (7.37 mg, 0.125 mmol) and CH_2Cl_2 (0.3 mL) stirred under an O_2 atmosphere (1 atm) at 25 °C for 14 h. The product was extracted with ethyl acetate. The organic layer was washed with saturated aqueous solution of $Na_2S_2O_3$, $NaHCO_3$ and then with the water. The combined organic layers were dried over $MgSO_4$ and concentrated under vacuum. The products were isolated using a preparative TLC plate to yield of LMC 1 (100%).

LMC 2 (50 mg, 0.2 mmol), TEMPO (4.57 mg, 0.03 mmol), NaNO$_2$ (3.37 mg, 0.05 mmol), 36% aq HCl (8.25 µL, 0.1 mmol), NaCl (5.7 mg, 0.1 mmol) and CH$_2$Cl$_2$ (0.3 mL) stirred under an O$_2$ atmosphere (1 atm) at 25 °C for 14 h The product was extracted with ethyl acetate. The organic layer was washed with saturated aqueous solution of Na$_2$S$_2$O$_3$, NaHCO$_3$ and then with the water. The combined organic layers were dried over MgSO$_4$ and concentrated under vacuum. The products were isolated using a preparative TLC plate to yield of LMC 2' (100%).

LMC 3 (50 mg, 0.14 mmol), TEMPO (3.2 mg, 0.021 mmol), NaNO$_2$ (2.4 mg, 0.035 mmol), 36% aq HCl (5.8 µL, 0.07 mmol), NaCl (4.06 mg, 0.07 mmol) and CH$_2$Cl$_2$ (0.3 mL) stirred under an O$_2$ atmosphere (1 atm) at 25 °C for 14 h. The product was extracted with ethyl acetate. The organic layer was washed with saturated aqueous solution of Na$_2$S$_2$O$_3$, NaHCO$_3$ and then with the water. The combined organic layers were dried over MgSO$_4$ and concentrated under vacuum. The products were isolated using a preparative TLC plate to yield of LMC 3' (81%).

LMC 4 (25 mg, 0.072 mmol), TEMPO (1.69 mg, 0.011 mmol), NaNO$_2$ (1.25 mg, 0.018 mmol), 36% aq HCl (3.24 µL, 0.036 mmol), NaCl (2.1 mg, 0.036 mmol) and CH$_2$Cl$_2$ (0.15 mL) stirred under an O$_2$ atmosphere (1 atm) at 25 °C for 14 h. The product was extracted with ethyl acetate. The organic layer was washed with saturated aqueous solution of Na$_2$S$_2$O$_3$, NaHCO$_3$ and then with the water. The combined organic layers were dried over MgSO$_4$ and concentrated under vacuum. The products were chromatographically immobile.

LMC 5 (50 mg, 0.13 mmol), TEMPO (3.11 mg, 0.02 mmol), NaNO$_2$ (2.29 mg, 0.033 mmol), 36% aq HCl (5.5 µL, 0.065 mmol), NaCl (3.89 mg, 0.067 mmol) and CH$_2$Cl$_2$ (0.3 mL) stirred under an O$_2$ atmosphere (1 atm) at 25 °C for 14 h. The product was extracted with ethyl acetate. The organic layer was washed with saturated aqueous solution of Na$_2$S$_2$O$_3$, NaHCO$_3$ and then with the water. The combined organic layers were dried over MgSO$_4$ and concentrated under vacuum. The products were isolated using a preparative TLC plate to yield of LMC 5' (80%).

LMC 6 (30 mg, 0.083 mmol), TEMPO (1.94 mg, 0.012 mmol), NaNO$_2$ (1.43 mg, 0.021 mmol), 36% aq HCl (3.4 µL, 0.042 mmol), NaCl (2.42 mg, 0.041 mmol) and CH$_2$Cl$_2$ (0.18

mL) stirred under an O_2 atmosphere (1 atm) at 25 °C for 14 h. The product was extracted with ethyl acetate. The organic layer was washed with saturated aqueous solution of $Na_2S_2O_3$, $NaHCO_3$ and then with the water. The combined organic layers were dried over $MgSO_4$ and concentrated under vacuum. The products were chromatographically immobile.

3.3.4 Baeyer-Villiger Oxidations

LMC 2' (50 mg, 0.2 mmol), 30% aq H_2O_2 (0.16 mL, 1.55 mmol), HCOOH (0.06 mL, 1.6 mmol) and 1, 2–dichloroethane (0.062 mL, 0.8 mmol) was refluxed at 50 °C for 24 h. The product was extracted with ethyl acetate, the organic layer was dried over $MgSO_4$ and concentrated under vacuum. The products were isolated using a preparative TLC plate to yield LMC 2' (90%) and (3-propylphenoxy)methyl benzoate (10%).

LMC 3' (50 mg, 0.14 mmol), 30% aq H_2O_2 (0.14 mL, 1.12 mmol), HCOOH (0.042 mL, 1.12 mmol) and 1, 2–dichloroethane (0.044 mL, 0.56 mmol) was refluxed at 50 °C for 24 h. The product was extracted with ethyl acetate, the organic layer was dried over $MgSO_4$ and concentrated under vacuum. The products were isolated using a preparative TLC plate to yield 3,4-dimethoxybenzoic acid (81%).

LMC 4'-P (132.2 mg, 0.305 mmol), 30% aq H_2O_2 (0.244 mL, 2.44 mmol), HCOOH (0.092 mL, 2.44 mmol) and 1, 2–dichloroethane (0.096 mL, 1.21 mmol) was refluxed at 50 °C for 24 h. The product was extracted with ethyl acetate, the organic layer was dried over $MgSO_4$ and concentrated under vacuum. The products were isolated using a preparative TLC plate to yield 4-benzyloxy-3-methoxybenzoicacid (80%).

LMC 5' (69 mg, 0.18 mmol), 30% aq H_2O_2 (0.15 mL, 1.46 mmol), HCOOH (0.056 mL, 1.48 mmol) and 1, 2–dichloroethane (0.06 mL, 0.76 mmol) was refluxed at 50 °C for 24 h. The product was extracted with ethyl acetate, the organic layer was dried over $MgSO_4$ and concentrated under vacuum. The products were isolated using a preparative TLC plate to yield 3,4-dimethoxybenzoic acid (40%).

LMC 6'-P (19 mg, 0.042 mmol), 30% aq H_2O_2 (0.0383 mL, 0.38 mmol), HCOOH (0.0155 mL, 0.344 mmol) and 1, 2–dichloroethane (0.0132 mL, 0.167 mmol) was refluxed at 50 °C for 24 h. The product was extracted with ethyl acetate, the organic layer was dried over $MgSO_4$ and concentrated under vacuum. The products were isolated using a preparative TLC plate to yield 4-benzyloxy-3-methoxybenzoicacid (80%).

3.4   Analytical methods and chemicals

^{1}H and ^{13}C NMR spectra were recorded on a Varian Inova 400MHz spectrometer. Gas chromatography-mass spectra (GC-MS) were recorded on a Agilent technologies 6890N instrument with 5973N electron impact ionization (EI) mass detector. Dry THF, diethyl ether, DMF and dichloromethane were purchased from Sigma-Aldrich. All other bulk solvent were purchased from Pharmco Aaper and used without further purification. Silica gel thin layer chromatography (TLC) plates (w/UV254, polyester backed, 200μm) were purchased from Sorbent technologies. Flash column chromatography was carried out with silica gel (60 Å) purchased from Sorbent technology. All reagents were purchased from commercial suppliers and used without further purification.

CHAPTER 4. DEPOLYMERIZATION OF ORGANOSOLV LIGNIN

4.1   Introduction

In the Organosolv pulping technique, lignin is extracted by dissolving it in organic solvent. The solid residue remains enriches with cellulose, whereas liquor contains degraded lignin free from sulphur. Later organosolv lignin is obtained by removing solvent from liquor by distillation. This solubilized form of lignin is prepared by treatment of lignocellulosic biomass with an aqueous organic solvent, usually methanol, ethanol, butanol, acetone, ethylene glycol or ethanolamine at elevated temperatures (≥140 °C), sometimes in the presence of inorganic acid catalysts.[162,163] In catalytic pulping processes, added reagents change the pH of the liquor. The base-catalyzed Organosolv process involves two stages: in the first-stage, lignocellulose biomass is cooked in 50% methanol/water solution, and then in the second stage the pulping mixture is basified by adding sodium hydroxide.[164] The alkali-sulfite-anthraquinone-methanol (ASAM) Organosolv is more is advance method.[164,165] In ASAM process, methanol and anthraquinone are added to alkaline sulphite liquor pulp. The methanol that is used as the organic solvent is completely recovered at the end of the process. The organosolv pulp obtained from this method has better optical (brightness) and strength properties than other conventional processes.[165] These pulping methods are superior to other pulping processes, and currently they are extensively used on large scales. The alkaline ethanol pulping process has been patented by Marton and co-workers, and according to their findings a mixture of ethanol and sodium hydroxide at elevated temperatures can be used for pulping of any type of wood.[166] Similarly, the use of other alcohols such as propanol, isopropanol, butanol and ethylene glycols have also reported in literature.[167] Methanol and ethanol are the preferred solvents, as they have lower boiling points and are less expensive than glycol. Some less common solvents that were also used include ethylacetate, ethylenediamine, methylamine, acetone and dioxane. The Acetosolv, Fomacell and Milox processes are acidic pulping processes, and they have also proven to be very effective methods. The Acetosolv pulping process is catalyzed by acetic acid and hydrochloric acid, the Fromocell process is catalyzed by

formic acid/acetic acid, and Milox pulping is performed by adding formic acid and hydrogen peroxide.[168,169]

In order to transfer our synthetic approach from a model molecule study to native lignin, an Organosolv lignin was employed in our depolymerization studies. This lignin is soluble in many commonly used polar solvents, making it a convenient substrate for lignin reactivity studies. The study of lignin depolymerization using organosolv lignin has many advantages over the use of another lignins. Organosolv lignin is soluble in several organic solvents, and homogeneous reactions process have advantages over heterogeneous processes, including an increase in activity, selectivity, and higher rapid mass transfer rates. In addition, analytical techniques such as NMR and GPC can be more conveniently used for soluble lignin polymers. Recently, many researchers have demonstrated catalytic depolymerization of Organosolv lignin into low molecular weight aromatic compounds. Lercher and co-workers have demonstrated the disassembly of Organosolv lignin by a base-catalyzed high temperature/high pressure reactions. Jones et al. reported depolymerization and hydrodeoxygenation of Organosolv lignin via formic acid and Pt/C treatment.[170] Another group showed an improved approach to hydrodeoxygenation of lignin by bimetallic Pd/C and Zn catalytic system.[171] Labidi et al. reported a method for producing phenolic compounds by microwave irradiation of lignin using a nickel-based catalyst.[172] Ford and group have showed the depolymerization of organosolv lignin using a copper-doped porous metal oxides in presence of methanol.[57]

Lignin seem to have large reactive plethora of functional groups. In all of the methods above, the fragmentation of lignin was not selective, which results in randomly fragmented products. Based on the product formed, many researchers have proposed fragmentation mechanisms,[173,174] however, changes in functional groups in the lignin polymer during depolymerization have not been characterized. Unambiguously, we have investigated step-wise specific oxidation reaction, which will react selectively. We have carefully characterized changes in functionality in each step of an oxidation, to ensure how each oxidation step proceeds and what all side products formed.

4.2   Protection phenolic hydroxyl group

^{31}P NMR spectroscopy is a valuable tool for the quantitative determination of hydroxyl groups present in lignin.[175,176] This technique is based upon phosphorus labeling of the hydroxyl groups present in lignin, and observation of the well-resolved resonances of ^{31}P-derivatized aliphatic, phenolic, and carboxylic acid hydroxyl groups, which can be further quantified using an internal standard. Hence, this method can be used to determine how well each step in the oxidation sequence has worked. Faix *et al.* have demonstrated that the hydroxyl groups determine by ^{31}P NMR correlate with other techniques such as ^{1}H NMR, [31]C NMR and FTIR spectroscopy, as well as wet chemical methods.[24] As previous reported by Argyropoulos, 2-chlor-1,3,2-dioxaphospholane is not universally effective in determination of hydroxyl group in lignin.[176] On other hand slight modified phosphitylation reagent, 2-chloro-4,4,5,5-tetramethyl-1,3,2-dioxaphospholane was more stable because of four methyl groups. Even though this reagent doesn't properly separate primary and secondary alcohol group, it is highly reliable.   The proportions of NMR solvent were kept constant 1.6:1 pyridine/$CDCl_3$ throughout depolymerization analysis, as it is reported that change in pyridine/$CDCl_3$ proportion may results in broadening of peaks because of solvent effect.[177] It is important to note that ^{31}P isotopes has 100% abundance, spin of ½ and magnetogyric ratio is relatively high. Because of all these reasons ^{31}P NMR spectroscopy is highly sensitive, and it is a rapid analytical method. Lately, ^{31}P NMR technique has been routinely used to study chemistry of biomass, biofuels and lignin.

The derivatizing agent (Figure 4.1) is prepared from pinacol, PCl_3 and NH_3 according to literature procedures.[24,175,176] PCl_3 (11.09 mL, 0.127 mol) in dry ether (35 mL) -THF (10 mL) was stirred at 0 °C for 5 mins. A solution NH_3 (35.4 mL, 0.254 mol) and pinacol (15 g, 0.127 mol) in dry ether (35 mL) -THF (11 mL) was added dropwise over 1 hrs, and the reaction mixture was stirred for 2 hrs at room temperature. The reaction was then filtered, to remove triethylamine hydrochloride. The residue was washed with ether, and then combine filtrate was concentrated under vacuum. The product was purified by vacuum-distillation above 180 °C to obtained 30% yield.[178]
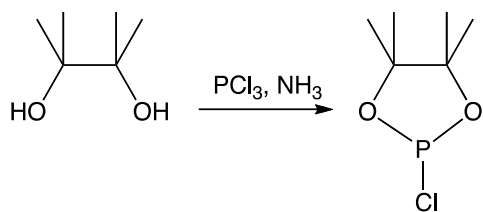
Figure 4. 1 Synthesis of 2-chloro-4,4,5,5-tetramethyl-1,3,2-dioxaphospholane (TMDP).

As previous reported,[175,176] Organosolv lignin (50 mg, ball-milled) was placed in a 1 mL volumetric flask. 100 μL of 0.1N benzoic acid solution (in 1.6:1 pyridine-d_6:CDCl3), 50 μL 2-chloro-4, 4, 5, 5-tetramethyl-1, 3, 2-dioxaphospholane (**7**), and 100 μL of a 0.01N solution of chromium (III) acetylacetonate (in 1.6:1 pyridine-d_6:CDCl$_3$) were added to the flask. The flask contents were diluted to 1.0 mL with 1.6:1 pyridine-d_6:CDCl$_3$.[176] ^{31}P NMR spectra were recorded at 25 °C on a 400 MHz (^{1}H frequency) spectrometer, using a previously reported method.[176] Our typical instrument setup involved a 90° ^{31}P pulse, 7.75 μs observation pulse, 0.919 s acquisition time and 12 s relaxation delay.
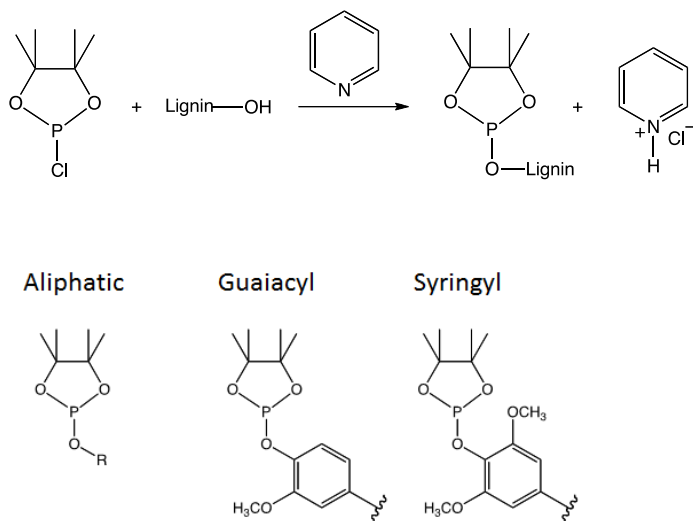
Figure 4. 2 Schematic representation of phosphitylation of hydroxyl group.

Quantitative phosphorous group derivatization of hydroxyl groups in lignin occurs by reaction between lignin and TMDP/ pyridine. Pyridine reacts with the HCl that is formed, to give pyridine hydrochloride.

72
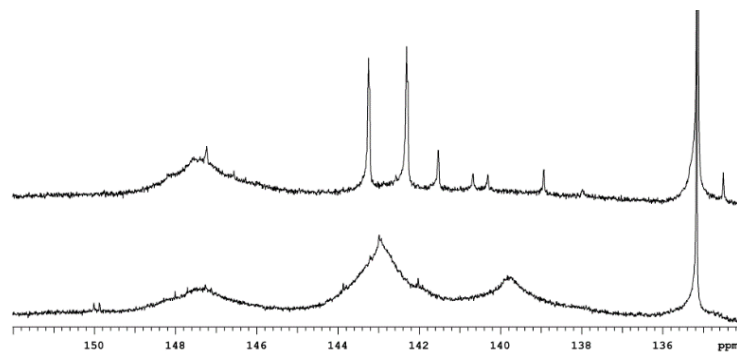
Figure 4. 3 Quantitative ^{31}P NMR spectra native Organosolv lignin and after hydroxyl group protection using benzyl bromide.

The ^{31}P spectra of derivatizated untreated Organosolv lignin has resonances between δ 151 to 134 ppm. This was consistent with literature reports for phosphorus-labeled aliphatic, phenolic (syringyl), phenolic (guaiacyl), and carboxylic hydroxyls. Addition of a known amount of benzoic acid prior to derivatization enabled quantification of these groups. The ^{31}P spectrum of TMCP-labeled Organosolv lignin (without previous addition of benzoic acid) shows no resonances between 137-134 ppm. The quantitative ^{31}P NMR spectrum in Fig. 8(a) shows 4 distinct peaks. The region between 149 to 145 ppm corresponds to aliphatic hydroxyl groups, the region between 145 to 141 ppm corresponds to syringyl phenolic hydroxyl groups, the region between 141 to 138 ppm corresponds to guaiacyl disubstituted phenolic hydroxyl groups and the sharp peak at 135.14 ppm corresponds to carboxylic hydroxyl groups.
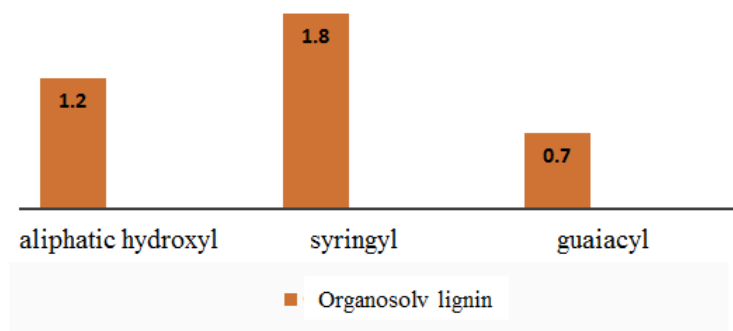
After comparing mmol g^{-1} of the hydroxyl group of Organosolv lignin (insoluble in water) with internal standard (benzoic acid), we found 1.2 mmol g^{-1} aliphatic hydroxyl group, 1.8

mmol g^{-1} syringyl phenolic hydroxyl group and 0.7 mmol g^{-1} guaiacyl phenolic hydroxyl group contained.

Our aim was to protect both phenolic hydroxyl groups selectively without protecting aliphatic hydroxyl group. In this study we tried various protecting groups like methyl, acyl and benzyl using different base and reaction conditions. And then organosolv lignin after protection of phenolic hydroxyl group was characterized by ^{31}P NMR spectroscopy. The protection group study result are as follow.

Protection of phenolic hydroxyl group using Me$_2$SO$_4$ and KOH: 50 mg of ball-milled organosolv lignin was dissolved in 3 mL solvent-1,2-dimethoxyethane, methanol, water (35:35:3, v/v). Dimethylsulphate was added to reaction mixture and then 15% KOH solution in the above solvent mixture was added to the reaction mixture under N$_2$ using additional funnel, and the addition rate was regulated to maintain the pH of the reaction at 11. Addition of KOH was stopped when the pH of the reaction mixture remained constant at pH 11. The reaction mixture was stirred further for 24 hrs at room temperature. The pH of the mixture was lowered to 3 by adding 0.5 M H$_3$PO$_4$, and after 30 minutes KOH was added again to adjust the pH to 6.5. The mixture was concentrated in vacuum. The product was washed with water and dried in vacuum oven.
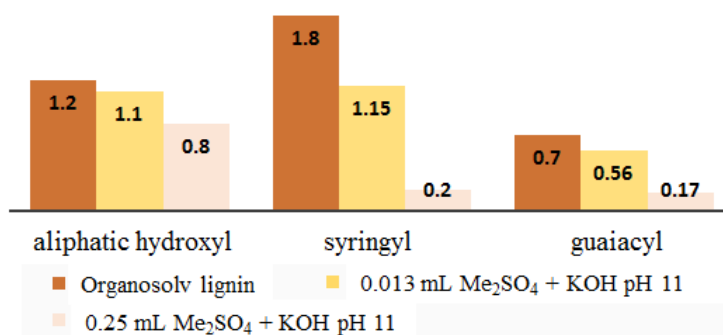
Figure 4. 4 Comparison of hydroxyl group content of organosolv lignin after Me$_2$SO$_4$/KOH protection of hydroxyl groups.

As shown in figure 4.3, 0.013 mL of Me$_2$SO$_4$ didn't lower the phenolic hydroxyl content, while similarly 0.25 mL of Me$_2$SO$_4$ significantly reduced the number of phenolic hydroxyl groups, although some of the aliphatic hydroxyl groups were also getting protected.

Protection of phenolic hydroxyl group using acetic anhydride and pyridine: A solution of 50 mg ball-milled organosolv lignin, pyridine was stirred in dry CH_2Cl_2 for 1hrs at ambient temperature. Acetic anhydride was added, and the mixture was then stirred at ambient temperature for 16 h. The mixture was concentrated in vacuum. The product was washed with water and dried in vacuum oven.
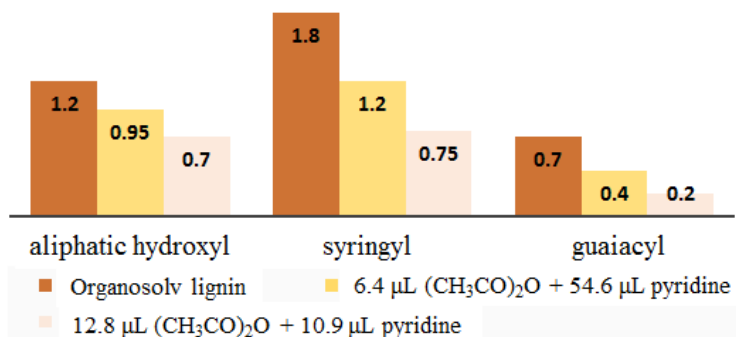
Figure 4. 5 Comparison of hydroxyl group content in organosolv lignin after $(CH_3CO)_2O$/pyridine protection of hydroxyl groups.

Acylation doesn't selectively protects phenolic hydroxyl group; aliphatic hydroxyl groups were also getting protected, i.e. in both the reaction conditions phenolic hydroxyl group contained is simultaneous get protected.

Protection of phenolic hydroxyl group using Me_2SO_4 and Et_3N: A solution of 50 mg ball-milled organosolv lignin and Et_3N in dry acetone was stirred for 5 mins at ambient temperature. Me_2SO_4 was added, and the mixture was then stirred at ambient temperature for 20 h. The mixture was concentrated in vacuum. The product was washed with water and dried in vacuum oven.
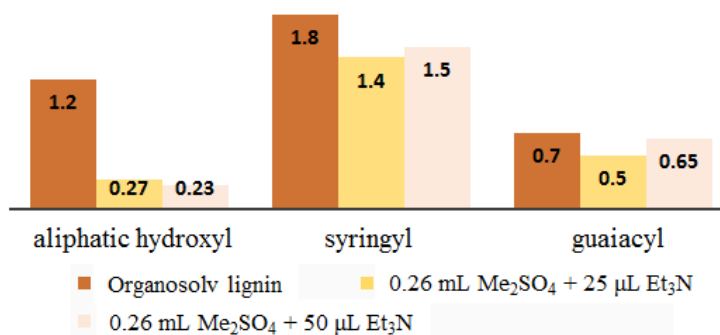
Figure 4. 6 Comparison of hydroxyl group content in organosolv lignin after Me_2SO_4/Et_3N protection of hydroxyl groups.

Protection of hydroxyl group with Me_2SO_4/Et_3N was not very useful, as methylation of alipahtic hydroxyl groups occurs to a considerable extent.

Protection of phenolic hydroxyl group using benzyl bromide (BnBr) and K_2CO_3: 50 mg ball-milled organosolv lignin, benzyl bromide and K_2CO_3 was reflux at 65°C for 5hrs in the presence of 13.6 ml acetone. The mixture was concentrated in vacuum. The product was washed with water and dried in vacuum oven.
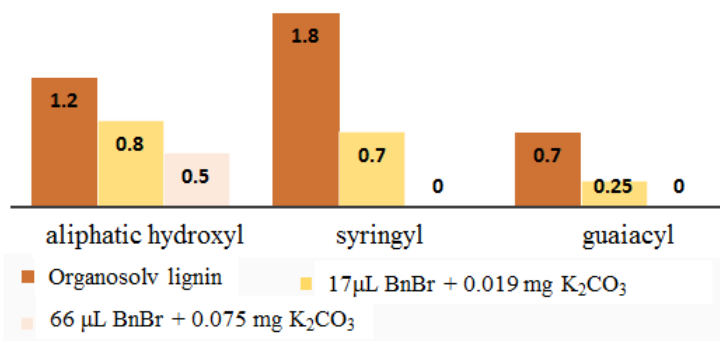
Figure 4. 7 Comparison of hydroxyl group content in organosolv lignin after $BnBr/K_2CO_3$ protection of hydroxyl groups

Figure 4.7 illustrate that benzyl bromide protection under condition 2 completely protects phenolic hydroxyl group. However, more than half aliphatic hydroxyl groups were also protected. Various attempts to selectively protect phenolic hydroxyl group were not completely successful. So far benzyl bromide protection were best, but further investigation is required.

76

4.3 Study of Organosolv lignin depolymerization using TEMPO/NaNO$_2$

Through the model studies reported above, we identified reagents suitable for the three steps required for cleavage of the β-O-4 linkage in lignin. The first two steps are oxidations (benzylic alcohol oxidation, then Baeyer-Villiger oxidation) and require the protection of the phenolic hydroxyl group to prevent oxidative coupling of phenols. While the success of the protection step and the oxidation steps was easy to monitor when working with small-molecule models, characterization is a significant challenge when working with lignin, even with a solubilized version such as Organosolv lignin.

Benzylation of Organosolv lignin: Organosolv lignin (0.725 g) and K$_2$CO$_3$ (0.558 g, 4.04 mmol) were stirred in acetone (32 mL). Benzyl bromide (0.96 mL, 8.07 mmol) was added to the reaction mixture which was refluxed for 14 h. The mixture was concentrated in vacuum. The product was refluxed in hexane for 15 min. The reaction mixture was the filtered, washed with water and dried in vacuum oven to yield benzylated Organosolv lignin 0.7 g.

Oxidation benzyl hydroxyl group Organosolv lignin using TEMPO/NaNO$_2$: Benzylated Organosolv lignin (0.45 g), TEMPO (29.25 mg, 0.188 mmol), NaNO$_2$ (21.56 mg, 0.312 mmol), 36% aq HCl (57.61 µL, 0.64 mmol), NaCl (36.56 mg, 0.62 mmol) and CH$_2$Cl$_2$ (2.7 mL) stirred under an O$_2$ atmosphere (1 atm) at 25 °C for 14 h. The mixture was concentrated in vacuum. The product was washed with water, filtered and dried in vacuum oven to yield 0.4 g product.

Baeyer-Villiger oxidation of TEMPO oxidized Organosolv lignin: TEMPO oxidized Organosolv lignin (0.18 g), 30% aq H$_2$O$_2$ (0.45 mL, 4.41 mmol), HCOOH (0.184 mL, 4.9 mmol) and 1, 2–dichloroethane (1.56 mL, 19.9 mmol) was refluxed at 50 °C for 24 h. The mixture was concentrated in vacuum to yield 0.15 g product.

4.3.1 ^{31}P NMR spectroscopy
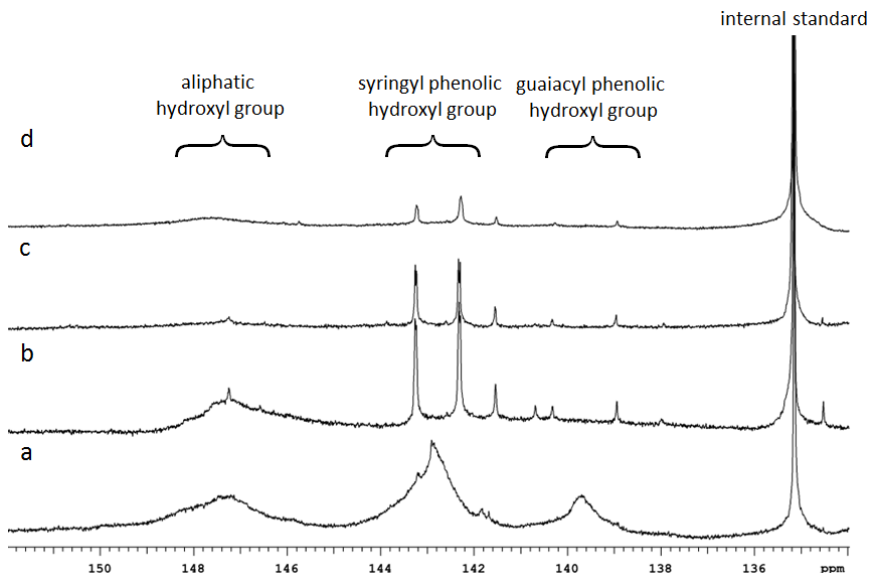
Figure 4. 8 Quantitative ^{31}P NMR spectra: (a) native Organosolv lignin; (b) after hydroxyl group protection using benzyl bromide; (c) after hydroxyl group oxidation using TEMPO/NaNO$_2$; (d) after Baeyer-Villiger oxidation using H$_2$O$_2$/ HCOOH.

The spectrum shown in figure. 4.8(b) clearly shows that the number of phenolic hydroxyl groups diminished after selective protection of phenolic hydroxyl groups via benzylation. Moreover, the spectrum in figure. 4.8(c) demonstrates that the resonance due to phosphorous-derivatized aliphatic hydroxyl groups diminished after TEMPO/ NaNO$_2$ oxidation of benzyl-protected Organosolv lignin. Finally, the spectrum in figure 4.8(d) indicates that Baeyer-Villiger oxidation of TEMPO/NaNO$_2$ oxidized Organosolv lignin resulted in an increased number of aliphatic hydroxyl groups, as expected when the esters that are formed in the Baeyer-Villiger step are hydrolyzed *in situ* by the highly acidic reaction conditions.

4.3.2 ATR-IR spectroscopy

Fourier transform infrared (FTIR) spectroscopy has been widely used for routine investigations of structural modifications in lignin.[179-182] FT-IR can be used for rapid characterization of changes in functional groups of solid as well as liquid samples. Emandi et al. reported the quantitative analysis of the ratio of lignin to cellulose and to

hemicellulose in fifteen different wood species by coupling integrated FT-IR spectroscopy with thermogravimetric (TGA) analysis.[183] FT-IR spectroscopy has been used to study the degradation of lignin caused by white rot fungus in wheat straw.[184] Another group studied the degradation of beech wood using FT-IR spectroscopy and pyrolysis gas chromatography.[179] Consequently, we compared the spectrum of native Organosolv lignin with the modified lignin after each oxidation step. The peaks present in the FTIR spectrum of Organosolv lignin are in accordance with their expected literature values.[181] IR spectra were recorded with a Nicolet 6700 FT-IR apparatus. The scanning was typically in the range 600 to 4000 cm^{-1} at a resolution of 4 cm^{-1}. Sixty-four scans were taken. Baseline correction was done using a three point linear approach at 3700 cm^{-1}, 1850 cm^{-1} and 670 cm^{-1} using previously reported method.[179-182]

The Organosolv lignin spectrum in figure 4.9 shows a broad absorption band between 3300 and 3500 cm^{-1} corresponding to phenolic and aliphatic hydroxyl groups, a band at 3000-2850 cm^{-1} which corresponds to sp^3 C-H bonds, and bands at 1710 and 1670 cm^{-1} corresponding to carbonyl groups. Other assignments are the sp^2 C=C vibration at 1587, 1512 cm^{-1}, C-H bending at 1458, 14224 cm^{-1} and peaks between 1100-1300 cm^{-1} which belong to characteristic C-O vibration bands.[179-182]
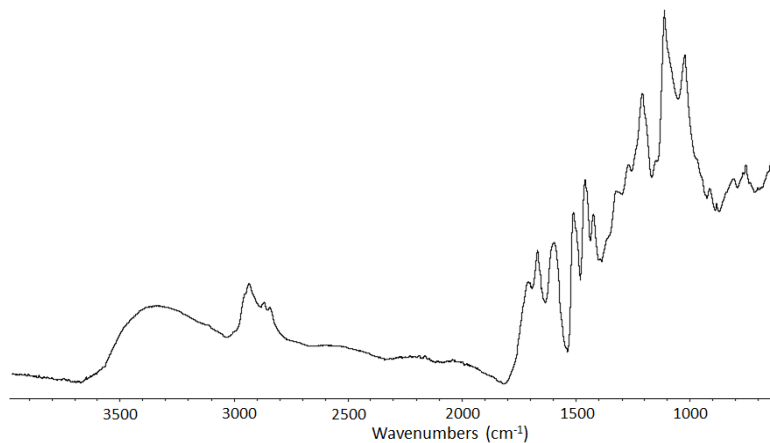
Figure 4. 9 FTIR spectra of the Organosolv lignin

Faix et al. have reported a method to determine carbonyl group content in lignin by correlating the intensity of the carbonyl IR peak with the aromatic absorption band.[180] We monitored the relative changes in carbonyl content in the sequence of oxidation reactions

by comparing the intensity of the carbonyl peak with the absorbance at 1587 cm^{-1} due to the aromatic rings. As shown in figure 4.10(b), the relative intensity of the aromatic peak at 1587 cm^{-1} increased after phenolic hydroxyl groups were protected via benzylation, while the intensity of the hydroxyl band between 3300 and 3500 cm^{-1} was significantly decreased. Figure 4.10(c) shows that little change in the relative intensity of the carbonyl peak took place after TEMPO oxidation, while for the last step (Figure 4.10(d)) a broad intense peak corresponding to carboxylic acids or esters was evident after Baeyer-Villiger oxidation.
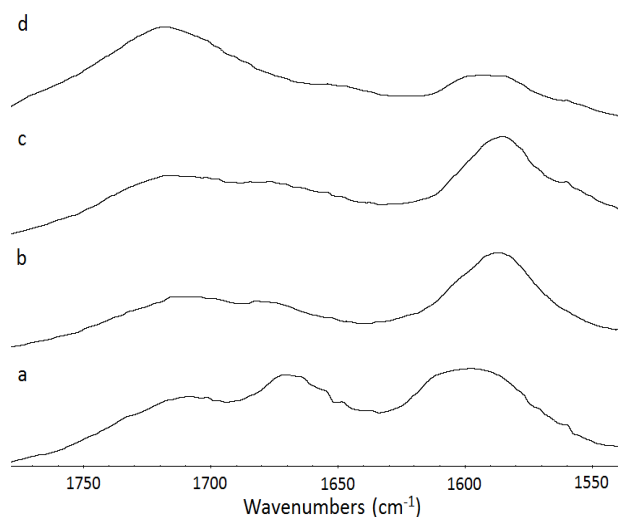
Figure 4. 10 FTIR spectra tracking the oxidative depolymerization of Organosolv lignin: (a) native Organosolv lignin; (b) hydroxyl group protection using benzyl bromide; (c) benzyl hydroxyl group oxidation using TEMPO/NaNO$_2$; (d) after Baeyer-Villiger oxidation using H$_2$O$_2$/ HCOOH

4.3.3 Gel permeation chromatography (GPC)

Analysis of the molecular weight distribution of Organosolv lignin after each oxidation step was achieved using gel permeation chromatography (GPC). Gel permeation chromatography (GPC) is a common analytical technique for the characterization of polymers. It is size exclusion chromatography (SEC) where the separation of polymers is based upon the hydrodynamic size of polymer molecules and the pore size of the column packing material. As lignin is a cross-linked polymer, we were not able to correlate elution time with the common internal standard (a linear polymer) used for molecular weight

distribution. We used GPC to detect changes in the elution time of untreated organosolv lignin to oxidized depolymerized lignin.

As reported in the literature, Organosolv lignin typically shows a bimodal molecular weight distribution,[185] the peak at higher retention time corresponding lower molecular lignin. Gel permeation chromatography (GPC) was performed on an Agilent 1260 Infinity Quaternary LC system equipped with a Polymer Standards Services (PSS) Suprema Linear S column (8 X 300 mm and a Suprema GPC Analytical Guard Column (8 X 50 mm), both of which had a 10µm particle size) and a DAD at 280nm. The mobile phase was 1:1 mixture of DMSO and THF at a flow of 0.6 mL/min. DMSO and THF, whose Hildebrand solubility parameters are 24.5 MPa$^{1/2}$ and 18.6 MPa$^{1/2}$ respectively, were chosen as solvents as they provided a good match for lignin (20-29 MPa$^{1/2}$).[186] It is important to note that GPC was only monitored on the soluble fraction of lignin. The typical sample size was 6 mg/mL of DMSO/THF. All chromatograms were normalized to their largest peak intensity to demonstrate molecular weight shifts. Lignin model compound 2 (LMC 2) was used as a point of reference.
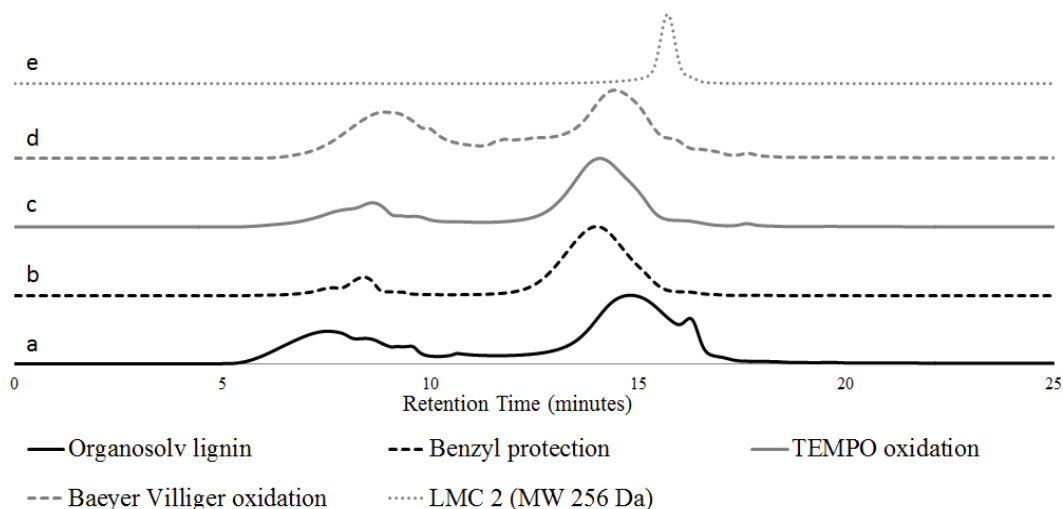
Figure 4. 11 Gel permeation chromatograms of Organosolv lignin subjected to oxidative depolymerization

Figures 4.11(a) and (b) show that after phenolic hydroxyl group protection, the molecular weight distribution of lignin shifted to slightly higher molecular weight. For molecular weight comparison lignin model compound 2 (LMC 2), which has a molecular weight of

256 Da, was displayed in Figure 4.11(e). In contrast, after TEMPO/NaNO$_2$ oxidation of the protected lignin, the molecular weight was not changed. After Baeyer-Villiger oxidation a slight shift towards lower molecular weight was observed, although the molecular weight distribution of the product was not significantly different from that of the initial Organosolv lignin starting material. This finding is likely due to a shift in the solubility of the lignin. While Organosolv lignin is highly soluble in DMSO/THF, benzylic oxidation resulted in a large insoluble fraction. However, after Baeyer-Villiger oxidation the sample was almost entirely soluble again. Thus GPC may not accurately portray the lignin depolymerization process and other analysis techniques are necessary to determine the degree of depolymerization.

4.4   Study of Organosolv lignin depolymerization using Swern oxidation

In order for our approach to depolymerization to be successful, we needed to ensure that the Baeyer-Villiger step is effective at introducing hydrolysable linkages into lignin. We turned to the Swern oxidation, a non-catalytic (but highly reliable) alcohol-to-ketone oxidation, so that the starting material for the Baeyer-Villiger step would have the maximum possible number of opportunities for oxidation of benzylic carbonyl groups.

Swern oxidation of Organosolv lignin: Oxalyl chloride (0.3 mL, 3.5 mmol), DMSO (0.5 mL, 7 mmol) and Organosolv lignin (soluble in water) (0.25 g) were placed in 3 individual one-neck round bottom flasks. The flasks were purged with N$_2$ for 15 min after which 11 ml dry CH$_2$Cl$_2$ was added to each flask. The solution of oxalyl chloride in CH$_2$Cl$_2$ was cooled to -78 °C and the solution of DMSO was added dropwise. The mixture was stirred to -78 °C for 15 min and then the Organosolv lignin solution was added dropwise. The resulting mixture was stirred at -40 °C and after 30 min the mixture was cooled to -78 °C and Et$_3$N (1.46 mL, 10.5 mmol) was added dropwise. The reaction was stirred 30 min at -78 °C then slowly allowed to warm to rt. CH$_2$Cl$_2$ (150 mL) was added and organic phase was washed with dilute HCl, water and concentrated under vacuum to yield 0.23 g product.[187]

<u>Baeyer Villiger oxidation of Swern oxidized Organosolv lignin</u>: Swern oxidized Organosolv lignin (0.1g), 30% aq H_2O_2 (0.22 mL, 2.22 mmol), HCOOH (0.084 mL, 2.22 mmol) and 1, 2–dichloroethane (0.348 mL, 4.35 mmol) was refluxed at 50 °C for 24 h. The reaction mixture was concentrated in vacuum to yield 0.092 g product.

4.4.1 ^{31}P NMR spectroscopy

This material also provided a useful reference material for comparison with the material produced by TEMPO oxidation of Organosolv lignin. After Swern oxidation of the Organosolv lignin, resonances due to ^{31}P-labeled aliphatic hydroxyl groups disappear from the quantitative ^{31}P NMR spectrum (Figure 4.12). The spectrum obtained after Baeyer-Villiger oxidation of the Swern-oxidized Organosolv lignin (Figure 4.12(c)) shows that new hydroxyl groups are formed, suggesting that after Baeyer-Villiger oxidation, hydrolysis of the new formed ester occurs and produces carboxylic acids and aliphatic hydroxyl groups.
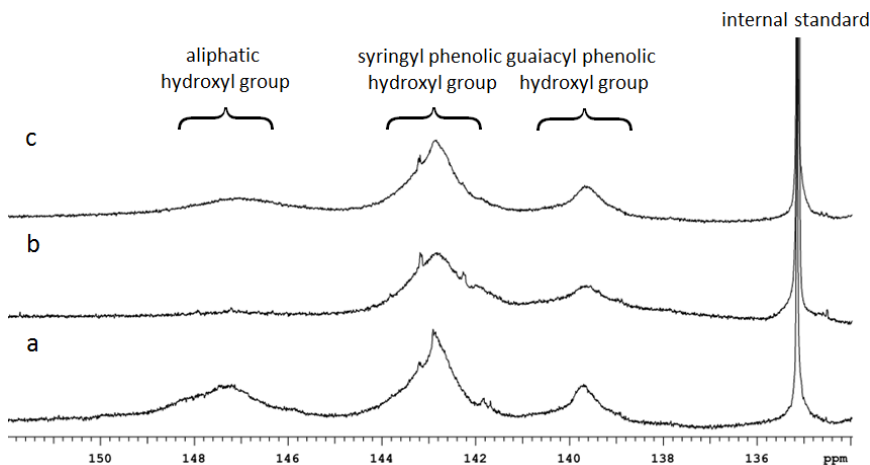
Figure 4. 12 Quantitative ^{31}P NMR spectra of the (a) native Organosolv lignin; (b) product obtained from Swern oxidation of native Organosolv lignin; (c) product obtained from Baeyer-Villiger oxidation using H_2O_2/HCOOH of Swern-oxidized Organosolv lignin.

4.4.2. ATR-IR spectroscopy
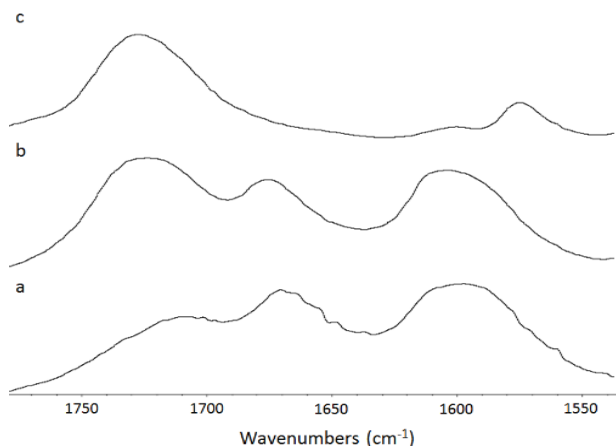
Figure 4. 13 FTIR spectra of Organosolv lignin subjected to oxidative depolymerization: (a) native Organosolv lignin; (b) Swern oxidation of native Organosolv lignin; (c) Baeyer-Villiger oxidation using H_2O_2/HCOOH of Swern-oxidized Organosolv lignin.

As shown in figure 4.13(b), the intensity of the carbonyl band at ca. 1710 cm^{-1} increased after Swern oxidation, while after Baeyer-Villiger oxidation (Figure 4.13(c)) a broad intense band corresponding to carboxylic acids or esters developed. The IR spectra demonstrate that after each step of the reaction, noticeable changes were observed that correspond to the expected outcome of selective oxidatively depolymerized lignin.

4.4.3 Gel permeation chromatography (GPC)
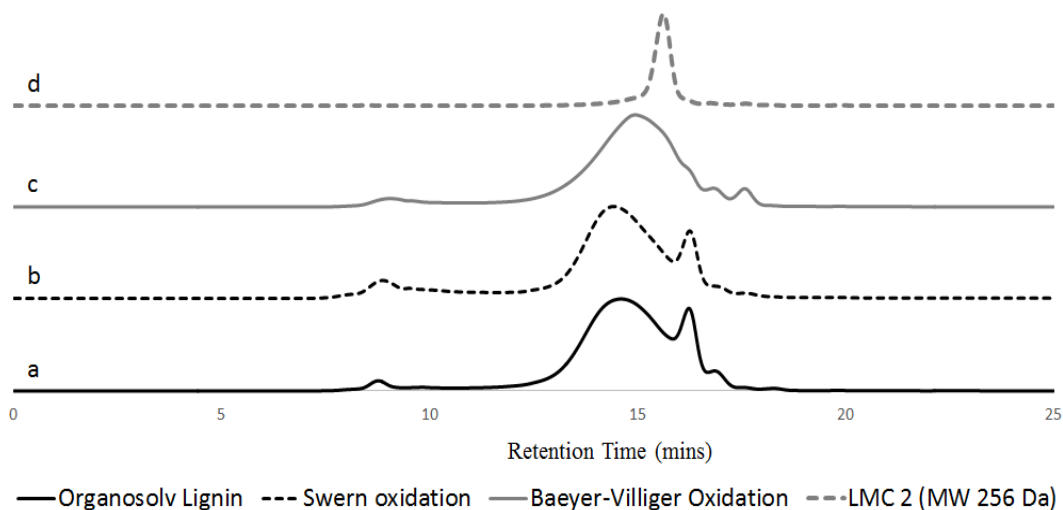
Figure 4. 14 Gel permeation chromatograms of Organosolv lignin subjected to oxidative depolymerization. Note: Chromatogram (a) corresponds to the Organosolv lignin CH_2Cl_2-soluble portion.

After Swern oxidation, the molecular weight distribution of the Organosolv lignin remained unchanged, as shown in figure 4.14(a). However, noticeable changes were observed after Baeyer-Villiger oxidation of the Swern-oxidized Organosolv lignin. Figure 4.14(c) shows the shift in the main lignin peak towards lower molecular weight.

4.4.4 ^{13}C NMR spectroscopy

^{13}C NMR spectroscopy is a valuable analytical method for determining linkages and functional groups present in lignin.[188,189] ^{13}C NMR spectra of Organosolv lignin itself and of its oxidized products are given in the Supporting Information. After Swern oxidation, we observed the appearance of a ketone carbonyl peak near 209 ppm, and after Baeyer-Villiger oxidation a carboxylic acid peaks at around 175-160 ppm.

120 mg of lignin sample and 1.8 mg of chromium (III) acetylacetonate were dissolved in 0.6 mL DMSO-d_6. An inverse gated decoupling pulse sequence was used for the measurements, employing a relaxation time delay of 1.7 s and an observation pulse of 5.17 μs (30°).
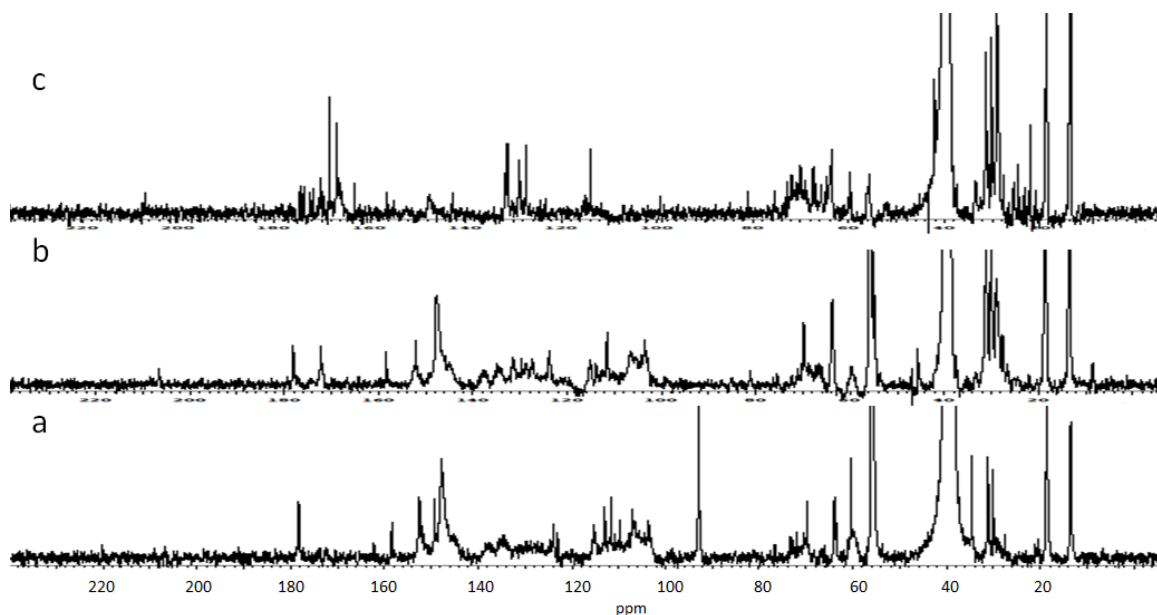
Figure 4. 15 ^{13}C NMR spectra of (a) native Organosolv lignin; (b) soluble product obtained from Swern oxidation of native Organosolv lignin; (c) Baeyer-Villiger oxidation using H_2O_2/ HCOOH of Swern-oxidized Organosolv lignin.

The ^{13}C NMR spectrum of the starting material showed satisfactory agreement with previously reported ^{13}C NMR data for Organosolv lignin.[57,188] A peak at 179 ppm corresponds to the carbonyl carbon of carboxylic acid/ester moieties, and signals from103 ppm to 153 ppm are assigned to the aromatic carbon region. Signals at 152-147 ppm belong to etherified/non-etherified C-3/C-5 carbons of syringyl (S) units and etherified C-3/C-4 carbon of guaiacyl (G) units. Resonances at 147-146 ppm belong to non-etherified C-4 carbon of G units, signals at 139-134 ppm are assigned to etherified C-1/C-4 carbon S units and C-1 carbon of G units, and signals at 128- 104 ppm belong to C-6/C-2 carbons. Signals at 75-55 ppm are assigned to C-γ, C-β, C-α and OCH$_3$ groups.

4.4.5 Matrix-assisted laser desorption/ionization time-of-flight mass spectrometry (MALDI-TOF MS)

Convenient, bench-top techniques such as GS-MS and pyrolysis GC-MS will not be appropriate to determine the molecular weight of lignin fragments. In those methods, a sample is vaporized by heating a solution or by heating a solid sample. Lignol dimers, trimers, or higher molecular units will likely not be vaporized and they may undergo degradation. MALDI-TOF MS is a soft ionization technique that has potential application in the study of larger molecules. In this method, the molecular ions generated by soft ionization generally undergo less fragmentation. In this regards, the literature is rich with examples where MALDI-TOF MS has been used in structural investigation of lignin polymers. Angelis and co-worker demonstrated an accurate determination molecular weight of synthetic lignin.[190] Awal et al. showed that MALDI-TOF data can give valuable information about the molecular weight distribution of lignin.[191] Metzger also demonstrated that this method is highly sensitive in wide range of molecules.[192]

MALDI-MS was performed on a Bruker Daltonics MALDI-TOF MS ultraflextreme, operating in position ion mode. Samples were dissolved in acetone and 2, 5-dihydroxybenoic acid was used as s matrix. MALDI-TOF MS was used to analyze the array of molecules formed upon depolymerization.[27,190]
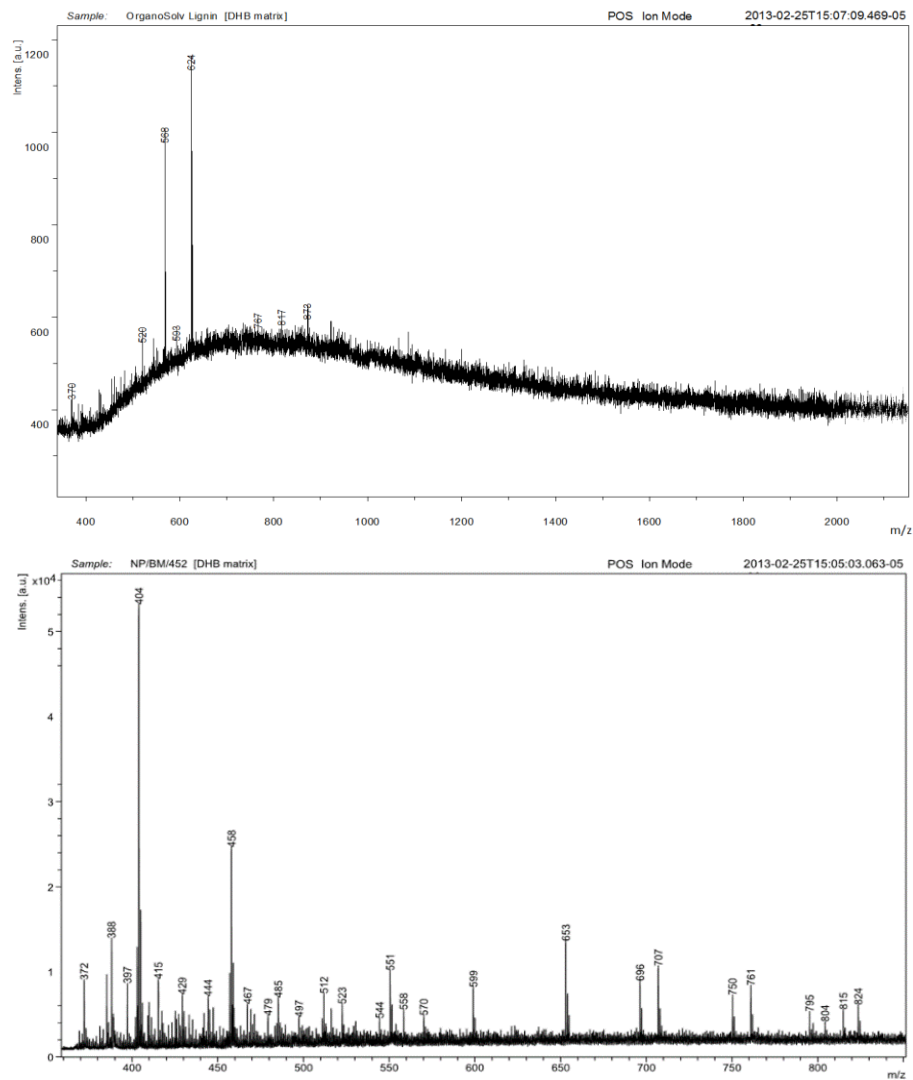
Figure 4. 16 MALDI-TOF MS spectrum of organosolv lignin and Swern-oxidized Organosolv lignin after Baeyer-Villiger oxidation

We observed significant ion current from ions in the range 372 to 824 Da (as shown in figure 4.16), in the range of masses expected for dimers, trimers and tetramers of lignols. In contrast, MALDI-TOF MS analysis of Organosolv lignin showed nothing more than background current, as did control samples of Organosolv lignin that had been subjected to Baeyer-Villiger oxidation, but not to the prior benzylic oxidation step.

CHAPTER 5. CONCLUSIONS

5.1   Conclusions

The overall approach for depolymerization of lignin was two-step process. However, in an attempt to perform aerobic oxidation of benzylic hydroxyl group in LMCs we had critical difficulties. In order to overcome this issue, we attempted to protect all phenolic hydroxyl group present in native lignin. The protection group study demonstrated that sterically hindered phenolic hydroxyl groups in lignin are difficult to protect selectively, and some degree of protection of aliphatic hydroxyls was unavoidable. However, the use of benzyl bromide gave satisfactory results, but completely selective protection of phenolic hydroxyl groups alone was not achieved. ^{31}P NMR and FTIR-ATR spectroscopy analyses suggested that in the protection step, the phenolic hydroxyl groups, along with some aliphatic hydroxyl groups, also were functionalized and some phenolic hydroxyl groups were not protected. Based on model compound studies, TEMPO oxidation process work exceptional good. The ^{31}P NMR and FTIR-ATR analysis of TEMPO oxidized Organosolv lignin illustrate oxidation of alcohol to desire products. Furthermore, after BVO, noticeable changes were observed at carbonyl region of FTIR-ATR. Finally, GPC results illustrated that after the BVO step, the molecular weight of the lignin polymer was not significantly reduced. These result suggest that overall three step depolymerized Organosolv lignin molecular weight does not reduces to larger extend. In addition, a non-catalytic oxidation pathway using Swern oxidation appears suitable for the oxidation of benzylic alcohol groups in lignin into ketones. ^{31}P NMR, ^{13}C NMR and FTIR-ATR spectroscopy analyses suggest that upon Swern oxidation of Organosolv lignin, aliphatic hydroxyl groups were successfully oxidized to ketones. Furthermore, GPC and MALDI-TOF MS results indicate that after Baeyer-Villiger oxidation the lignin polymer fragmented into lower molecular weight compounds. This selective two-step oxidation process successfully achieves the reduction of the molecular weight of Organosolv lignin.

In summary, we have developed a process for selective cleavage of the $C\alpha$-$C\beta$ linkage in the depolymerization of Organosolv lignin, via Baeyer-Villiger oxidation. The further research targets on study of depolymerization of switch grass lignin.

LIST OF ABBREVIATIONS

ASAM	Alkali-sulfite-anthraquinone-methanol
ATR-IR	Attenuated total reflectance Infrared spectroscopy
BVO	Baeyer-Villiger oxidation
CAN	Ceric ammonium nitrate
DDQ	2,3-Dichloro-5,6-dicyano-1,4-benzoquinone
DMPA	Dimethylolpropionic acid
EI	Electron impact ionization
EMAL	Enzymatic mild acidolysis lignin
EPR	Electronic paramagnetic resonance spectroscopy
FTIR	Fourier transform infrared spectroscopy
GC-MS	Gas chromatography-mass spectroscopy
GPC	Gel permeation chromatography
LMCS	Lignin model compounds
MALDI	Matrix-assisted laser desorption/ionization
m-CPBA	m-chloroperbenzoic acid
NHPI	N-hydroxyphthalimide
NMR	Nuclear magnetic spectroscopy
PTC	Phase-transfer catalyst
TEMPO	(2,2,6,6-Tetramethylpiperidin-1-yl)oxyl
TFPAA	Trifluoroperacetic acid
TGA	Thermogravimetric analysis
TMDP	2-chloro-4, 4, 5, 5-tetramethyl-1, 3, 2-dioxaphospholane
TOF	Time-of-flight
TPP	Iron tetraphenylporphyrin
TPPFeCl	5,10,15,20-Tetraphenyl-21H,23H-porphine iron(III) chloride

REFERENCES

(1)   McLaren, J. S. *Trends Biotechnol* **2005**, *23*, 339.

(2)   Zhang, Y. H. P. *J Ind Microbiol Biot* **2008**, *35*, 367.

(3)   Huber, G. W.; Iborra, S.; Corma, A. *Chemical reviews* **2006**, *106*, 4044.

(4)   Qin, Z. C.; Zhuang, Q. L.; Zhu, X. D.; Cai, X. M.; Zhang, X. *Environ Sci Technol* **2011**, *45*, 10765.

(5)   Farrell, A. E. *Science* **2006**, *312*, 1748.

(6)   Carriquiry, M. A.; Du, X. D.; Timilsina, G. R. *Energ Policy* **2011**, *39*, 4222.

(7)   Perlack, R. D.; Wright, L. L.; Turhollow, A. F.; Graham, R. L. "http://feedstockreview.ornl.gov/pdf/billion_ton_vision.pdf," 2005.

(8)   He, H.; Rodgers, R. P.; Marshall, A. G.; Hsu, C. S. *Energ Fuel* **2011**, *25*, 4770.

(9)   Dodds, D. R.; Gross, R. A. *Science* **2007**, *318*, 1250.

(10)   Zakzeski, J.; Bruijnincx, P. C. A.; Jongerius, A. L.; Weckhuysen, B. M. *Chemical reviews* **2010**, *110*, 3552.

(11)   Ritter, S. K. *Chem Eng News* **2008**, *86*, 57.

(12)   Lewis, N. G., Sarkanen, S *Lignin and Lignan Biosynthesis* American Chemical Society, 1998.

(13)   Marton, J. *Technical Lignin Structure and Reactions (Advances in Chemistry)*

june 19, 1966.

(14)   Freudenb.K *Holzforschung* **1968**, *22*, 65.

(15)   Onnerud, H.; Zhang, L. M.; Gellerstedt, G.; Henriksson, G. *Plant Cell* **2002**, *14*, 1953.

(16)   Freudenberg, K.; Schraube, H. *Chem Ber-Recl* **1955**, *88*, 16.

(17)   Syrjanen, K.; Brunow, G. *J Chem Soc Perk T 1* **2000**, 183.

(18)   Tobimatsu, Y.; Chen, F.; Nakashima, J.; Escamilla-Trevino, L. L.; Jackson, L.; Dixon, R. A.; Ralph, J. *Plant Cell* **2013**, *25*, 2587.

(19)   Ralph, J.; Lundquist, K.; Brunow, G.; Lu, F.; Kim, H.; Schatz, P. F.; Marita, J. M.; Hatfield, R. D.; Ralph, S. A.; Christensen, J. H.; Boerjan, W. *Lignins: Natural polymers from oxidative coupling of 4-hydroxyphenylpropanoids*; Kluwer Academic Publishers., 2004; Vol. 3.

(20)   Chakar, F. S.; Ragauskas, A. J. *Ind Crop Prod* **2004**, *20*, 131.

(21)   Faix, O.; Meier, D.; Fortmann, I. *Holz Roh Werkst* **1990**, *48*, 351.

(22)   Lapierre, C.; Pollet, B.; Monties, B. *Phytochemistry* **1991**, *30*, 659.

(23)   Tien, M.; Kirk, T. K. *Science* **1983**, *221*, 661.

(24)   Faix, O.; Argyropoulos, D. S.; Robert, D.; Neirinck, V. *Holzforschung* **1994**, *48*, 387.

(25)   Atalla, R. H.; Agarwal, U. P. *Science* **1985**, *227*, 636.

(26)   Beste, A.; Buchanan, A. C. *J Org Chem* **2009**, *74*, 2837.

(27)   Reale, S.; Di Tullio, A.; Spreti, N.; De Angelis, F. *Mass Spectrom Rev* **2004**, *23*, 87.

(28)   Adler, E. *Wood Sci Technol* **1977**, *11*, 169.

(29)   Adler, P. R.; Sanderson, M. A.; Boateng, A. A.; Weimer, P. I.; Jung, H. J. G. *Agron J* **2006**, *98*, 1518.

(30)   Mann, D. G. J.; Labbe, N.; Sykes, R. W.; Gracom, K.; Kline, L.; Swamidoss, I. M.; Burris, J. N.; Davis, M.; Stewart, C. N. *Bioenerg Res* **2009**, *2*, 246.

(31)   Anterola, A. M.; Lewis, N. G. *Phytochemistry* **2002**, *61*, 221.

(32)   Guerra, A.; Filpponen, I.; Lucia, L. A.; Argyropoulos, D. S. *J Agr Food Chem* **2006**, *54*, 9696.

(33)   Chiang, V. L.; Funaoka, M. *Holzforschung* **1990**, *44*, 147.

(34)   Davison, B. H.; Drescher, S. R.; Tuskan, G. A.; Davis, M. F.; Nghiem, N. P. *Appl Biochem Biotech* **2006**, *130*, 427.

(35)   Pilate, G.; Guiney, E.; Holt, K.; Petit-Conil, M.; Lapierre, C.; Leple, J. C.; Pollet, B.; Mila, I.; Webster, E. A.; Marstorp, H. G.; Hopkins, D. W.; Jouanin, L.; Boerjan, W.; Schuch, W.; Cornu, D.; Halpin, C. *Nat Biotechnol* **2002**, *20*, 607.

(36)   Fu, C. X.; Mielenz, J. R.; Xiao, X. R.; Ge, Y. X.; Hamilton, C. Y.; Rodriguez, M.; Chen, F.; Foston, M.; Ragauskas, A.; Bouton, J.; Dixon, R. A.; Wang, Z. Y. *P Natl Acad Sci USA* **2011**, *108*, 3803.

(37)   Brunow, G. *Methods to Reveal the Structure of Lignin, Biopolymers Online*, 2005.

(38)   Brandt, A.; Grasvik, J.; Hallett, J. P.; Welton, T. *Green Chem* **2013**, *15*, 550.

(39)   Hsu, T. A.; Ladisch, M. R.; Tsao, G. T. *Chemtech* **1980**, *10*, 315.

(40)   Moura, J. C. M. S.; Bonine, C. A. V.; Viana, J. D. F.; Dornelas, M. C.; Mazzafera, P. *J Integr Plant Biol* **2010**, *52*, 360.

(41)   Hames, B. R.; Kurek, B.; Pollet, B.; Lapierre, C.; Monties, B. *J Agr Food Chem* **1998**, *46*, 5362.

(42)   Crist, R. H.; Martin, J. R.; Crist, D. R. *Environ Sci Technol* **2002**, *36*, 1485.

(43)   Rogers, L. A.; Dubos, C.; Cullis, I. F.; Surman, C.; Poole, M.; Willment, J.; Mansfield, S. D.; Campbell, M. M. *J Exp Bot* **2005**, *56*, 1651.

(44)   Leinhos, V.; Bergmann, H. *J Appl Bot-Angew Bot* **1995**, *69*, 206.

(45)   Masingale, M. P.; Alves, E. F.; Korbieh, T. N.; Bose, S. K.; Francis, R. C. *Bioresources* **2009**, *4*, 1139.

(46)   Harman-Ware, A. E.; Crocker, M.; Kaur, A. P.; Meier
, M. S.; Kato, D.; Lynn, B. *J Anal Appl Pyrol* **2013**, *99*, 161.

(47)   Gellerstedt, G.; Lindfors, E. L. *Holzforschung* **1984**, *38*, 151.

(48)   Wu, L. C. F.; Glasser, W. G. *Biotechnol Bioeng* **1979**, *21*, 1679.

(49)   Zhang, J. H.; Deng, H. B.; Lin, L. *Molecules* **2009**, *14*, 2747.

(50)   Parpot, P.; Bettencourt, A. P.; Carvalho, A. M.; Belgsir, E. M. *J Appl Electrochem* **2000**, *30*, 727.

(51)   Kuwahara, M.; Glenn, J. K.; Morgan, M. A.; Gold, M. H. *Febs Lett* **1984**, *169*, 247.

(52)   Evtuguin, D. V.; Neto, C. P.; Rocha, J.; de Jesus, J. D. P. *Appl Catal a-Gen* **1998**, *167*, 123.

(53)   Gupta, K. C.; Sutar, A. K.; Lin, C. C. *Coordin Chem Rev* **2009**, *253*, 1926.

(54)   Harris, E. E.; D'Ianni, J.; Adkins, H. *J Am Chem Soc* **1938**, *60*, 1467.

(55)   Pepper, J. M.; Steck, W. F.; Swoboda, R.; Karapall.Jc *Adv Chem Ser* **1966**, 238.

(56)   Pepper, J. M.; Lee, Y. W. *Can J Chemistry* **1969**, *47*, 723.

(57)   Barta, K.; Matson, T. D.; Fettig, M. L.; Scott, S. L.; Iretskii, A. V.; Ford, P. C. *Green Chem* **2010**, *12*, 1640.

(58)   Cyr, A.; Chiltz, F.; Jeanson, P.; Martel, A.; Brossard, L.; Lessard, J.; Menard, H. *Can J Chem* **2000**, *78*, 307.

(59)   Januszkiewicz, K. R.; Alper, H. *Organometallics* **1983**, *2*, 1055.

(60)   Nasar, K.; Fache, F.; Lemaire, M.; Beziat, J. C.; Besson, M.; Gallezot, P. *J Mol Catal* **1994**, *87*, 107.

(61)   Nagy, M.; David, K.; Britovsek, G. J. P.; Ragauskas, A. J. *Holzforschung* **2009**, *63*, 513.

(62)   Beste, A.; Buchanan, A. C., 3rd *The Journal of organic chemistry* **2011**, *76*, 2195.

(63)   Beste, A.; Buchanan, A. C., 3rd *J Org Chem* **2009**, *74*, 2837.

(64)   Beste, A.; Buchanan, A. C., 3rd; Harrison, R. J. *J Phys Chem A* **2008**, *112*, 4982.

(65)   Britt, P. F.; Buchanan, A. C., 3rd; Cooney, M. J.; Martineau, D. R. *The Journal of organic chemistry* **2000**, *65*, 1376.

(66)   Olcese, R. N.; Francois, J.; Bettahar, M. M.; Petitjean, D.; Dufour, A. *Energ Fuel* **2013**, *27*, 975.

(67)   Lu, Q. A.; Zhang, Z. F.; Dong, C. Q.; Zhu, X. F. *Energies* **2010**, *3*, 1805.

(68)   Mukkamala, S.; Wheeler, M. C.; van Heiningen, A. R. P.; DeSisto, W. J. *Energ Fuel* **2012**, *26*, 1380.

(69)   Kantarelis, E.; Yang, W.; Blasiak, W. *Energy Fuels* **2014**, *28*, 591.

(70)   Ferdous, D.; Dalai, A. K.; Bej, S. K.; Thring, R. W. *Energ Fuel* **2002**, *16*, 1405.

(71)   Son, S.; Toste, F. D. *Angew Chem Int Edit* **2010**, *49*, 3791.

(72)   Hanson, S. K.; Wu, R.; Silks, L. A. *Angew Chem Int Ed Engl* **2012**.

(73)   Hanson, S. K.; Baker, R. T.; Gordon, J. C.; Scott, B. L.; Thorn, D. L. *Inorg Chem* **2010**, *49*, 5611.

(74)   Crestini, C.; Pastorini, A.; Tagliatesta, P. *Eur J Inorg Chem* **2004**, 4477.

(75)   Rahimi, A.; Azarpira, A.; Kim, H.; Ralph, J.; Stahl, S. S. *J Am Chem Soc* **2013**, *135*, 6415.

(76)   Biannic, B.; Bozell, J. J. *Org Lett* **2013**, *15*, 2730.

(77)   Martinez, A. T.; Rencoret, J.; Nieto, L.; Jimenez-Barbero, J.; Gutierrez, A.; del Rio, J. C. *Environ Microbiol* **2011**, *13*, 96.

(78)   Glenn, J. K.; Morgan, M. A.; Mayfield, M. B.; Kuwahara, M.; Gold, M. H. *Biochem Bioph Res Co* **1983**, *114*, 1077.

(79)   Kirk, T. K.; Connors, W. J.; Bleam, R. D.; Hackett, W. F.; Zeikus, J. G. *P Natl Acad Sci USA* **1975**, *72*, 2515.

(80)   Gold, M. H.; Kuwahara, M.; Chiu, A. A.; Glenn, J. K. *Arch Biochem Biophys* **1984**, *234*, 353.

(81)   Li, H.; Poulos, T. L. *Structure* **1994**, *2*, 461.

(82)   Poulos, T. L.; Edwards, S. L.; Wariishi, H.; Gold, M. H. *J Biol Chem* **1993**, *268*, 4429.

(83)   Edwards, S. L.; Raag, R.; Wariishi, H.; Gold, M. H.; Poulos, T. L. *P Natl Acad Sci USA* **1993**, *90*, 750.

(84)   Cui, F.; Dolphin, D. *Can J Chemistry* **1995**, *73*, 2153.

(85)   Cui, F. T.; Dolphin, D. *Can J Chem* **1992**, *70*, 2314.

(86)   Renganathan, V.; Miki, K.; Gold, M. H. *Arch Biochem Biophys* **1985**, *241*, 304.

(87)   Kirk, T. K.; Tien, M.; Kersten, P. J.; Mozuch, M. D.; Kalyanaraman, B. *Biochem J* **1986**, *236*, 279.

(88)   Tsutsui, M.; Srivasta.Ts *Ann Ny Acad Sci* **1973**, *206*, 404.

(89)   Brunink, J. A. J.; DiNatale, C.; Bungaro, F.; Davide, F. A. M.; DAmico, A.; Paolesse, R.; Boschi, T.; Faccio, M.; Ferri, G. *Anal Chim Acta* **1996**, *325*, 53.

(90)   Renganathan, V.; Miki, K.; Gold, M. H. *Arch Biochem Biophys* **1986**, *246*, 155.

(91)   Baciocchi, E.; Fabbri, C.; Lanzalunga, O. *The Journal of organic chemistry* **2003**, *68*, 9061.

(92)   Baciocchi, E.; Gerini, M. F.; Harvey, P. J.; Lanzalunga, O.; Prosperi, A. *J Chem Soc Perk T 2* **2001**, 1512.

(93)   Tien, M.; Kirk, T. K. *P Natl Acad Sci USA* **1984**, *81*, 2280.

(94)   Labat, G.; Meunier, B. *J Org Chem* **1989**, *54*, 5008.

(95)   DeRosa, M. C.; Crutchley, R. J. *Coordin Chem Rev* **2002**, *233*, 351.

(96)   Mimoun, H. *Pure Appl Chem* **1981**, *53*, 2389.

(97)   Wang, L. Y.; Li, J.; Lv, Y.; Zhang, H. Y.; Gao, S. *J Organomet Chem* **2011**, *696*, 3257.

(98)   Schultz, M. J.; Park, C. C.; Sigman, M. S. *Chem Commun* **2002**, 3034.

(99)   Peterson, K. P.; Larock, R. C. *J Org Chem* **1998**, *63*, 3185.

(100)   An, G.; Lim, M.; Chun, K. S.; Rhee, H. *Synlett* **2007**, 95.

(101)   Matsumoto, M.; Watanabe, N. *J Org Chem* **1984**, *49*, 3435.

(102)   Makwana, V. D.; Son, Y. C.; Howell, A. R.; Suib, S. L. *J Catal* **2002**, *210*, 46.

(103)   Zhou, L. P.; Chen, Y.; Yang, X. M.; Su, Y. L.; Zhang, W.; Xu, J. *Catal Lett* **2008**, *125*, 154.

(104)   Sharma, G. V. M.; Lavanya, B.; Mahalingam, A. K.; Krishna, P. R. *Tetrahedron Lett* **2000**, *41*, 10323.

(105)   Nohl, H.; Jordan, W.; Youngman, R. J. *Adv Free Radical Bio* **1986**, *2*, 211.

(106)   Frontana, C.; Vazquez-Mayagoitia, A.; Garza, J.; Vargas, R.; Gonzalez, I. *Journal of Physical Chemistry A* **2006**, *110*, 9411.

(107)   Zhu, X. Q.; Wang, C. H. *J Org Chem* **2010**, *75*, 5037.

(108)   Zhang, W.; Ma, H.; Zhou, L. P.; Sun, Z. Q.; Du, Z. T.; Miao, H.; Xu, J. *Molecules* **2008**, *13*, 3236.

(109)   Muramatsu, W.; Nakano, K.; Li, C. J. *Org Lett* **2013**.

(110) Ohki, A.; Nishiguchi, T.; Fukuzumi, K. *Tetrahedron* **1979**, *35*, 1737.

(111) Guin, P. S.; Das, S.; Mandla, P. C. *International Journal of Electrochemistry* **2011**, *816202*, 22.

(112) Joshi, B. P.; Sharma, A.; Sinha, A. K. *Tetrahedron* **2006**, *62*, 2590.

(113) Liu, L.; Floreancig, P. E. *Org Lett* **2009**, *11*, 3152.

(114) Yadav, J. S.; Chandrasekhar, S.; Sumithra, G.; Kache, R. *Tetrahedron Lett* **1996**, *37*, 6603.

(115) Becker, H. D.; Bjork, A.; Adler, E. *J Org Chem* **1980**, *45*, 1596.

(116) Walker, D.; Hiebert, J. D. *Chemical reviews* **1967**, *67*, 153.

(117) Brown, D. R.; Turner, A. B. *J Chem Soc Perk T 2* **1975**, 1307.

(118) Chandrasekhar, S.; Sumithra, G.; Yadav, J. S. *Tetrahedron Lett* **1996**, *37*, 1645.

(119) Luca, O. R.; Wang, T.; Konezny, S. J.; Batista, V. S.; Crabtree, R. H. *New J Chem* **2011**, *35*, 998.

(120) Noyes, W. A. *J Am Chem Soc* **1925**, *47*, 2170.

(121) Galliker, B.; Kissner, R.; Nauser, T.; Koppenol, W. H. *Chem-Eur J* **2009**, *15*, 6161.

(122) Astolfi, P.; Panagiotaki, M.; Greci, L. *Eur J Org Chem* **2005**, 3052.

(123) Wang, L. Y.; Li, J.; Yang, H.; Lv, Y.; Gao, S. *J Org Chem* **2012**, *77*, 790.

(124) Wang, L.; Li, J.; Yang, H.; Lv, Y.; Gao, S. *The Journal of organic chemistry* **2012**, *77*, 790.

(125) Kumar, T. V.; Veeraiah, T.; Venkateshwarlu, G. *P Indian as-Chem Sci* **2000**, *112*, 119.

(126) Zhang, W.; Ma, H.; Zhou, L. P.; Miao, H.; Xu, J. *Chinese J Catal* **2009**, *30*, 86.

(127) Cella, J. A.; Kelley, J. A.; Kenehan, E. F. *J Org Chem* **1975**, *40*, 1860.

(128) Boutevin, B.; Hervaud, Y.; Boulahna, A.; El Asri, M. *Macromolecules* **2002**, *35*, 6511.

(129) Zweier, J. L.; Kuppusamy, P. *P Natl Acad Sci USA* **1988**, *85*, 5703.

(130) Conte, M.; Ma, Y.; Loyns, C.; Price, P.; Rippon, D.; Chechik, V. *Org Biomol Chem* **2009**, *7*, 2685.

(131) http://www.silicycle.com/products/siliacat-heterogeneous-catalysts/r723-100.

(132) Einhorn, J.; Einhorn, C.; Ratajczak, F.; Pierre, J. L. *J Org Chem* **1996**, *61*, 7452.

(133) Miyazawa, T.; Endo, T.; Shiihashi, S.; Okawara, M. *J Org Chem* **1985**, *50*, 1332.

(134) Miyazawa, T.; Endo, T. *J Mol Catal* **1985**, *31*, 217.

(135) Semmelhack, M. F.; Chou, C. S.; Cortes, D. A. *J Am Chem Soc* **1983**, *105*, 4492.

(136) Anelli, P. L.; Biffi, C.; Montanari, F.; Quici, S. *J Org Chem* **1987**, *52*, 2559.

(137) Denooy, A. E. J.; Besemer, A. C.; Vanbekkum, H. *Tetrahedron* **1995**, *51*, 8023.

(138)   Inokuchi, T.; Matsumoto, S.; Nishiyama, T.; Torii, S. *J Org Chem* **1990**, *55*, 462.

(139)   Bailey, W. F.; Bobbitt, J. M.; Wiberg, K. B. *J Org Chem* **2007**, *72*, 4504.

(140)   Sen, V. D.; Golubev, V. A. *J Phys Org Chem* **2009**, *22*, 138.

(141)   Liu, R. H.; Liang, X. M.; Dong, C. Y.; Hu, X. Q. *J Am Chem Soc* **2004**, *126*, 4112.

(142)   Liu, R. H.; Dong, C. Y.; Liang, X. M.; Wang, X. J.; Hu, X. Q. *J Org Chem* **2005**, *70*, 729.

(143)   Kim, S. S.; Jung, H. C. *Synthesis-Stuttgart* **2003**, 2135.

(144)   Wang, X. L.; Liu, R. H.; Jin, Y.; Liang, X. M. *Chem-Eur J* **2008**, *14*, 2679.

(145)   Hawthorne, M. F.; Emmons, W. D.; Mccallum, K. S. *J Am Chem Soc* **1958**, *80*, 6393.

(146)   Strukul, G. *Angew Chem Int Edit* **1998**, *37*, 1199.

(147)   Doering, W. V.; Speers, L. *J Am Chem Soc* **1950**, *72*, 5515.

(148)   ten Brink, G. J.; Arends, I. W. C. E.; Sheldon, R. A. *Chemical reviews* **2004**, *104*, 4105.

(149)   Liu, B.; Meng, X. G.; Li, W. Y.; Zhou, L. C.; Hu, C. W. *Journal of Physical Chemistry A* **2012**, *116*, 2920.

(150)   Alvarez-Idaboy, J. R.; Reyes, L.; Mora-Diez, N. *Org Biomol Chem* **2007**, *5*, 3682.

(151)   Mora-Diez, N.; Keller, S.; Alvarez-Idaboy, J. R. *Org Biomol Chem* **2009**, *7*, 3682.

(152)   Klein, M. T.; Virk, P. S. *Ind Eng Chem Fund* **1983**, *22*, 35.

(153)   Nichols, J. M.; Bishop, L. M.; Bergman, R. G.; Ellman, J. A. *J Am Chem Soc* **2010**, *132*, 12554.

(154)   Kandanarachchi, P. H.; Autrey, T.; Franz, J. A. *The Journal of organic chemistry* **2002**, *67*, 7937.

(155)   Compton, D. R.; Prescott, W. R., Jr.; Martin, B. R.; Siegel, C.; Gordon, P. M.; Razdan, R. K. *J Med Chem* **1991**, *34*, 3310.

(156)   Cordoba, R.; Tormo, N. S.; Medarde, A. F.; Plumet, J. *Bioorgan Med Chem* **2007**, *15*, 5300.

(157)   Head, F. S. H.; Lund, G. *J Chem Soc C* **1969**, 37.

(158)   Cardillo, G.; Shimizu, M. *J Org Chem* **1977**, *42*, 4268.

(159)   Tanaka, H.; Kato, I.; Ito, K. *Chem Pharm Bull* **1986**, *34*, 628.

(160)   Pericas, A.; Shafir, A.; Vallribera, A. *Tetrahedron* **2008**, *64*, 9258.

(161)   Tanemura, K.; Suzuki, T.; Nishida, Y.; Satsumabayashi, K.; Horaguchi, T. *Chem Commun* **2004**, 470.

(162)   Quesada-Medina, J.; Lopez-Cremades, F. J.; Olivares-Carrillo, P. *Bioresource technology* **2010**, *101*, 8252.

(163)   Jimenez, L.; Maestre, F.; Perez, I. *Wood Sci Technol* **1999**, *33*, 97.

(164)   Lindner, A.; Wegener, G. *J Wood Chem Technol* **1988**, *8*, 323.

(165)   Shatalov, A. A.; Pereira, H. *Bioresource technology* **2008**, *99*, 472.

(166)   Marton, R.; Granzow, S. G.; Patent, P., Ed. 1982; Vol. PCT Patent WO 82/01568.

(167)   Thring, R. W.; Chornet, E.; Overend, R. P. *Biomass* **1990**, *23*, 289.

(168)   Sixta, H.; Harms, H.; Dapia, S.; Parajo, J. C.; Puls, J.; Saake, B.; Fink, H. P.; Roder, T. *Cellulose* **2004**, *11*, 73.

(169)   Arnoldy, P.; Petrus, L. 1989; Vol. DE patent 38.30.993. A1.

(170)   Xu, W. Y.; Miller, S. J.; Agrawal, P. K.; Jones, C. W. *Chemsuschem* **2012**, *5*, 667.

(171)   Parsell, T. H.; Owen, B. C.; Klein, I.; Jarrell, T. M.; Marcum, C. L.; Haupert, L. J.; Amundson, L. M.; Kenttamaa, H. I.; Ribeiro, F.; Miller, J. T.; Abu-Omar, M. M. *Chem Sci* **2013**, *4*, 806.

(172)   Toledano, A.; Serrano, L.; Balu, A. M.; Luque, R.; Pineda, A.; Labidi, J. *Chemsuschem* **2013**, *6*, 529.

(173)   Roberts, V. M.; Stein, V.; Reiner, T.; Lemonidou, A.; Li, X. B.; Lercher, J. A. *Chem-Eur J* **2011**, *17*, 5939.

(174)   Bauer, S.; Sorek, H.; Mitchell, V. D.; Ibanez, A. B.; Wemmer, D. E. *J Agr Food Chem* **2012**, *60*, 8203.

(175)   Pu, Y. Q.; Cao, S. L.; Ragauskas, A. J. *Energ Environ Sci* **2011**, *4*, 3154.

(176)   Granata, A.; Argyropoulos, D. S. *J Agr Food Chem* **1995**, *43*, 1538.

(177)   Argyropoulos, D. S.; Bolker, H. I.; Heitner, C.; Archipov, Y. *Holzforschung* **1993**, *47*, 50.

(178)   Morita, I.; Kunimoto, K.; Tsuda, M.; Tada, S.; Kise, M.; Kimura, K. *Chem Pharm Bull* **1987**, *35*, 4144.

(179)   Faix, O.; Bremer, J.; Schmidt, O.; Stevanovic, T. *J Anal Appl Pyrol* **1991**, *21*, 147.

(180)   Faix, O.; Andersons, B.; Zakis, G. *Holzforschung* **1998**, *52*, 268.

(181)   Vallejos, M. E.; Felissia, F. E.; Curvelo, A. A. S.; Zambon, M. D.; Ramos, L.; Area, M. C. *Bioresources* **2011**, *6*, 1158.

(182)   Buta, J. G.; Galletti, G. C. *J Sci Food Agr* **1989**, *49*, 37.

(183)   Emandi, A.; Vasiliu, C. I.; Budrugeac, P.; Stamatin, I. *Cell Chem Technol* **2011**, *45*, 579.

(184)   Buta, J. G.; Zadrazil, F.; Galletti, G. C. *J Agr Food Chem* **1989**, *37*, 1382.

(185)   El Mansouri, N. E.; Salvado, J. *Ind Crop Prod* **2006**, *24*, 8.

(186)   Barton, A. F. M. *CRC Handbook of Solubility Parameters and other Cohesion Parameters*; CRC: Boca Raton, Fl., 1983.

(187)   Omura, K.; Swern, D. *Tetrahedron* **1978**, *34*, 1651.

(188)   Nimz, H. *Angewandte Chemie-International Edition in English* **1974**, *13*, 313.

(189)   Wen, J. L.; Sun, S. L.; Xue, B. L.; Sun, R. C. *Materials* **2013**, *6*, 359.

(190)   DeAngelis, F.; Fregonese, P.; Veri, F. *Rapid Commun Mass Sp* **1996**, *10*, 1304.

(191)   Awal, A.; Sain, M. *J Appl Polym Sci* **2011**, *122*, 956.

(192)   Metzger, J. O.; Bicke, C.; Faix, O.; Tuszynski, W.; Angermann, R.; Karas, M.; Strupat, K. *Angewandte Chemie-International Edition in English* **1992**, *31*, 762.

AN INVESTIGATION OF THE CHANNELING REACTION IN NITROGEN-DOPED

MULTIWALLED CARBON NANOTUBES (N-MWCNTS)

CHAPTER 6. GENERAL INTRODUCTION

6.1   Introduction

Carbon materials have been under intense study for the last few decades because of their unique electronic and mechanical properties.[1-3] Diamond, graphite, fullerenes, and carbon nanotubes are the most widely studied allotropes of carbon. Every allotrope of carbon has distinct chemical and physical properties. In diamond, sp^3 hybridized carbon atoms are covalently bonded in a three-dimensional network to form an extremely hard solid. Graphene is the planar sheet of sp^2 hybridized carbon and graphite are stacked of graphene sheets with an interplanar spacing of 0.335 nm. Fullerenes are hollow spherical, ellipsoidal or tubular atomic structure entirely made from sp^2 hybridized carbon. The extended tubular fullerene structure to form a long tube is distinctly known as carbon nanotubes. The carbon nanotube structure is between that of fullerenes and graphite. Altogether, the structure of carbon nanomaterials, from zero-dimensional (0D) to three-dimensional (3D) structure, is an exciting, but challenging research topic for the future application developers.

6.2   Carbon nanotubes (CNTs)

Carbon nanotubes are elongated cylindrical tubes formed from one or more graphene sheets. Carbon nanotubes, first described in 1991 by Iijima, were called helical microtubules of graphite carbon.[4] The tubes designated were made from 2 to 50 graphene sheets, and they were later known as multiwalled carbon nanotubes (MWCNTs). One-atom thick graphene cylinders are most commonly known as single walled carbon nanotubes (SWCNTs). The SWCNTs and MWCNTs diameter typically range from between 0.8-2 nm and 5 to 100 nm respectively, and have lengths of several micrometers.[5] In recent times, an enormous amount of progress has been made on synthesis of CNTs. Every year hundred tons of MWCNTs are produced.[6]

There are three types of CNTs: armchair (n, n), zigzag (n, 0) and chiral (n, m),[7] depending on how the cylinder is rolled relative to the arrangement of hexagons in the graphene. The degree of the helical arrangement of the carbon hexagons in graphene sheet is defined by rolling indices (n, m). Every type of tube is distinguished from other based on degree of the helical arrangement of the carbon hexagons. The wrapping vector R, is represented by a pair of integers (n, m). n is nth hexagon from origin (0, 0).[8]
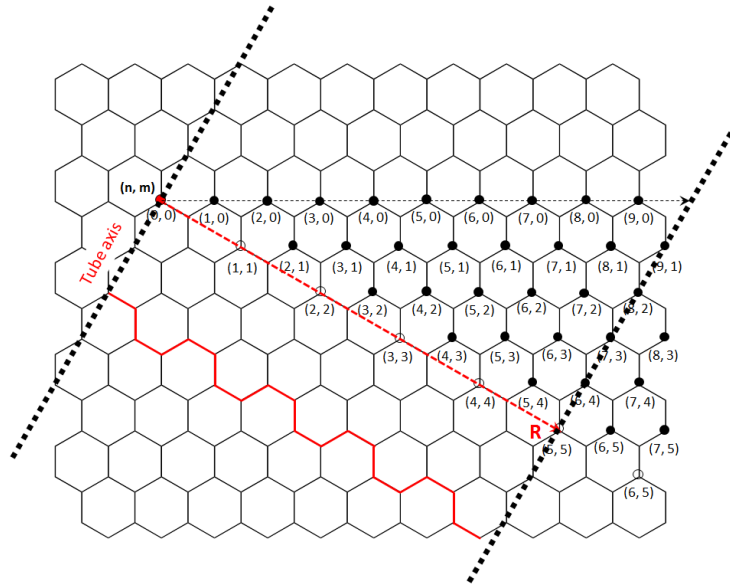
Figure 6. 1 Armchair (5, 5) carbon nanotubes hexagon lattice of graphene monoatomic layer sheet.

In armchair carbon nanotubes, the wrapping angle ϕ is 0° and n=m. The armchair nanotubes shown in figure 6.1 have rolling index (5, 5). The bold dashed lines are perpendicular to vector R and is the axis of the armchair tubes.[8] All armchair CNTs are metallic in nature.
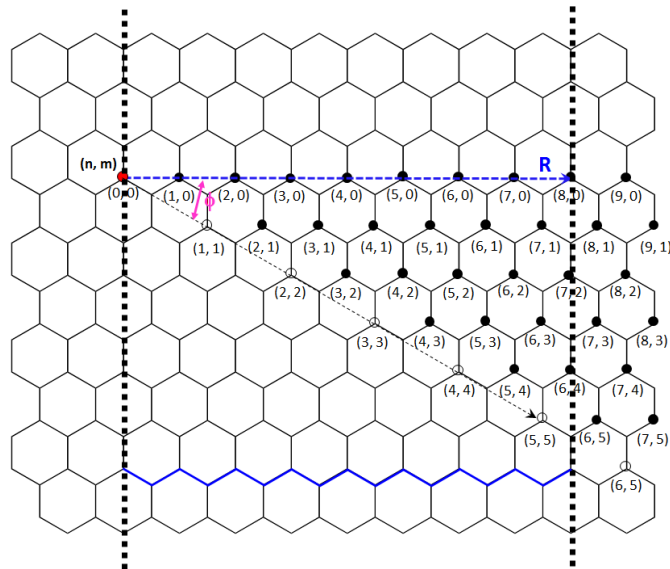
Figure 6. 2 Zigzag (8, 0) carbon nanotubes hexagon lattice of graphene monatomic layer sheet.

In zigzag carbon nanotubes, the wrapping angle ϕ is 30° and m=0. The zigzag nanotubes shown in figure 6.2 have rolling index (8, 0). The bold dashed lines are perpendicular to R and is the axis of the armchair tubes.[8]
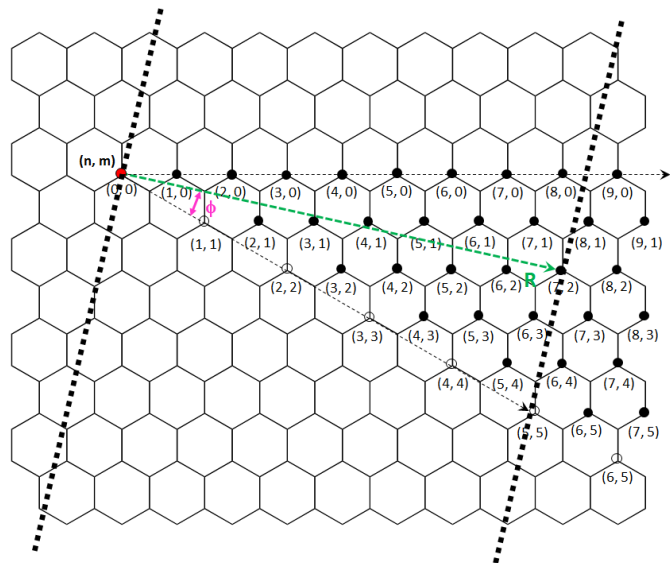
Figure 6. 3 Chiral (7, 2) carbon nanotubes hexagon lattice of graphene monoatomic layer sheet.

In chiral carbon nanotubes $n \neq m$, and a chiral angle which is greater than 0º and less than 30º. The chiral nanotubes shown in figure 6.3 have rolling index (7, 2). The bold dashed lines are perpendicular to R and is the axis of the armchair tubes.[8]

Carbon nanotubes are either metallic or semiconducting in nature. The electronic properties of SWCNTs primarily depend upon rolling index (n, m) and tube diameter.[9] Such that when n-m value is divisible of three, tubes are metallic in nature. In past, tubes synthesized had mixed chirality, which lead to amphibious electronic properties. However, recently many researchers have demonstrated synthesis of chirality-controlled SWCNTs.[10,11]

The structure of MWCNTs is described by two models: the Russian doll model and the scroll models as shown in figure 6.4.[12] In the Russian doll model, many single walled carbon nanotube are arranged as nested concentric cylinders. In the scroll model, a one-atom thick graphene sheet is rolled around itself multiple times.
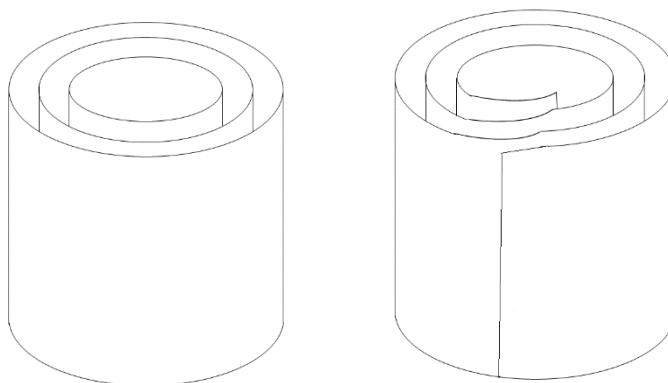
Figure 6. 4 Schematic representation of Russian doll and Scroll models for MWCNTs.

In MWCNTs, the interstitial distance between graphene sheets is 3.59 - 3.62 A°, which is slightly more than observed in graphite. The interstitial spacing between graphene sheets increases with a decrease in tube diameter.[13] Based on high electron microscopic imaging and an electron diffraction morphology study, MWCNTs appear to exist as shown in the Russian doll model.[14] However, this model is still disputed and the exact structure of MWCNTs remains unclear.[15] It is possible that some MWCNTs have a Russian doll structure and other have a scroll structure, depending upon the specific synthesis method.

Beyond the MWCNT structures discussed above, there are two additional important types of MWCNT structures - herringbone and bamboo tubes (figure 6.5). Herringbone and bamboo tubes have a different graphene plane angle with respect to the axis of the tube.[16] These tubes are often prepared with nitrogen-containing feedstocks, and such materials are known as N-MWCNTs.

Figure 6. 5 Schematic representation of herringbone MWCNTs and nesting cup (bamboo) MWCNTs.

6.3   Annual number of publications, patents and production capacity of CNTs
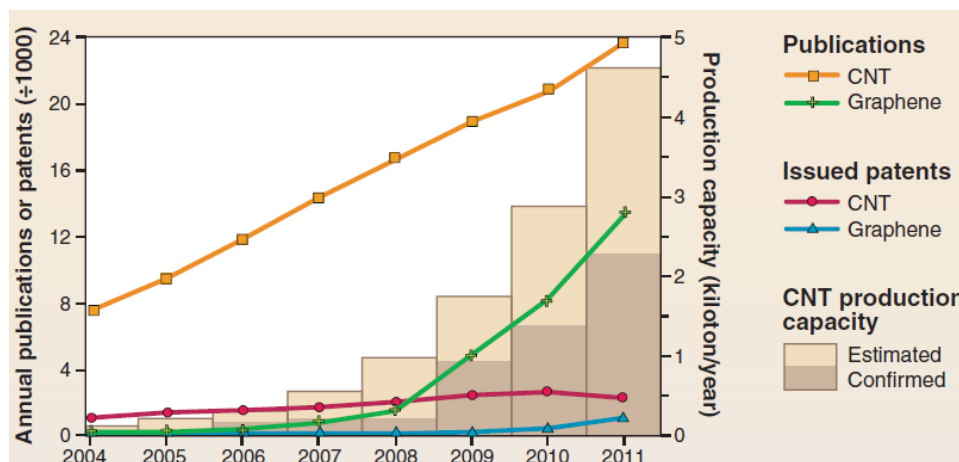
Figure 6. 6 Annual number of publication, patents and production capacity on CNTs. Image reprinted from Reference.[6] Copyright 2013, Science AAAs

As previous reported by De Volder, the annual number of publication and commercial production of CNTs increase steadily in past couple of decades.[6] The data in figure 6.6 clear shows that during last two decades, considerable attention has been paid to carbon nanotubes research. Likewise, the CNTs production capacity increased 10 times since 2006. In the past, most of the publications were focused on characterization of CNTs and

towards understanding it properties, it is clearly seen from the graph that issue patent of graphene and CNTs is not astonishingly increased. But recently research has more driven towards its applications.

6.4   Synthesis of N-MWCNTs

Since the discovery of carbon nanotubes, various synthesis methods have been reported in literature. The commonly used methods to synthesis carbon nanotubes are arc-discharge[17], laser vaporization,[18] and chemical vapor deposition[19]. The carbon nanotubes prepared by chemical vapor deposition (CVD) has significant advantages over the other conventional methods. CVD method is the cheap and thus used for commercial synthesis of nanotubes.[20] Carbon nanotubes (CNTs) obtained by the CVD method are uniformly aligned on the substrate and have narrow distributions of length and diameter. Two common CVD methods are two-stage method or continuous method. In the two-stage CVD method, the catalyst is first deposited on a substrate, then the CNTs growth occurs in a discrete second step. In the continuous CVD process, organometallic precursors are continuously injected into a pre-heated quartz tube reactor. The formation of catalyst nanoparticles and growth of CNTs occur at the same time throughout the reaction process.[20-23] Diameter of tubes entirely depends upon the diameter of metal nanoparticles deposited in the first step of synthesis. But, length of tubes can be control by adjusting reaction time.

Incorporation of another elements in the feedstock presents a way to tune the properties of carbon nanotubes in a well-defined manner. Doping CNTs with electron donors or electron acceptors is an interesting approach to tune their properties.[24] The doping an electron donors nitrogen and electron accepter boron typically leads to semi-conductive CNTs.[25] The atomic radius of nitrogen is close to carbon, and it is certainly possible to incorporate nitrogen in a graphite network.[26] The use of nitrogen-containing feedstocks during the synthesis process produces CNTs that are doped with nitrogen. In the literature, several groups have reported the synthesis of nitrogen doped multiwalled carbon nanotubes (N-MWCNTs). Sung et al. demonstrated a method using electron cyclotron resonance (ECR)

plasma by alumina template.[27] CVD is an effective method for synthesis of N-MWCNTs arrays, the nitrogen precursors commonly used is ammonia or volatile nitrogen containing organic compounds (pyridine, acetonitrile, melamine, phthalocyanine). Sen et al. synthesized well-aligned N-MWCNTs by the pyrolysis of pyridine over pre-deposited Co powder and Fe nanoparticles.[21,28] Walton and group produces nanofibers via melamine over laser etched thin films Fe/Ni nanoparticle catalyst deposited on a substrate and one-step process through mixture of melamine powder/ferrocene at 950–1050 °C.[29] Wang and group developed a microwave plasma-assisted CVD continuous growth method using N_2/CH_4.[30] In 2011, two different groups reported synthesis of N-MWCNTs using CVD methods. Lv and group demonstrate using iron phthalocyanine/pyridine[22] and D. Higgins et al. reports using three distinct feedstocks: ethylenediamine, 1, 3-diaminopropane and 1, 4-diaminobutane, all in the presence of ferrocene.[31] Coville, N. J. describes a simple method of using sealed quartz tubes and ferrocenylmethyimidazole precursor.[26]

Our interest lies mainly in synthesis of N-MWCNTs arrays on a quartz substrate. In this study, we synthesized arrays of nitrogen-doped multiwall carbon nanotubes (N-MWCNTs) by floating catalyst chemical vapor deposition (CVD) on quartz substrates (figure 6.7). The arrays of N-MWCNTs were synthesized on the quartz plates by the floating catalytic chemical vapor deposition (CVD) method, at the Center for Applied Research (CAER). The pyridine-ferrocene mixtures were pyrolyzed at 800°C in a four-inch diameter tube reactor with N_2 as carrier gas.[23]
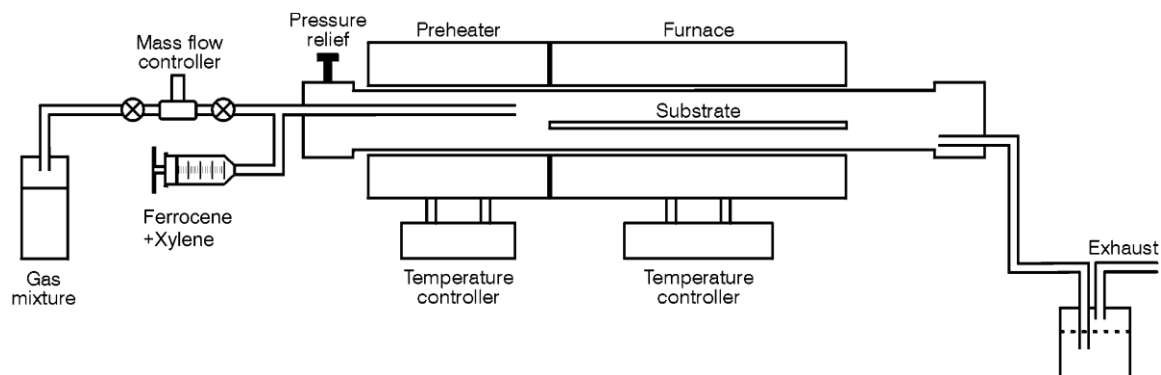
Figure 6. 7 Schematic of floating catalytic CVD reactor system to produce N-MWCNTs.[23,32] Image reprinted with permission from Reference.[32] Copyright (2002) American Chemical Society.

A CVD reactor consists of a quartz tube equipped with an exhaust port and an inlet to introduced hydrocarbon and catalyst feedstock. The center portion of the tube is called the reaction zone (furnace). A silica plate is placed in the reaction zone acting as an additional substrate for nanotube growth. The continuous CVD process growth of N-MWCNTs then takes place by a root growth mechanism.[23]
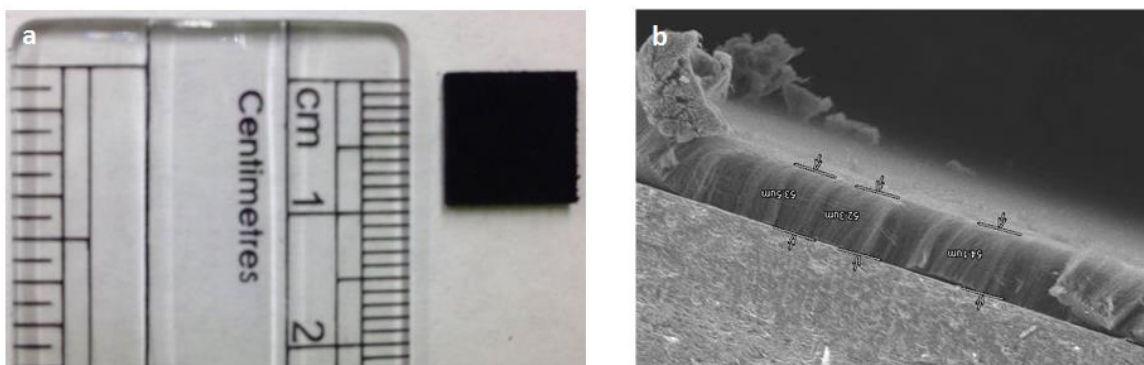
Figure 6. 8 (a) Photographic image of N-MWCNTs array, (b) SEM image of array of N-MWCNTs grown on quartz substrate.

The well-aligned arrays of nanotubes produced by this method were typically 55 to 66 μm in thickness, as shown in figure 6.8(b). Figure 6.8(a) is a photographic image of N-WMCNTs grown on 1×1 cm^2 quartz slides. The initial studies were carried out on nanotubes grown on 1×1 cm^2 quartz slides. However, for surface area analysis, 50-100 mg of sample is required, so for convenience this study was done using 2.5×2.5 cm^2 quartz slides of N-MWCNTs arrays. The one CVD batch typically generates sixteen 2.5×2.5 cm^2 quartz slides of N-MWCNTs arrays.

6.5   Growth mechanism

According to the most widely accepted CNTs growth mechanism, the synthesis of CNTs occurs in three steps.[33] In first step, the catalyst nanoparticles grow on the substrate, then in the second step hydrocarbon vapors decompose to form metal carbides as they come in contact with catalyst nanoparticles.[34] In the last step, carbon rapidly diffuses through the

metal and precipitates out as a crystalline graphitic structure in the form of tubes.[33] Kunadian et al. clarify the actual process of the growth mechanism; according to their findings CNTs growth does not occur in the vapor phase, but rather from catalyst nanoparticles that are first deposited on the substrate.[35] It is observed by many researchers that catalyst nanoparticles are mostly present at the tip or at the bottom of the tubes. The tubes growth process occurs via either a root growth or a tip growth process, depending upon substrate and catalyst used in synthesis of CNTs. In the root growth process, catalyst nanoparticles attach to the substrate with a firm interaction. Carbon diffuses through the catalyst and elongation of tubes occurs over the catalyst particle. According to Fan and his group, elongation of CNTs occurs by the extrusion of carbon from the bottom of tube, presumably between the particle and the grown tubes as shown in figure 6.9.[36,37] In contrast, in the tip growth process, nanoparticles have weak interaction with substrate, and the carbon diffuses through the catalyst and pushes the nanoparticles off the substrate.
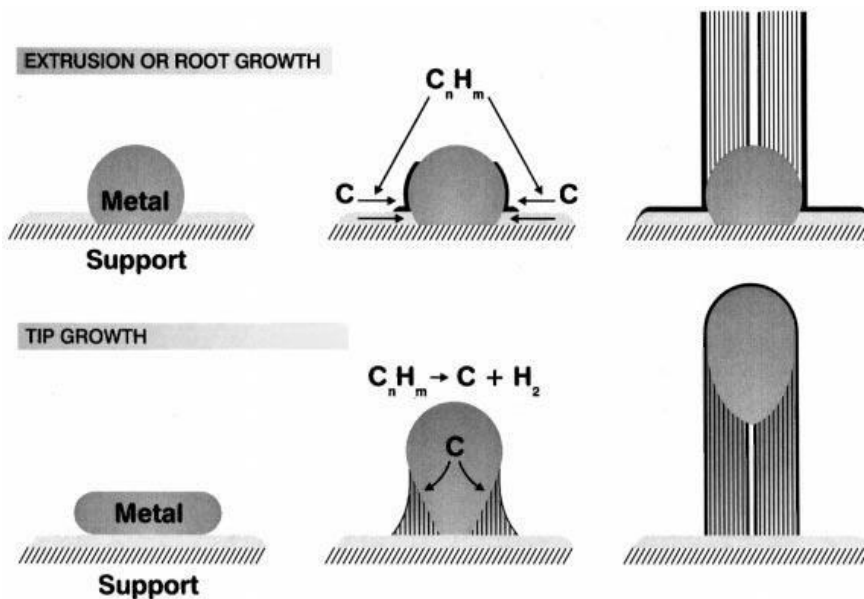
Figure 6. 9 Schematic representation of root growth and tip growth process in carbon nanotubes.[38] Image reprinted with permission from Reference.[39] Copyright 1999 Elsevier.

The morphological structure and properties of tubes produced depend on various factors like reactor size, reaction parameter, carbon feedstock, nature of catalyst nanoparticles and carrier gas.

6.6   Structure of N-MWCNTs
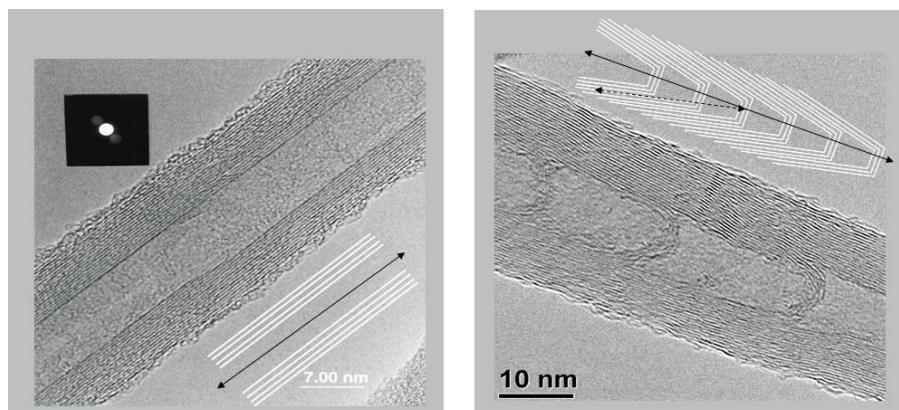
Figure 6. 10 TEM image of hollow, cylindrical tube (MWCNTs) and bamboo tube (N-MWCNTs).

The cylindrical MWCNTs shown in figure 6.10 was made from a hydrocarbon feedstock (xylene) containing ferrocene as a source of the Fe catalyst. The graphene planes in classical MWCNTs are parallel to the axis of the tubes. Unlike classical, cylindrical MWCNTs, the graphene planes of N-MWCNTs are not parallel to the longitudinal axis of the nanotube, and there are periodic compartments within the core (figure 6.10).[18] TEM images reveal that the outer surface of the N-MWCNTs is composed of a stack of graphene plane edges (as expected for 'nesting cups'). The origin of this morphology lies in the pyridine-ferrocene feedstock used in the CVD synthesis.[23,40]
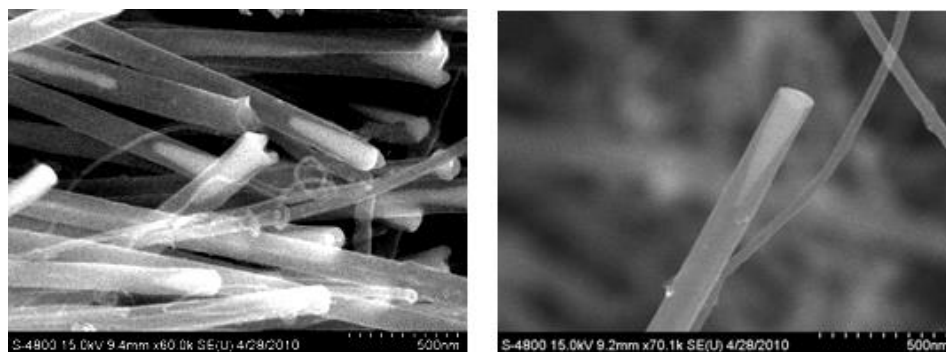
Figure 6. 11 Cone shaped catalyst at the root end of the N-MWCNTs.

Many researchers have reported that cone-shaped nanoparticles that are produced in first step of synthesis play a crucial role in the growth mechanism and morphology of the tubes.

The cone-shaped catalyst particles would be expected to produce nested cups of carbon.[13,40,41]

Furthermore, Lee el al. have proposed that nitrogen also plays an important role in changing the morphology of the tubes. The X-ray photoelectron spectroscopic (XPS) data indicates that nitrogen is present as a substituent of carbon in the nanotube's walls and not in the spaces between graphene layers.[42] The XPS results indicate the presence of three of the most important types of nitrogen present in N-MWCNTs: quaternary, pyridinic (sp^2 hybridized nitrogen) and pyrrolic nitrogen.
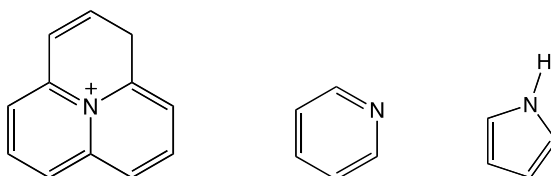
The concentration of pyrrolic nitrogen is greater than pyridinic nitrogen.[42] Pyridinic nitrogen is present at the edge of the graphene sheet as well as within the graphene sheet. Pyridinic nitrogen is sp^2 hybridized with a non-bonding pair of electrons in an sp^2 orbital oriented perpendicular to conjugated π system.[43] Pyridinic nitrogen generates holes within graphene sheets, which increases the flexibility of the sheet and decreases the strain in smaller diameter cylinders of graphene sheets.[43-45] It has been reported by Andrews and co-workers based on electron energy loss spectroscopy (EELS) elemental analysis that nitrogen concentration is higher within the inner shell of tubes and the outer shell contains a reduced amount of nitrogen.[23] Bitter et al. N-MWCNTs synthesize study reveal that concentration of nitrogen decrease with increase in reaction temperature.[46] The compartment size decreases as nitrogen concentration in feedstock increases. Furthermore, nitrogen changes the overall physical and chemical properties of the material, pyridinic nitrogens promotes the basicity and metallic behavior.[46,47]

6.7   Properties and Applications

CNTs have extraordinary electronic, physical, and optical properties because of this, they have beneficial value in electronic, material science, optics and technology. Apart from

this, their weight is extremely light, and they have astonishing mechanical properties. The recent advances in the production CNTs composite increase the potential for their use in application including bicycle frames, baseball bats, tennis racquets, and others.[6,48] CNTs coating on ship hulls act as anti-fouling.[49] CNTs are also used extensively in lithium ion batteries, microelectronic, biosensor and medical devices.

CNTs obtained from some synthesis processes are randomly oriented. Many researchers have put effort into orienting the CNTs vertically because vertical well-aligned CNTs appear to have numerous applications which may not be possible without alignment. Vertically-aligned CNT arrays have been extensively studied for various electron field emitter arrays,[50] thin-film transistors[51] and electronic applications.[52] Moreover, micropatterned array CNTs possess advantages for various multifunctional applications,[53,54] optoelectronic ultrasensitive label-free DNA analysis.[55] Polymer infiltrated, aligned arrays of CNTs have been also used to create a nanoporous membrane structures. Membranes have been proven promising for water purification,[56] gas separation, water desalination,[57] and sensing applications.[58]

6.8   Channeling of carbon nanotubes

Recently, many researchers have demonstrated techniques for unzipping of cylindrical CNTs to produce graphite nanosheets; the resulting graphene nanomaterial shows promise for applications in nanoelectronic devices.[59,60] Ci and Ajayan illustrated a method to cut the graphene sheet in a controlled manner.[61] In their method nickel nanoparticles deposited on graphite, cut the graphite sheet on high-temperature hydrogenation. According to their findings, unzipping of graphene sheets occurs along straight lines and the resulting nano-graphene sheets produced commonly have zigzag or armchair edges. Datta and co-workers have demonstrated the similar cutting process by thermally active metallic nanoparticles.[41] On other hand, the Tour group reported a method to produced oxidized nanoribbons by exfoliation of MWCNTs by $KMnO_4/H_2SO_4$ and thermal treatment.[62] In their $KMnO_4$ oxidation process, a manganate ester formed in first step further undergoes oxidization

reaction to produce a diketone, which eventually initiates linear longitudinal unzipping of the tubes. Dai and co-workers show a unique approach to making graphene nanoribbons (GNRs) by plasma etching, and similar work has done by Mohajerzadeh on unzipping of CNTs using oxygen and hydrogen plasma.[63,64] Terrones et al. have reported unzipping of nanotubes by thermal expansion of N_2 gas trapped within the hollow core of the tube.[65] Recently Hu and Chen group showed a clean unzipping method via steam etching process.[66] The unzipping and exfoliation of SWCNTs was achieved via direct current pulse and microwave-intercalation by Kim.[67] The sputter-etching method to convert part of SWCNTs into GNRs has demonstrated by Wee.[68] In 2008, our group reported the unzipping ("channeling") of nitrogen-doped multiwall carbon nanotubes (N-MWCNTs) by reductive alkylation using Li/NH_3 and further, in 2010 we reported linear and spiral forms of unzipping graphitized N-MWCNTs.[69,70] We have found that upon Birch reduction, deep fractures appear in the sidewall of N-MWCNTs, cutting deep enough to reach the inner core of the tube,[69] and running the entire length of the tubes. The mechanism for this unzipping by a reductive process is unclear.

6.9   Characterization of nanotubes

The conventional analytical techniques (NMR and mass spectroscopy) used to characterized organic compound are inadequately sensitivity to characterize CNTs. The characterization of CNTs seems to be very challenging because CNTs absorb across a broad range of the electromagnetic spectrum, and they are insoluble in most solvents. Lately, many methods available to characterized CNTs are classified in two categories: characterization of individual CNTs and characterization of bulk sample. Commonly used techniques for the characterization of individual nanotubes include scanning electron microscopy (SEM), scanning transmission electron microscope (STEM), scanning tunneling microscopy (STM), transmission electronic microscopy (TEM), energy dispersive x-ray spectroscopy (EDX), atomic force microscopy (AFM), photoluminescence spectroscopy, and electron energy-loss spectroscopy (EELS).[71,72] In all of the methods listed above, individual nanotubes are separated from bundles by ultra-

sonication. These methods are recommended for the measurement of length, diameter, surface coating, and the results of the channeling reaction. Another class of methods, useful for the characterization of bulk samples, are X-ray photoelectron spectroscopy (XPS),[73] infrared and Raman spectroscopy,[74] X-ray/neutron diffraction,[75] thermogravimetry[76] and BET surface area analysis.[69] Bulk characterization methods are helpful to determine impurities, chirality, helicity, functionalization, porosity, intershell spacing, and the extent of the channeling reaction. These characterization techniques have brought great improvements in the understanding the properties and chemistry of CNTs. Every method has its strength as well as its limitations, because of inhomogeneity and impurities present in the sample. Therefore, it is a good practice to use several of these techniques in complementary ways. In our studies we extensively used thermogravimetric analysis (TGA) and BET surface area analysis for bulk sample characterization and SEM/STEM spectroscopy for characterization of individual tubes.

6.10   Motivation

In N-MWCNTs, exposed graphene edges should provide access for lithium ions to intercalate between layers of graphene, and we hypothesize that the forces involved in lithium intercalation push apart gaps or seams in the graphene layers, producing the appearance of a 'channel' in the nanotube. If the fracturing process is driven by lithium intercalation and if lithium is not able to reach these sites, then the fracturing process should not occur, even if electrons are able to access the carbon.

In this study, we were interested in performing chemistry at only one the end of the tubes. If the unzipping reaction occurs only when one specific end of the tube is exposed, this will suggest the unzipping process is unidirectional. These observation will be extremely useful to understand the morphological structure of the tubes. Our finding provides some insight into the mechanism of the unzipping process, and provides evidence that the unzipping process has a directional preference- unzipping from the root end towards the tip end. In this overall process, we may be able to functionalization of

113

the interior of tubes selectively and create a new form of nanotube-based porous membrane.

CHAPTER 7. INVESTIGATION OF CHANNELING REACTION

7.1   Overview

CNTs produced by these different methods are normally packed in bundles because of weak Van der Waals bonding between them. The agglomerated bundles of CNTs are insoluble in most solvents and because of this, their utility in fundamental research and technological developments is restricted.[77] Several investigators have done considerable research into methods for functionalization and chemical modification of CNTs to enhance their dispersibility in common organic solvents.[78] It is important to note that functionalization of CNTs also helps in the exploration its utility in various applications like CNTs-composites, catalyst supports and sensors. The functionalization of CNTs by chemical modification using various derivatizing agents such as thionychloride/octadecylamine,[79] fluorination,[80] $H_2SO_4/HNO_3/HCl$,[81] 3-dipolar cycloaddition,[77][82] and reductive alkylation.[83] The functionalization preferentially occurs at exposed edges and at the defect sites.[84-86]

7.1.1 Birch reductive alkylation

The Birch reductive alkylation is a commonly-used method for functionalization of aromatic compounds.[87] In this method, the aromatic compound is reduced by lithium dissolved in liquid ammonia. The reduced aromatic compounds are then alkylated by treating with alkyl halide.
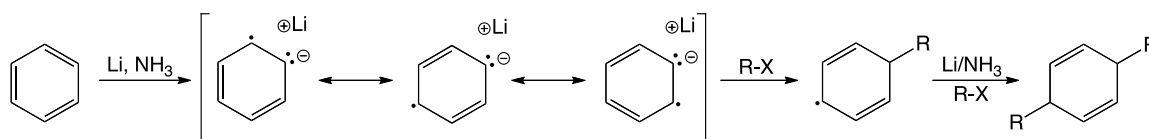
Figure 7. 1 Schematic representation of Birch reductive alkylation.

The carbon nanotubes entirely made from sp^2 hybridized conjugated carbon atoms are referred to as aromatic compound. Under Birch reductive conditions, carbon nanotubes are reduced to form polyanions as their lithium salts. Birch reductive functionalization of SWCNTs and MWCNTs have been reported by many researcher. [84-86]

Figure 7.2 illustrate SEM image of reductive alkylation of unzipped channeled N-MWCNTs.[69,70] The deep channel runs all the way from the outer wall to the inner core of the tube. The SEM and TEM images suggest that all the tubes in the sample have undergone the channeling reactions. The bulk-sample characterization methods like TGA and BET surface area analysis also confirmed that channeling reaction is not limited to a few nanotubes. SWCNTs and MWCNTs do not undergo channeling reaction under these conditions, whilst this key finding of unzipping in N-MWCNTs was highly exceptional.
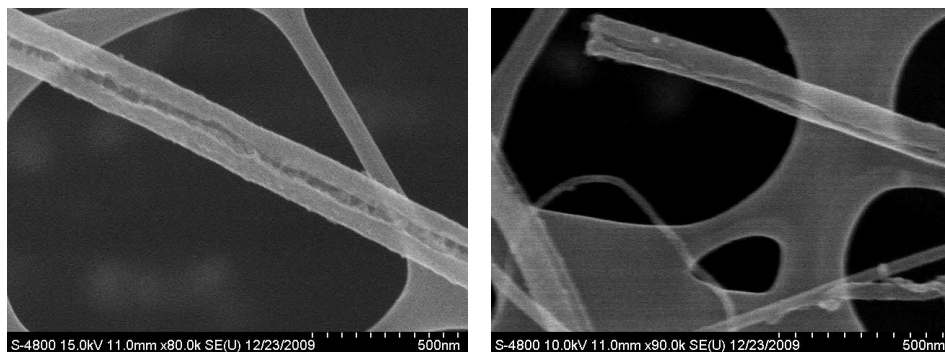
Figure 7. 2 SEM image of longitudinal cutting in N-MWCNTs after Birch reductive methylation.[88]

7.1.2 Graphite Intercalation Compound (GICs)

The insertion of an atom or molecule into interstitial graphene planes is a well-studied phenomenon. When treated with electron donor species like lithium, graphite gets reduced to form a charge transfer complex. Furthermore, graphite stabilizes the positively charged lithium by accommodating it between graphene sheets. The complex substance thus formed is called a graphite intercalation compound (GIC). The GICs is more specifically describe by stage number, this number is conveys how many graphite layers are separated from adjacent intercalated layers.

GICs have the general formula XC_y, where X is intercalant and y is number of carbon atoms. Various electron donor species like Na, K, Rb, Cs, Ba, Eu and Sm intercalate in graphite.[89] Similarly, a number of electron acceptor species like F, Cl, and Br also intercalate in graphite.[89,90] The amount of intercalation depends upon the ionization potential and the ionic radius of the intercalating element. Intercalation of alkali metals has been extensively studied by many researchers.[91,92] In solvent phase reaction, the solvent molecule (NH_3) also intercalates along with the intercalating metal ion.[91] After intercalation, the bond distance between carbons within a graphene sheet remains the same, but the graphene sheets spread apart.[93] It is also known that intercalation of electron donor atoms (K, Rb) into graphene layers increases its electrical conductivity.[20]

Multiwalled carbon nanotubes are commonly referred to as multi-rolled graphene sheets. The exposed graphene sheet edge could possibly be present only at the bottom end or at the top end of the tubes. However, the exposed edges are also presumably present at the site of structural defects. Henn et al. reports electrochemical intercalation of lithium into multiwalled carbon nanotubes, according to their finding, intercalation of lithium into the MWCNTs occurs through the defects.[94] Beguin and co-workers report intercalation of lithium into the less graphitized carbon nanotubes by high-pressure liquid-phase process.[95] The graphite intercalation compound undergoes thermal expansion on heating, and after cooling the graphite retains its original structure. The intercalation and de-intercalation in graphite is a reversible process, and the morphological structure remains unchanged.[93] However, in carbon nanotubes expansion may result in rupture of the nanotube structure. Recently, Vega-Cantu reports exfoliation of MWCNTs, in their process Li/NH_3 intercalated MWCNTs is treated with acid.[96] The author proposed that the exothermic reaction between acid and lithiated-MWCNTs results in exfoliation.[96]
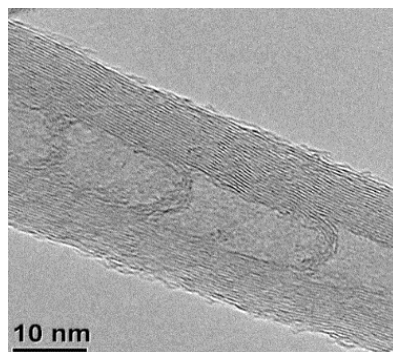
Figure 7. 3 TEM image of N-MWCNTs (Bamboo or nesting cups tubes).

TEM images (figure 7.3) illustrate that the outer surface of the N-MWCNTs is composed of a stack of graphene plane edges (as expected for 'nesting cups'). The MWCNTs has very few exposed graphene edges, as compared to N-MWCNTs. The exposed graphene edges should provide access for lithium ions to intercalate between layers of graphene, and we hypothesize that the forces involved in lithium intercalation push apart gaps or seams in the graphene layers, producing the appearance of 'channel' in the nanotube. Figure 7.4 illustrate possible mechanism for channeling process.
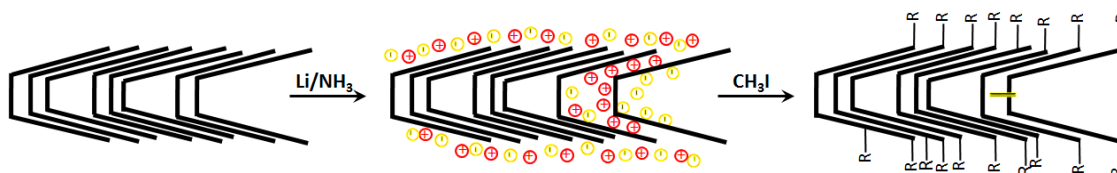
Figure 7. 4 Schematic representation intercalation of lithium in interstitial spaces between graphene layers.

7.2 Experiment designed to investigation of the channeling reaction

7.2.1 Materials

Methyl methacrylate (MMA, contains ≤30 ppm MEHQ as inhibitor, 99%), 2, 2′-azobis(2-methylpropionitrile) (AIBN, 98%) and 1-decanethiol (96%) were purchased from Sigma Aldrich and used without purification. All other bulk solvent were purchased from Pharmco Aaper and used without further purification. Polyethylene adhesive-back film

(UHMW, 0.042 inch thick) was purchased from McMaster-Carr and adhesive tape (3M Co) was purchased from an office supplies company.

7.2.2 Overview

It is difficult to rationalize the observed 'unzipping' process if the underlying carbon morphology is truly that of nested cups, so it seems likely that these fractures are the result of a physical (mechanical) process rather than the result of a purely chemical process. If the fracturing process is driven by lithium intercalation and if lithium is not able to reach these sites, then the fracturing process should not occur even if electrons are able to access the carbon.

The anisotropy of N-MWCNTs offers the opportunity to test this hypothesis. As shown in figure 7.5, coating N-MWCNTs in polymer with only the tips exposed would permit electrons to reach the carbon but prevent lithium ions from reaching the core or the interstitial spaces between layers. Alternatively, if N-MWCNTs are coated such that only the root (catalyst) end is exposed, then electrons can reach the carbon and lithium ions can reach both the interlayer spaces and the core of the nanotube.
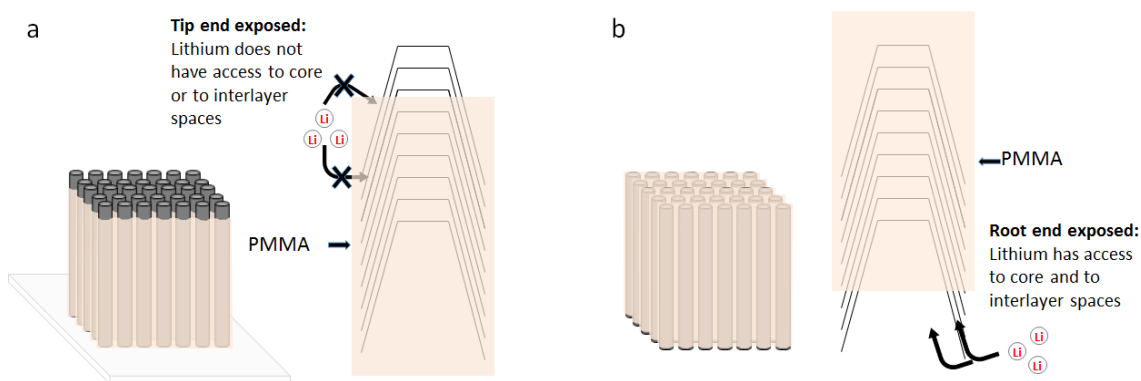
Figure 7. 5 Schematic illustration of the use of polymer-filled N-MWCNT arrays. (a) tip ends exposed, (b) root ends exposed.[88]

The anisotropy of N-MWCNTs offers the opportunity to test this hypothesis. As shown in figure 7.5, coating N-MWCNTs in polymer with only the tips exposed would permit electrons to reach the carbon but prevent lithium ions from reaching the core or the interstitial spaces between layers. Alternatively, if N-MWCNTs are coated such that only

the root (catalyst) end is exposed, then electrons can reach the carbon and lithium ions can reach both the interlayer spaces and the core of the nanotube.

7.2.3 Process to remove amorphous carbon from topmost surface of as produced N-MWCNTs array

Figure 7.6, SEM images of the as-produced arrays show amorphous carbon particles were present on the topmost surface of the tubes, and the tips of the nanotubes were not visible under this crust. Removing this amorphous carbon was essential so that we can perform chemistry on the top ends of the nanotubes alone.
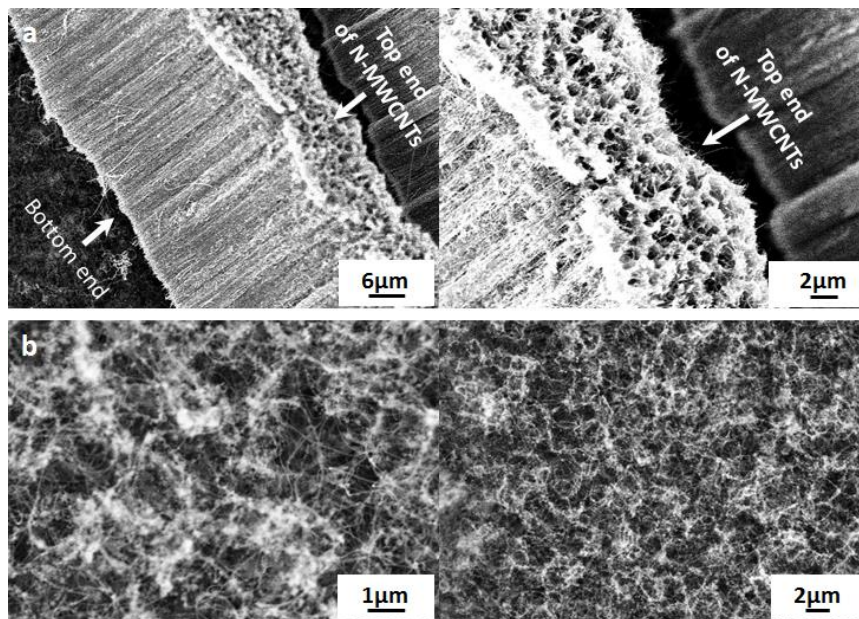
Figure 7. 6 SEM images (a) cross section of array as-produced N-MWCNTs array, (b) topmost surface of as produced N-MWCNTs array.[88]

Recently, Qu, *et al.* published a simple technique to remove CNTs from an array selectively.[97] We used this technique to clean the top surface of N-MWCNTs. The array of tubes (on the quartz substrate) was fixed to a glass slide with the help of double-sided tape. Amorphous carbon was removed from the top surface of the array by repeatedly applying and removing adhesive tape as shown in figure 7.7.
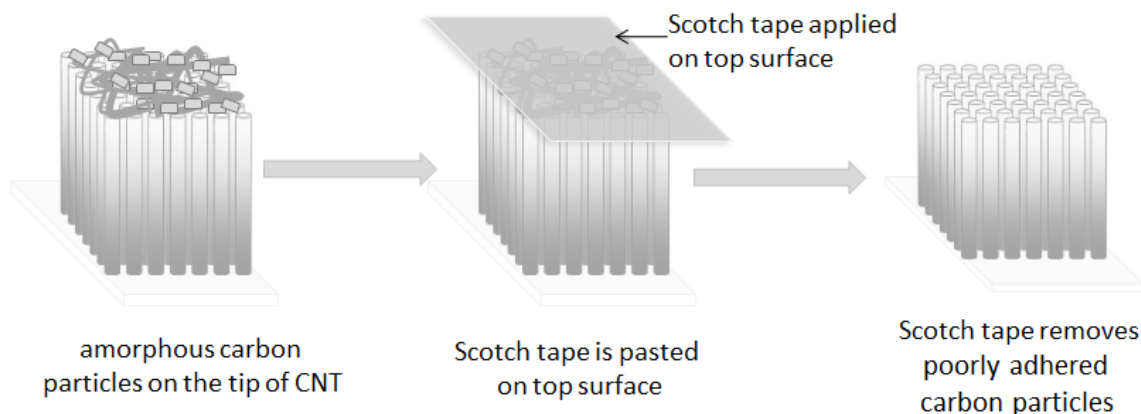
Figure 7. 7 Schematic representation of cleaning amorphous carbon particles from the topmost surface of the tubes.

When the tape was removed, poorly adhered carbon particles (and a few carbon nanotubes) were removed. After repeating the process seven times, the carbon debris from the surface was almost completely eliminated. SEM images of the top ends were taken after this process, and these images (Figure 7.8) indicate that the number of carbon particles was significantly reduced after every step. We found that repeating this step for 7 times remove almost all of the debris from the surface. This technique is very selective, as the adhesive surface of the tape removes weakly adhered material and the N-MWCNTs remained intact. In this process, few nanotubes removed are not concerned.
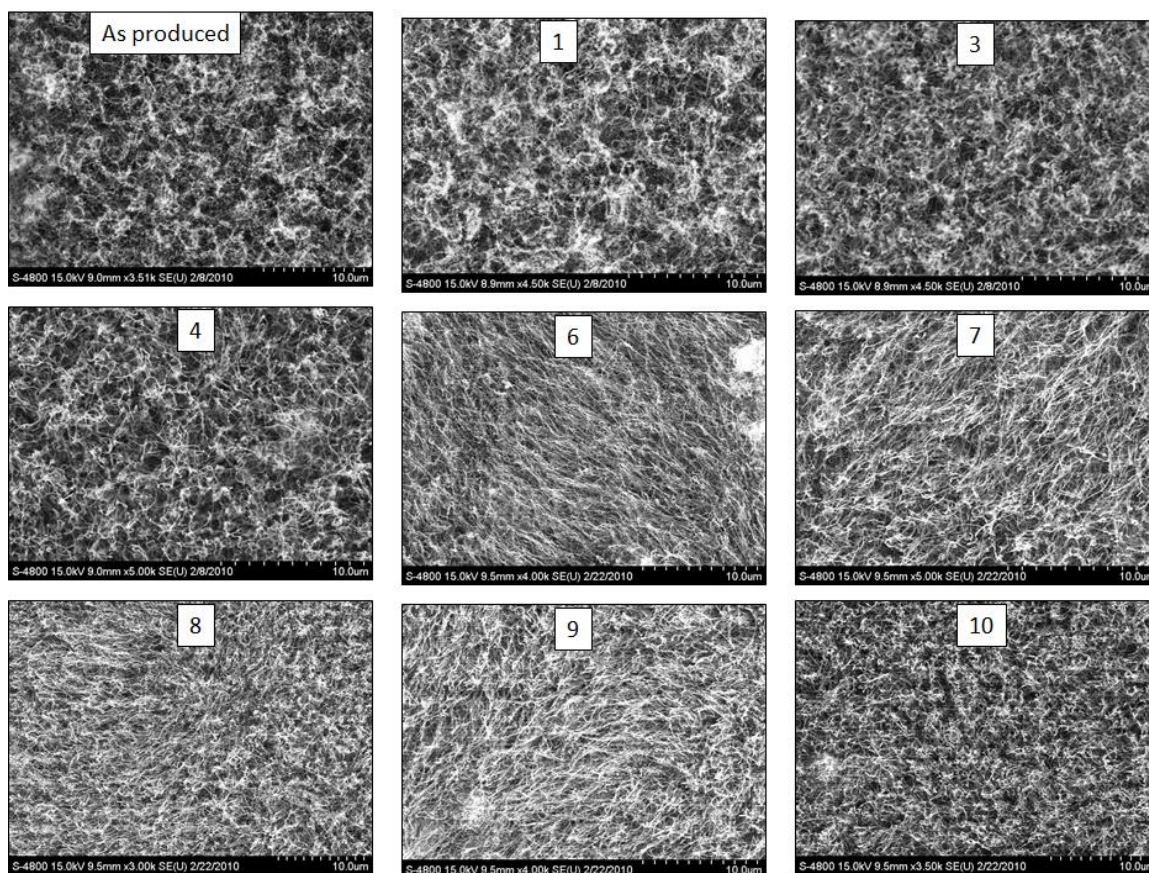
Figure 7. 8 SEM image of top surface of N-MWCNTs array after each cleaning step to amorphous carbon with scotch tape.

7.2.4 Process to infiltrate poly(methyl methacrylate) (PMMA) into interstitial spaces between N-MWCNTs array

The key to being able to conduct chemistry on either end of the nanotubes, but not in the middle, was the ability to prepare polymer-filled arrays, then to expose one end of the nanotubes without exposing the sidewalls. In the infiltration process, the polymer filled the interspatial space between the CNTs and wrapped around the tubes to form a protective coating. Different CNTs-coating methods have been reported in literature. Some of the well-known methods are spin-based methods, vacuum-based methods, dip-coating methods and in-situ polymerization methods. Linda Schadler and her coworkers reported the process for infiltration by in-situ polymerization.[98] Mijangos reports polymer

122

infiltration of nanofibers and nanotubes by three different methods: wetting-based methods, vacuum-based methods, and spin-based methods.[99]

Dip-coating method: We initially attempted to coat N-MWCNTs array by PMMA using dip-coating method. In the dip-coating process,[100] the array of N-MWCNTs was dipped in solution of PMMA and toluene for 8 hrs at 80 °C. The PMMA coated N-MWCNTs array was allowed to dry at room temperature for 4 hrs and then dried in vacuum oven for 8 hrs at 55 °C. We performed coating using different concentration of PMMA from 10 to 40%.
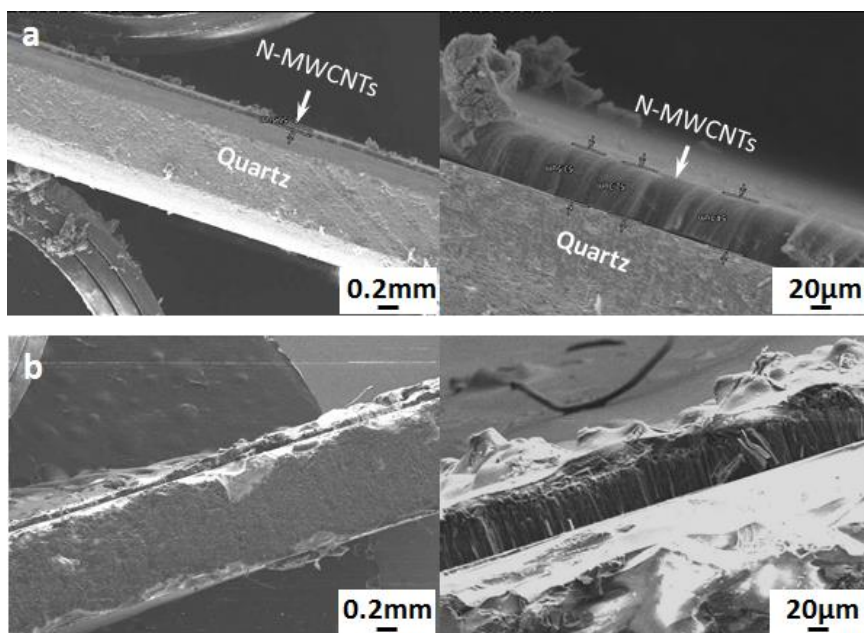
Figure 7. 9 Cross-sectional SEM image of (a) as produced N-MWCNTs, (b) PMMA infiltrated N-MWCNTs by dip-coating.

We found that when dilute PMMA solution was used interspatial space between the CNTs was not completely filled. Furthermore, on using concentrated PMMA solution uneven PMMA-layer was formed on the top surface, as shown in figure 7.9(b).

Spin-coating method: Hinds group carried out infiltration of MWCNTs with polystyrene using the spin-coating method.[58] In the spin-coating method, the polymer solution is applied on the center of the substrate, and the substrate is revolved at high speed. As the substrate rotated the polymer solution drew away from the center because of centrifugal force, which result into forming a uniform coating. Figure 7.10 shows SEM image of N-

MWCNTs after spin coating. In spin-coating method, we had similar difficulties as we have in a dip-coating process.
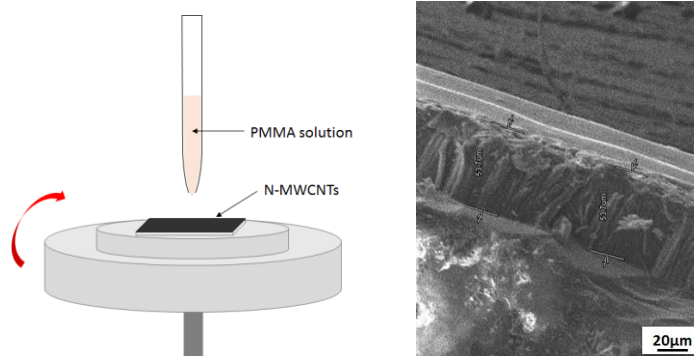
Figure 7. 10 Schematic representation of spin coating process and infiltration of PMMA in N-MWCNTs by spin-coating.

In-situ Polymerization process: To accomplish this, N-MWCNTs arrays were infiltrated with PMMA by an in-situ polymerization technique.[98] In order to prepare PMMA infiltrated N-MWCNTs arrays without a large excess of polymer covering the top of the array, we fabricated an ultra-high-molecular-weight polyethylene (UHMWPE) spacer as shown in a figure 7.11(a). The self-adhesive polyethylene sheet was affixed to a glass slide, and then an N-MWCNTs array on the 1 x 1 inch substrate was placed at the center of the spacer. Another glass slide was placed on top of the spacer, and the entire assembly was clamped together with small metal binder clips. The assembly was placed in specially designed wide mouth vessel equipped with a provision for a vacuum adapter and a ground glass joint. The apparatus was then evacuated to remove air between the slides, including the air trapped in the spaces between of the tubes. The space between the glass slides was filled with the mixture of methyl methacrylate (MMA) monomer, azobisisobutyronitrile (AIBN, initiator) and 1-decanethiol (chain transfer agent).[98] The top opening was sealed, and whole assembly was heated in an oven at 55°C for 24 hrs. After cooling, the metal clips were removed and the top glass slide was removed. A hot cutter was used to remove the polymer from around the array. The thickness of the membrane was measured by SEM imaging, as illustrated in figure 7.12

(a)

(b)
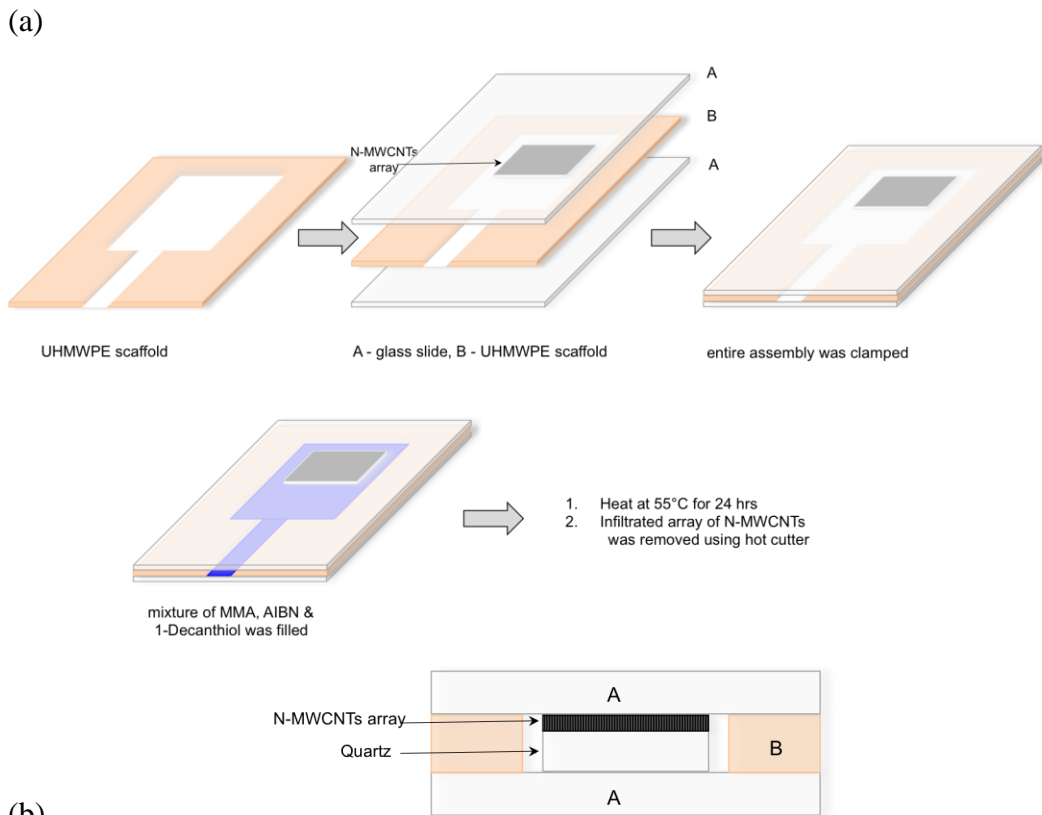
Figure 7. 11 (a) Schematics of representation of the infiltration process, (b) cross-section of entire assembly.[88]
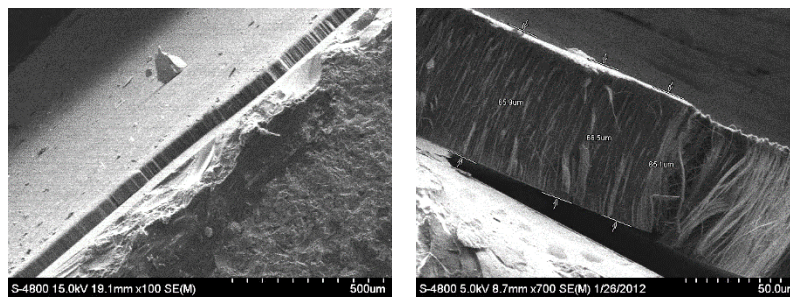
Figure 7. 12 SEM images of the edge of arrays of N-MWCNTs that have been infiltrated with PMMA.[88]

7.2.5 Birch reductive methylation and removal of polymer

Anhydrous liquid ammonia was condensed in the 250 ml three neck round bottom flask using Dewar condenser and dry ice-acetone under nitrogen atmosphere. Lithium metal (high sodium granules, 99%, Aldrich) was added and stirred for 10 min. The stirring was then stopped and a 1 cm square array of N-MWCNTS, clipped to stainless

125

steel wire, was immersed the dark blue liquid ammonia/lithium solution. After immersion for half an hour, the array was lifted from the solution and quenched with iodomethane (99+%, stabilized with copper). The resulting N-MWCNTs were then washed with water, ethanol and methylene chloride. The N-MWCNTs were then removed from the quartz substrate by scraping with sharp razor blade. The polymer around the tubes was removed by refluxing the nanotube-polymer composite in toluene, then hot vacuum filtering the resulting suspension through a nylon membrane filter membrane. This was repeated three times to remove the PMMA completely from the sample. N-MWCNTs were dried in vacuum oven for 24 hr at 55 °C.

7.3   Exposing the top end of nanotubes array to Li/NH$_3$

The last step required for exposing the top of the nanotubes within the array was to remove the thin layer of polymer covering the top of the array (figure 7.13) without removing the polymer covering the walls of the nanotubes.

| As-produced | Amorphous carbon | Infiltrated with | Polishing & plasma oxidation, | Birch reductive |
| N-MWCNTs array | removed | PMMA | tip ends exposed | methylation |
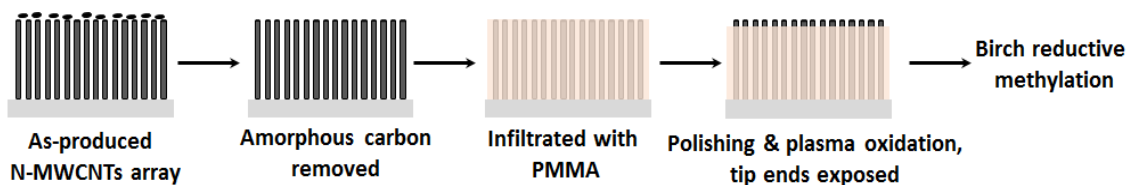
Figure 7. 13 Schematic illustration of the key steps involved in infiltration of polymer into interstitial spaces between N-MWCNTs in the array and exposing top ends of the tubes to performed chemistry on the open ends alone.[88]

The polymer layer on the top surface was reduced in thickness by gently polishing with 2000 grit sand paper, and the last bit of polymer was removed by H$_2$O plasma etching. The rate of etching was established by measuring etching rate of PMMA sheet, so we were able to etch down to a point where nanotube tops protrude from the polymer-infiltrated array. The figure 7.14(a) is top view SEM image of infiltrate N-MWCNTs after polishing. The image illustrate that tubes are completely coated with PMMA after polishing, however after plasma etching the polymer is removed and top ends of the tubes are again exposed.

The resulting tubes walls are completely coated with PMMA, only top end are exposed to performed the necessitate chemistry.
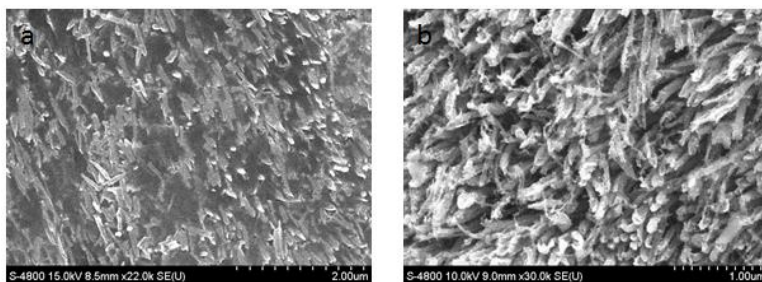
Figure 7. 14 SEM images (a) topmost surface after polishing the infiltrated N-MWCNTs, (b) topmost surface of polished infiltrated N-MWCNTs after 20 min H_2O plasma oxidation.[88]

7.4 Exposing bottom end of N-MWCNTs

Figure 7. 15 Schematic illustration of the key steps involved in infiltration of polymer into interstitial spaces between N-MWCNTs in the array and exposing bottom ends of the tubes to performed chemistry alone.[88]

To prepare an array where only the bottom (root) ends of the nanotubes are exposed, we infiltrated N-MWCNT arrays as shown figure 7.11(a), then separated the intact, infiltrated array from the quartz substrate with a sharp razor blade. The substrate was carefully remove from the substrate as often membrane breaks into pieces. SEM images of the bottom (substrate) side of the array shows the root ends of the nanotubes, with the catalyst particles remaining from the synthesis (figure 7.16).
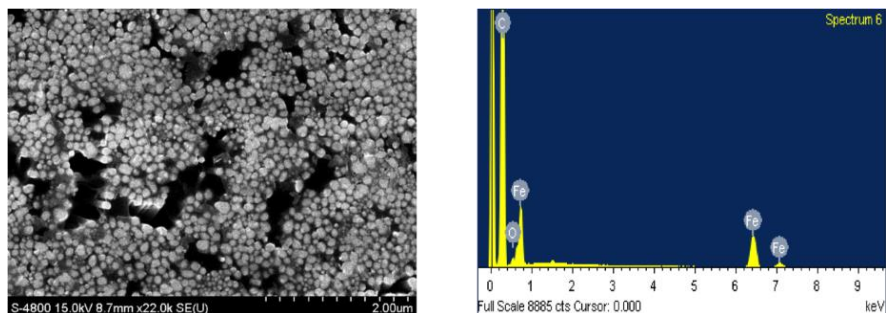
Figure 7. 16 SEM images of bottom end of the N-MWCNTs and corresponding EDX spectra of element present.

Element analysis on this surface was carried out by energy dispersive X-ray spectroscopy (EDS), and these results are consistent with iron particles filling the ends of the nanotubes. EDS data obtained by JEOL 2010F field-emission TEM. The absolute levels of each element from EDS are not accurate, these results gave us a rough idea about element present.
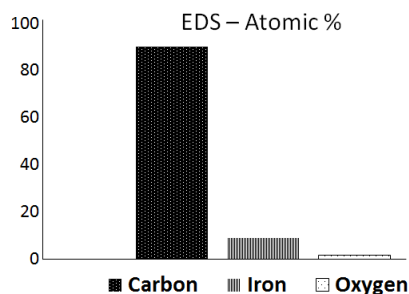
Figure 7. 17 Atomic percentage of element present at bottom end of the N-MWCNTs from EDS analysis.[88]

Figure 7.17 shows the atomic % of element present at the end of the nanotubes. These EDS results confirm that iron content is 9.17%. We were able to remove these catalyst particles by treating the infiltrated array with 5% HF solution. The PMMA infiltrated array of N-MWCNTs array was immersed in 5% HF solution for 8Hrs and dried in vacuum oven. Figure 7.17 shows an SEM image of the bottom (substrate) side of the array after HF treatment, and the image reveals that the catalyst particles have been removed from the bottom end of the tubes.
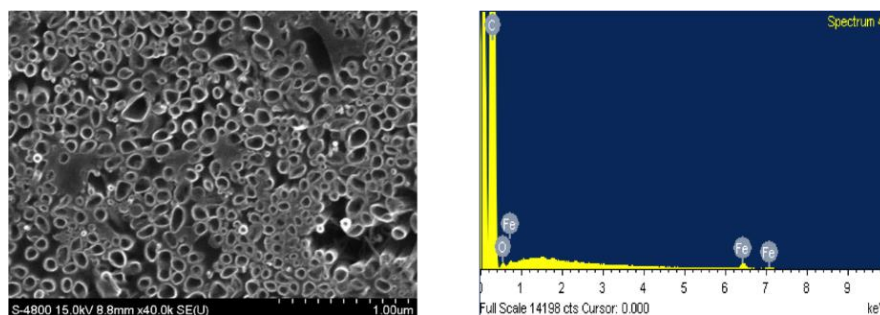
Figure 7. 18 SEM images of bottom end of the N-MWCNTs after HF treatment and corresponding EDX spectra of element present.
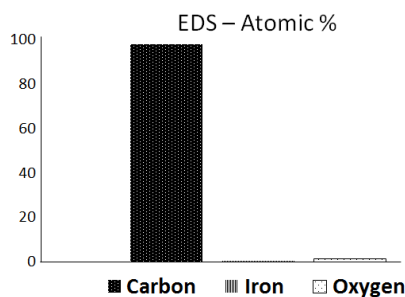
Figure 7. 19 Atomic percentage of element present at bottom end of the N-MWCNTs after HF treatment from EDS analysis.[88]

EDS results after the HF treatment show only a small amount (0.5 %) of iron remaining after HF treatment. After tubes are treated with HF solution, only the bottom end is exposed for intercalation of lithium between layers of graphene. On other hand when catalyst particle is intake to the bottom end, the electron will able to access the carbon but lithium will not intercalate. Each of these arrays (tip end exposed and root end exposed) was subjected to Birch reductive methylation in liquid ammonia, followed by quenching with methyl iodide.[69]

CHAPTER 8. CHARACTERISATION OF CHANNELING REACTION

8.1   Results and discussions

The individual tubes were characterized by SEM and STEM spectroscopy. The bulk samples were analyzed by thermogravimetric analysis and surface area analysis. The N-MWCNTs produced from different batches can have different diameters and radii. Likewise, the decomposition temperature and the surface areas of the samples from different batches are not necessarily identical. The initial set of experiments were characterized by SEM and TGA analysis, as only a few milligrams of sample are required for analysis. The analysis of the channeling reaction were characterized by SEM and TGA analysis many time. However, bulk characterization methods, particularly by BET surface area analysis, were used to provide independent confirmation. BET surface area analysis was repeated twice, using N-MWCNTs produced from two different batches. For surface area analysis, 50-100 mg of sample is required for better precision. The surface area comparison of N-MWCNTs produced from single batch has been used to carry-out all four sets of experiments.

8.2   Thermal analysis

The oxidation of diamond, fullerenes, as well as carbon nanotubes, has been well studied by thermogravimetric analysis (TGA) in past decade.[101] In this method, a sample is heated at a constant rate under an argon, nitrogen, air, or O_2 atmosphere, and the change in mass is monitored as the function of temperature. Carbon nanotubes decomposed at lower temperature in an O_2 atmosphere than in an inert gas atmosphere, and the decomposition process in the O_2 atmosphere is largely simple combustion. In this oxidation process, carbon nanotubes are combusted to CO_2. The TGA analysis of carbon nanotubes reveal important information about impurities presents, the oxidative stability of the material, and the residual mass due to impurities. The impurities present may result from amorphous

carbon or from foreign materials used in chemical processing of the CNTs. The combustion temperature represents the thermal stability of the CNTs, and the residue mass largely represents the catalyst nanoparticles used while synthesizing the tubes. The width of the oxidation peak reflects the inhomogeneity of the sample - a single sharp mass loss suggests homogeneity in the sample. TGA analysis is used to study changes in the physical or chemical properties of the modified CNTs, and has proven to be very useful. Annealed CNTs decomposed at higher temperature in air, because annealing results in fewer defect sites and higher crystallinity of the tubes is improved. Functionalized CNTs usually have two or more stages of degradation, including a low-temparature degradation stage that results from decomposition of functional groups. It has also been reported that the catalyst particle present in the CNTs does not significantly affect the combustion temperature of the CNTs.[76,102] Some researcher have also studies effect of tubes diameter on the combustion temperature.[102] Nanotubes obtained from different batches do not exactly coincide with each other. Therefore we endeavored to ensure that all comparisons are between nanotubes from the same batch, but the results obtained agree with results from all other batches.

TGA was performed using a TA TGA Q5000 thermogravimetric analyzer, 4-7 mg of samples were analyzed in platinum pans with a standard heating rate of 10°C/min from ambient temperature to 800°C. The oxidative stability of different N-MWCNTs samples were studied by thermogravimetric analysis (TGA) under air atmosphere.
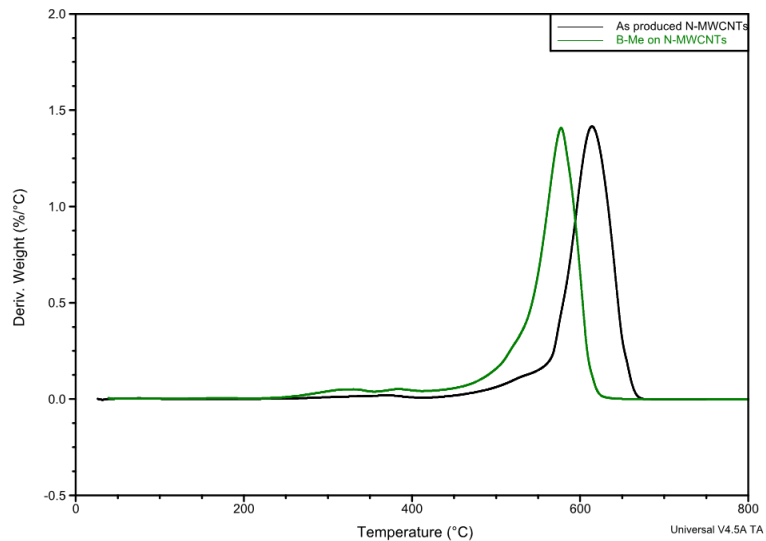
Figure 8. 1 Thermogravimetric curves for (a) as produced N-MWCNTs — black line, (b) Birch reductive methylated N-MWCNTs (B-Me N-MWCNTs) — green line.

The TGA of as-produced and B-Me N-MWCNTs (figure 8.1) shows that as-produced N-MWCNTs decomposed at 625 °C and channeled N-MWCNTs decomposed at lower temperature (575 °C). These results suggested that after channeling reaction, tube become thermally less stable.
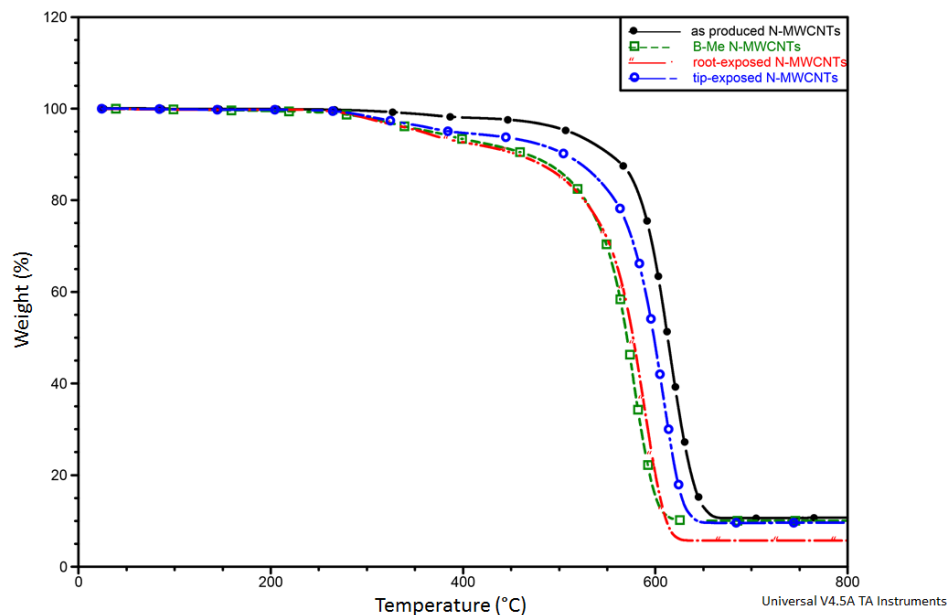
Figure 8. 2 Thermogravimetric curves for (a) as produced N-MWCNTs — black line, (b) Birch reductive methylated N-MWCNTs (B-Me N-MWCNTs) — green line, (c) Birch reductive methylated N-MWCNTs exposed bottom end alone (BB-Me N-MWCNTs) — red, (d) Birch reductive methylated N-MWCNTs exposed bottom end alone (TB-Me N-MWCNTs) — blue[88]

Figure 8.2(a) shows that oxidation of as-produced N-MWCNTs occurs between 550 to 650°C, while figure 8.2(b) shows that nanotubes that have been subjected to Birch reductive methylation (without polymer coating) have a combustion temperature from 500-600°C. Under the conditions of Birch reduction, channels are formed in these unprotected nanotubes and not surprisingly, the nanotubes become thermally less stable in air. The residual weight of channeled tubes is ~3% less than it is in as-produced tubes, and this is likely to be the result of partially removal of catalyst particle in reduction step. Evidence that complete coverage of N-MWNTs by PMMA completely prevents the unzipping process was provided by analysis of an array where the nanotubes were completely covered by polymer. This array was subjected to the Birch reductive methylation, and after the nanotubes were liberated from the polymer, TGA analysis reveals that they behave in essentially identical manner to as-produced, intact nanotubes. This provides evidence that the PMMA coating protects the nanotubes from the reaction mixture. In addition, this result demonstrates that the formation of the PMMA-infiltrated array does not modify the nanotubes and change their nature. Further, birch reductive methylation of infiltrated N-

133

MWCNTs membrane after peeling off from the quartz demonstrate no channeling reaction. From this result it is presumably seen that catalyst particle inhibits lithium intercalation into interstitial spaces between nanotube graphite layers. In order to remove the catalyst particle, infiltrated tubes were treated with 5% HF solution. Figure 8.2(c) shows the TGA of root-exposed N-MWCNTs and the combustion temperature is very similar to that of unzipped tubes. This result suggests that nanotubes where only the root end is exposed unzip to the same extent as completely uncoated N- MWNTs. In bottom end exposed experiment (BB-Me N-MWCNTs) catalyst from the bottom of the tube was removed by HF treatment. Because of this catalyst from entire tube reduce to 5%. However, the TGA of tip-exposed N-MWCNTs has combustion temperature between 525-625°C, which is intermediate between the fully unzipped material (Birch reduced uncoated N-MWCNTs) and completely unmodified, as-produced N-MWNTs.

8.3   BET surface area

Carbon nanotubes have been extensively used as a support for heterogeneous catalysis, anodes in Li-ion batteries and for gas storage. For all these applications the study of specific surface area as well as distribution of pores is often measured using Brunauer-Emmett-Teller (BET) isotherm. In our work, BET surface area has proven to be a useful tool for investigating the extent of the channeling reaction. As produced N-MWCNTs happened to have few defects and mesoporosity, therefore, total surface area of the tubes is relatively less. However, when these nanotubes undergo the Birch Reduction-triggered channeling reaction, the inner surface is exposed and this results in an increase in total surface area of the tubes. Like TGA, nitrogen physisorption is another quantitative measurement technique.

In our study, the surface area of N-MWCNTs was determined via nitrogen physisorption using an ASAP 2020 V3.00H analyser. The BET model was used to calculate surface areas and pore size distributions. Degassing was done by heating the sample under vacuum for 24 hrs at 250 °C. The degassing is done to remove physically adsorbed gas,

moisture or any adsorbed contaminants that might be present on the surface. After degassing, the sample is again weighed accurately, and further surface area analysis was carried out at 77 °K, by immersing sample probe into liquid nitrogen. In BET analysis, the quantity of nitrogen multilayer adsorption on the surface of the solid sample is calculated as a function of the relative pressure from adsorption isotherm using the BET equation.

In past, the nitrogen physisorption and desorption method has been widely used to study the surface area of carbon nanotubes.[103] However because of the tendency for carbon nanotubes to form bundles, the measured surface area of nanotubes is imprecise.[104,105] Cukierman and co-workers have studied the effect of N-MWCNTs alignment on N_2 adsorbed isotherm. The study reveals that well-aligned MWCNTs has higher surface area then sonicated dispersed tubes. The tubes randomly orient over each other on ultra-sonication, due to which interstitial space between tubes as well as surface area decreases.[105,106] In order to minimize experimental error we treated all samples identically. Figure 8.3 show N_2 adsorption-desorption isotherms plot of volume of N_2 adsorbed per unit mass of adsorbent against relative pressure (P/P°), where P is the equilibrium pressure and P°, the saturation pressure of the adsorbate at standard temperature and pressure.
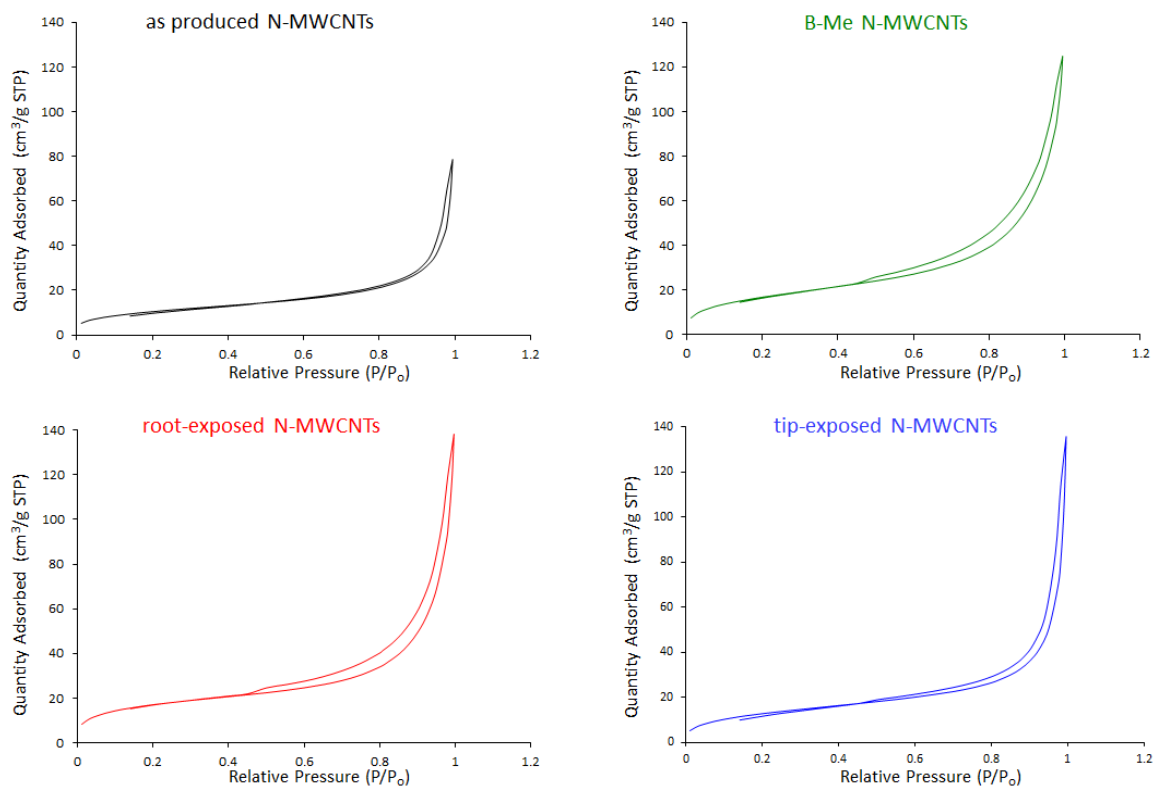
Figure 8. 3 N_2 adsorption–desorption isotherms of the (a) as-produced, (b) B-Me N-MWCNTs, (c) root-exposed N-MWCNTs and (d) tip-exposed N-MWCNTs.

An N_2 adsorption isotherm of as produced N-MWCNTs (Figure 8.3(a)) corresponds to the type II isotherms, as shown quantity of adsorption rises gradually with increase in relative pressure from 0.05 to 0.994, and at low relative pressure quantity of adsorption is negligible because of insignificant amount of microporous. The adsorption from 0.05 onwards resulting from mesoporous and macroporous pore. In N_2 adsorption-desorption isotherm of B-Me N-MWCNTS, desorption curve deviate from adsorption curve from $P/P°=1$ to $P/P°=0.44$, and again merge with adsorption curve. The N_2 adsorption isotherm of channeled N-MWCNTs show hysteresis loop between 0.4 to 0.5 $P/P°$ corresponds to the type IV isotherms. Similarly, the isotherm of root-exposed N-MWCNTs is identical to completely channeled tubes, the isotherm results shows agreement with TGA results. Although, isotherm of tip-exposed N-MWCNTs does not have hysteresis loop, the adsorption-desorption curve is not identical to as-produced N-MWCNTs

136

Table 8. 1 Comparison of surface area and porosity of different N-MWCNTs.

Sample BET	Surface Area m2/g	% Mesoporosity	% Macroporosity
As produce N-MWCNTs[a]	37.9	40.2	59.1
B-Me N-MWCNTs[a]	64.5	74.7	25.3
BB-Me N-MWCNTs[a]	64.9	60.4	39.3
TB-Me N-MWCNTs[b]	56.1	44.4	55.6

Note: a — average of 2 runs, b — average of 4 runs
[#]Surface area of tip-exposed N-MWCNTs is an average of 4 runs (1st and 2nd runs used small samples and as such were subject to greater experimental error). Actual measurements: 68.1, 65.0, 47.1, and 44.2 m^2/g, % Mesoporosity: 47.3, 51.5, 38.0, and 40.7.[88]

IUPAC segregates porous materials into three categories. The classification is based upon the size of the pores: the pore diameter of mesoporous material is greater than 50 nm, macroporous material between 2 nm to 50 nm and microporous less than 2 nm. Pore size distribution is another bulk-sample characterization that provides information on the extent of unzipping is surface area analysis. The surface area of as-produced N-MWCNTs was found to be 37.9 m^2/g (BET model), whereas Birch reduced (unzipped) N-MWCNTs surface area was found to be 64.5 m^2/g. Similarly, the fraction of mesopores of unzipped N-MWCNTs increases from 40.2% to 74.7%. The surface area and mesoporosity data on N-MWCNTs from infiltrated arrays suggest that root end exposed N-MWCNTs suffer complete unzipping in essentially the same manner that uncoated N-MWCNTs, but tip exposed N-MWCNTs undergo only a partial unzipping reaction, consistent with the TGA results, above.

8.4   SEM image
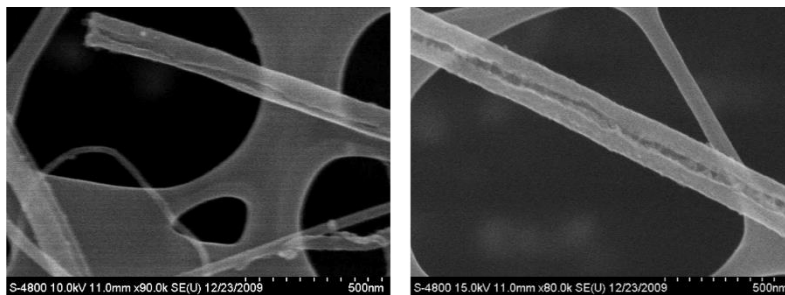
Figure 8. 4 SEM image of longitudinal cutting in N-MWCNTs after Birch reductive methylation of (a) as-produced tubes, (b) after Birch reductive methylation with tip end exposed only.

Microscopy was performed using a scanning electron microscope (SEM) Hitachi S-4800 operated at 5-15 kV. SEM results (figure 8.4) further confirmed that when bottom end of tubes is exposed to Li/NH_3 followed by alkylation, the complete unzipping reaction occurs and nearly all tubes display longitudinal cut that are essentially identical to the cuts formed in dispersed, as-produced N-MWCNTs that were not coated in polymer.

In other words, *channeling occurs with equal efficiency when only the bottom end is exposed as when the entire nanotube is exposed* (figure 8.5). On other hand, when only the top end of the tubes are exposed to Li/NH_3 followed by alkylation, only few tubes undergo the channeling reaction, and those are only channeled for part of the length. These SEM results are in agreement with surface area and TGA results. Taken together, these results indicate that the unzipping of N- MWCNTs under the conditions of Birch reductive methylation (Li in anhydrous NH_3) occurs preferentially from the root end where there is easy access to the interstitial spaces and the core of the nanotube. This conclusion strongly supports the notion that the unzipping process is driven by intercalation.
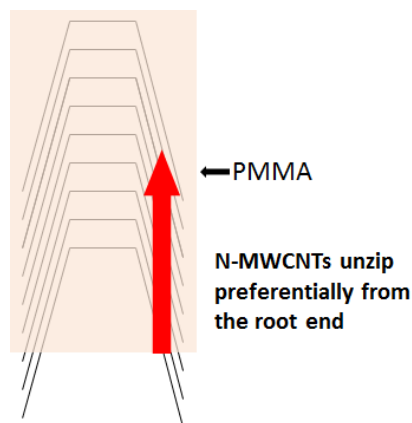
Figure 8. 5 Model for unzipping process when only the bottom ends are exposed.[88]

The partial unzipping of tip exposed N-MWCNTs is likely due to imperfections in the top surface of the array. Removal of the amorphous carbon, polishing off excess PMMA, and plasma oxidation of the remaining surface coating of polymer could result in the formation of occasional gaps and breaks in the polymer, permitting the Li/NH$_3$ reaction mixture to come into contact with the sidewalls of some of the N-MWCNTs. As a result, some of the nanotubes from those samples are unzipped as far down into the array as the reaction mixture could reach, resulting in a sample where some of the nanotubes are unzipped and some are not.

CHAPTER 9. CONCLUSIONS

9.1 Conclusions

In summary, we demonstrate that arrays of N-MWCNTs grown on quartz and disengage free N-MWCNTs substrate behave identical to under Birch reductive condition, such that they both undergoes channeling reaction under Birch reductive conditions. We have established a method for the preparation of PMMA-infiltrated arrays of aligned N-MWCNTs membrane, such that the thickness of the membrane obtained is exactly 66 μm. Our in-situ method, use to prepare PMMA membrane prove to be versatile that spin-coating and dip-coating method, as interstitial space between N-MWCNTs array is properly filled with PMMA. And PMMA coated tubes does not undergoes channeling reaction under Birch reductive condition. We demonstrate an excellent method to remove amorphous carbon from the topmost surface of as produced N-MWCNTs array. Further, we show that the PMMA from tip end or the root end can be remove selectively, without un-coating walls of the tubes. The TGA, BET surface area analysis and SEM imaging proves that when only the tip ends of the nanotubes are exposed to a Li/NH$_3$ reaction mixture, there is little evidence of the unzipping reaction that we have reported in N-MWCNTs. However, when the root ends of the nanotubes are exposed to the reaction mixture, the N-MWCNTs unzip in a manner that is indistinguishable from as-produced, uncoated N-MWCNTs. These results indicate that the unzipping process is likely driven by intercalation and proceeds from the root end toward the tip end.

LIST OF ABBREVIATIONS

AFM	Atomic force microscopy
AIBN	2,2′-azobis(2-methylpropionitrile)
BET	Brunauer-Emmett-Teller
CNTs	Carbon nanotubes
CVD	Chemical vapor deposition
ECR	Electron cyclotron resonance
EDS	X-ray spectroscopy
EDX	Energy dispersive x-ray spectroscopy
EELS	Electron energy-loss spectroscopy
GICs	Graphite intercalation compounds
GNRs	Graphene nanoribbons
MMA	Methyl methacrylate
MWCNTs	Multiwalled carbon nanotubes
N-MWCNTs	Nitrogen-doped multiwalled carbon
PMMA	Poly(methyl methacrylate)
SEM	Scanning electron microscopy
STEM	Scanning transmission electron microscope
SWCNTs	Singel walled carbon nanotubes
TEM	Transmission electronic microscopy
TGA	Thermogravimetric analysis
UHMWPE	Ultra-high-molecular-weight polyethylene
XPS	X-ray photoelectron spectroscopic

REFERENCES

(1)   Geim, A. K.; Novoselov, K. S. *Nat Mater* **2007**, *6*, 183.

(2)   Castro Neto, A. H.; Guinea, F.; Peres, N. M. R.; Novoselov, K. S.; Geim, A. K. *Rev Mod Phys* **2009**, *81*, 109.

(3)   Lee, C.; Wei, X. D.; Kysar, J. W.; Hone, J. *Science* **2008**, *321*, 385.

(4)   Iijima, S. *Nature* **1991**, *354*, 56.

(5)   Popov, V. N. *Mat Sci Eng R* **2004**, *43*, 61.

(6)   De Volder, M. F. L.; Tawfick, S. H.; Baughman, R. H.; Hart, A. J. *Science* **2013**, *339*, 535.

(7)   Ajayan, P. M.; Ebbesen, T. W. *Rep Prog Phys* **1997**, *60*, 1025.

(8)   Wildoer, J. W. G.; Venema, L. C.; Rinzler, A. G.; Smalley, R. E.; Dekker, C. *Nature* **1998**, *391*, 59.

(9)   Bulusheva, L. G.; Okotrub, A. V.; Romanov, D. A.; Tomanek, D. *J Phys Chem A* **1998**, *102*, 975.

(10)   Sankaran, R. M. *J Phys D Appl Phys* **2011**, *44*.

(11)   Li, H. B.; Page, A. J.; Irle, S.; Morokuma, K. *J Am Chem Soc* **2012**, *134*, 15887.

(12)   Amelinckx, S.; Lucas, A.; Lambin, P. *Rep Prog Phys* **1999**, *62*, 1471.

(13)   Katayama, T.; Araki, H.; Yoshino, K. *J Appl Phys* **2002**, *91*, 6675.

(14)   Ajayan, P. M.; Ichihashi, T.; Iijima, S. *Chem Phys Lett* **1993**, *202*, 384.

(15)   Harris, P. J. F.; John, P. *Carbon Nanotubes and Related Structures: New Materials for the Twenty-first* 1991.

(16)   Rodriguez, N. M.; Chambers, A.; Baker, R. T. K. *Langmuir* **1995**, *11*, 3862.

(17)   Ebbesen, T. W.; Ajayan, P. M. *Nature* **1992**, *358*, 220.

(18)   Guo, T.; Nikolaev, P.; Rinzler, A. G.; Tomanek, D.; Colbert, D. T.; Smalley, R. E. *J Phys Chem-Us* **1995**, *99*, 10694.

(19)   Joseyacaman, M.; Mikiyoshida, M.; Rendon, L.; Santiesteban, J. G. *Appl Phys Lett* **1993**, *62*, 202.

(20)   Sharifi, T.; Nitze, F.; Barzegar, H. R.; Tai, C. W.; Mazurkiewicz, M.; Malolepszy, A.; Stobinski, L.; Wagberg, T. *Carbon* **2012**, *50*, 3535.

(21)   Nath, M.; Satishkumar, B. C.; Govindaraj, A.; Vinod, C. P.; Rao, C. N. R. *Chem Phys Lett* **2000**, *322*, 333.

(22)   Lv, W. X.; Zhang, R.; Xia, T. L.; Bi, H. M.; Shi, K. Y. *J Nanopart Res* **2011**, *13*, 2351.

(23)   Qian, D. L.; Andrews, R.; Jacques, D.; Kichambare, P.; Lian, G.; Dickey, E. C. *J Nanosci Nanotechno* **2003**, *3*, 93.

(24)   Duclaux, L. *Carbon* **2002**, *40*, 1751.

(25)   Satishkumar, B. C.; Govindaraj, A.; Harikumar, K. R.; Zhang, J. P.; Cheetham, A. K.; Rao, C. N. R. *Chem Phys Lett* **1999**, *300*, 473.

(26)   Nxumalo, E. N.; Chabalala, V. P.; Nyamori, V. O.; Witcomb, M. J.; Coville, N. J. *J Organomet Chem* **2010**, *695*, 1451.

(27)   Sung, S. L.; Tsai, S. H.; Liu, X. W.; Shih, H. C. *J Mater Res* **2000**, *15*, 502.

(28)   Sen, R.; Satishkumar, B. C.; Govindaraj, A.; Harikumar, K. R.; Raina, G.; Zhang, J. P.; Cheetham, A. K.; Rao, C. N. R. *Chem Phys Lett* **1998**, *287*, 671.

(29)   Terrones, M.; Redlich, P.; Grobert, N.; Trasobares, S.; Hsu, W. K.; Terrones, H.; Zhu, Y. Q.; Hare, J. P.; Reeves, C. L.; Cheetham, A. K.; Ruhle, M.; Kroto, H. W.; Walton, D. R. M. *Adv Mater* **1999**, *11*, 655.

(30)   Ma, X. C.; Wang, E. G. *Appl Phys Lett* **2001**, *78*, 978.

(31)   Higgins, D.; Chen, Z.; Chen, Z. W. *Electrochim Acta* **2011**, *56*, 1570.

(32)   Andrews, R.; Jacques, D.; Qian, D. L.; Rantell, T. *Accounts Chem Res* **2002**, *35*, 1008.

(33)   Kumar, M.; Ando, Y. *J Nanosci Nanotechno* **2010**, *10*, 3739.

(34)   Liu, K.; Jiang, K. L.; Feng, C.; Chen, Z.; Fan, S. S. *Carbon* **2005**, *43*, 2850.

(35)   Kunadian, I.; Andrews, R.; Qian, D. L.; Menguc, M. P. *Carbon* **2009**, *47*, 384.

(36)   Amelinckx, S.; Zhang, X. B.; Bernaerts, D.; Zhang, X. F.; Ivanov, V.; Nagy, J. B. *Science* **1994**, *265*, 635.

(37)   Fan, S. S.; Liu, L.; Liu, M. *Nanotechnology* **2003**, *14*, 1118.

(38)   Baker, R. T. K.; Chludzinski, J. J.; Dudash, N. S.; Simoens, A. J. *Carbon* **1983**, *21*, 463.

(39)   Sinnott, S. B.; Andrews, R.; Qian, D.; Rao, A. M.; Mao, Z.; Dickey, E. C.; Derbyshire, F. *Chem Phys Lett* **1999**, *315*, 25.

(40)   Brown, B.; Parker, C. B.; Stoner, B. R.; Glass, J. T. *Carbon* **2011**, *49*, 266.

(41)   Datta, S. S.; Strachan, D. R.; Khamis, S. M.; Johnson, A. T. C. *Nano Lett* **2008**, *8*, 1912.

(42)   Jang, J. W.; Lee, C. E.; Lyu, S. C.; Lee, T. J.; Lee, C. J. *Appl Phys Lett* **2004**, *84*, 2877.

(43)   van Dommele, S.; Romero-Izquirdo, A.; Brydson, R.; de Jong, K. P.; Bitter, J. H. *Carbon* **2008**, *46*, 138.

(44)   Miyamoto, Y.; Cohen, M. L.; Louie, S. G. *Solid State Commun* **1997**, *102*, 605.

(45)   Nxumalo, E. N.; Coville, N. J. *Materials* **2010**, *3*, 2141.

(46)   van Dommele, S.; de Jong, K. P.; Bitter, J. H. *Chem Commun* **2006**, 4859.

(47)   Czerw, R.; Terrones, M.; Charlier, J. C.; Blase, X.; Foley, B.; Kamalakaran, R.; Grobert, N.; Terrones, H.; Tekleab, D.; Ajayan, P. M.; Blau, W.; Ruhle, M.; Carroll, D. L. *Nano Lett* **2001**, *1*, 457.

(48)   Chou, T. W.; Gao, L. M.; Thostenson, E. T.; Zhang, Z. G.; Byun, J. H. *Compos Sci Technol* **2010**, *70*, 1.

(49)   Beigbeder, A.; Degee, P.; Conlan, S. L.; Mutton, R. J.; Clare, A. S.; Pettitt, M. E.; Callow, M. E.; Callow, J. A.; Dubois, P. *Biofouling* **2008**, *24*, 291.

(50)   Fan, S. S.; Chapline, M. G.; Franklin, N. R.; Tombler, T. W.; Cassell, A. M.; Dai, H. J. *Science* **1999**, *283*, 512.

(51)   Kocabas, C.; Hur, S. H.; Gaur, A.; Meitl, M. A.; Shim, M.; Rogers, J. A. *Small* **2005**, *1*, 1110.

(52)   Kang, S. J.; Kocabas, C.; Kim, H. S.; Cao, Q.; Meitl, M. A.; Khang, D. Y.; Rogers, J. A. *Nano Lett* **2007**, *7*, 3343.

(53)   Qu, L. T.; Vaia, R. A.; Dai, L. M. *Acs Nano* **2011**, *5*, 994.

(54)   Qu, L.; Dai, L. *J Mater Chem* **2007**, *17*, 3401.

(55)   Koehne, J.; Chen, H.; Li, J.; Cassell, A. M.; Ye, Q.; Ng, H. T.; Han, J.; Meyyappan, M. *Nanotechnology* **2003**, *14*, 1239.

(56)   Kar, S.; Bindal, R. C.; Tewari, P. K. *Nano Today* **2012**, *7*, 385.

(57)   Dumee, L.; Sears, K.; Schutz, J.; Finn, N.; Duke, M.; Gray, S. *Desalin Water Treat* **2010**, *17*, 72.

(58)   Hinds, B. J.; Chopra, N.; Rantell, T.; Andrews, R.; Gavalas, V.; Bachas, L. G. *Science* **2004**, *303*, 62.

(59)   Li, X. L.; Wang, X. R.; Zhang, L.; Lee, S. W.; Dai, H. J. *Science* **2008**, *319*, 1229.

(60)   Luo, B.; Liu, S. M.; Zhi, L. J. *Small* **2012**, *8*, 630.

(61)   Ci, L.; Xu, Z. P.; Wang, L. L.; Gao, W.; Ding, F.; Kelly, K. F.; Yakobson, B. I.; Ajayan, P. M. *Nano Res* **2008**, *1*, 116.

(62)   Kosynkin, D. V.; Higginbotham, A. L.; Sinitskii, A.; Lomeda, J. R.; Dimiev, A.; Price, B. K.; Tour, J. M. *Nature* **2009**, *458*, 872.

(63)   Jiao, L. Y.; Zhang, L.; Wang, X. R.; Diankov, G.; Dai, H. J. *Nature* **2009**, *458*, 877.

(64)   Mohammadi, S.; Kolahdouz, Z.; Mohajerzadeh, S. *J Mater Chem C* **2013**, *1*, 1309.

(65)   Morelos-Gomez, A.; Vega-Diaz, S. M.; Gonzalez, V. J.; Tristan-Lopez, F.; Cruz-Silva, R.; Fujisawa, K.; Muramatsu, H.; Hayashi, T.; Mi, X.; Shi, Y. F.; Sakamoto, H.; Khoerunnisa, F.; Kaneko, K.; Sumpter, B. G.; Kim, Y. A.; Meunier, V.; Endo, M.; Munoz-Sandoval, E.; Terrones, M. *Acs Nano* **2012**, *6*, 2261.

(66)   Zhuang, N. F.; Liu, C. C.; Jia, L. N.; Wei, L.; Cai, J. D.; Guo, Y. L.; Zhang, Y. F.; Hu, X. L.; Chen, J. Z.; Chen, X. D.; Tang, Y. X. *Nanotechnology* **2013**, *24*.

(67)   Kim, W. S.; Moon, S. Y.; Park, N. H.; Huh, H.; Shim, K. B.; Ham, H. *Chem Mater* **2011**, *23*, 940.

(68)   Wei, D. C.; Xie, L. F.; Lee, K. K.; Hu, Z. B.; Tan, S. H.; Chen, W.; Sow, C. H.; Chen, K. Q.; Liu, Y. Q.; Wee, A. T. S. *Nat Commun* **2013**, *4*.

(69)   Meier, M. S.; Andrews, R.; Jacques, D.; Cassity, K. B.; Qian, D. *J Mater Chem* **2008**, *18*, 4143.

(70)   Meier, M. S.; Selegue, J. P.; Cassity, K. B.; Kaur, A. P.; Qian, D. L. *J Phys-Condens Mat* **2010**, *22*.

(71)   Belin, T.; Epron, F. *Mat Sci Eng B-Solid* **2005**, *119*, 105.

(72)   Wepasnick, K. A.; Smith, B. A.; Bitter, J. L.; Fairbrother, D. H. *Anal Bioanal Chem* **2010**, *396*, 1003.

(73)   Wildgoose, G. G.; Lawrence, N. S.; Leventis, H. C.; Jiang, L.; Jones, T. G. J.; Compton, R. G. *J Mater Chem* **2005**, *15*, 953.

(74)   Kim, U. J.; Furtado, C. A.; Liu, X. M.; Chen, G. G.; Eklund, P. C. *J Am Chem Soc* **2005**, *127*, 15437.

(75)   Cao, A. Y.; Xu, C. L.; Liang, J.; Wu, D. H.; Wei, B. Q. *Chem Phys Lett* **2001**, *344*, 13.

(76)   Bom, D.; Andrews, R.; Jacques, D.; Anthony, J.; Chen, B. L.; Meier, M. S.; Selegue, J. P. *Nano Lett* **2002**, *2*, 615.

(77)   Georgakilas, V.; Kordatos, K.; Prato, M.; Guldi, D. M.; Holzinger, M.; Hirsch, A. *J Am Chem Soc* **2002**, *124*, 760.

(78)   Fernando, K. A. S.; Lin, Y.; Sun, Y. P. *Langmuir* **2004**, *20*, 4777.

(79)   Chen, J.; Hamon, M. A.; Hu, H.; Chen, Y. S.; Rao, A. M.; Eklund, P. C.; Haddon, R. C. *Science* **1998**, *282*, 95.

(80)   Boul, P. J.; Liu, J.; Mickelson, E. T.; Huffman, C. B.; Ericson, L. M.; Chiang, I. W.; Smith, K. A.; Colbert, D. T.; Hauge, R. H.; Margrave, J. L.; Smalley, R. E. *Chem Phys Lett* **1999**, *310*, 367.

(81)   Osorio, A. G.; Silveira, I. C. L.; Bueno, V. L.; Bergmann, C. P. *Appl Surf Sci* **2008**, *255*, 2485.

(82)   Barthos, R.; Mehn, D.; Demortier, A.; Pierard, N.; Morciaux, Y.; Demortier, G.; Fonseca, A.; Nagy, J. B. *Carbon* **2005**, *43*, 321.

(83)   Borondics, F.; Bokor, M.; Matus, P.; Tompa, K.; Pekker, S.; Jakab, E. *Fuller Nanotub Car N* **2005**, *13*, 375.

(84)   Wunderlich, D.; Hauke, F.; Hirsch, A. *J Mater Chem* **2008**, *18*, 1493.

(85)   Stephenson, J. J.; Sadana, A. K.; Higginbotham, A. L.; Tour, J. M. *Chem Mater* **2006**, *18*, 4658.

(86)   Liang, F.; Alemany, L. B.; Beach, J. M.; Billups, W. E. *J Am Chem Soc* **2005**, *127*, 13941.

(87)   Hook, J. M.; Mander, L. N. *Nat Prod Rep* **1986**, *3*, 35.

144

(88)   Patil, N. D.; Meier, M. S. *Mater. Res. Express* **2014**, *1*, 015603.

(89)   Charlier, A.; Charlier, M. F.; Fristot, D. *J Phys Chem Solids* **1989**, *50*, 987.

(90)   Dresselhaus, M. S.; Dresselhaus, G. *Adv Phys* **2002**, *51*, 1.

(91)   York, B. R.; Solin, S. A. *Phys Rev B* **1985**, *31*, 8206.

(92)   Le Normand, F.; Hommet, J.; Szorenyi, T.; Fuchs, C.; Fogarassy, E. *Phys Rev B* **2001**, *64*.

(93)   Salamancariba, L.; Dresselhaus, M. S. *Carbon* **1986**, *24*, 261.

(94)   Maurin, G.; Bousquet, C.; Henn, F.; Bernier, P.; Almairac, R.; Simon, B. *Chem Phys Lett* **1999**, *312*, 14.

(95)   Nalimova, V. A.; Sklovsky, D. E.; Bondarenko, G. N.; AlvergnatGaucher, H.; Bonnamy, S.; Beguin, F. *Synthetic Met* **1997**, *88*, 89.

(96)   Cano-Marquez, A. G.; Rodriguez-Macias, F. J.; Campos-Delgado, J.; Espinosa-Gonzalez, C. G.; Tristan-Lopez, F.; Ramirez-Gonzalez, D.; Cullen, D. A.; Smith, D. J.; Terrones, M.; Vega-Cantu, Y. I. *Nano Lett* **2009**, *9*, 1527.

(97)   Qu, L. T.; Zhao, Y.; Hu, Y.; Zhang, H.; Li, Y.; Guo, W.; Luo, H. X.; Dai, L. M. *J Mater Chem* **2010**, *20*, 3595.

(98)   Raravikar, N. R.; Schadler, L. S.; Vijayaraghavan, A.; Zhao, Y. P.; Wei, B. Q.; Ajayan, P. M. *Chem Mater* **2005**, *17*, 974.

(99)   Martin, J.; Mijangos, C. *Langmuir* **2009**, *25*, 1181.

(100)   Ko, H.; Peleshanko, S.; Tsukruk, V. V. *J Phys Chem B* **2004**, *108*, 4385.

(101)   Zhou, L.; Gao, C.; Zhu, D.; Xu, W.; Chen, F. F.; Palkar, A.; Echegoyen, L.; Kong, E. S. W. *Chem-Eur J* **2009**, *15*, 1389.

(102)   Singh, D. K.; Iyer, P. K.; Giri, P. K. *J Appl Phys* **2010**, *108*.

(103)   Peigney, A.; Laurent, C.; Flahaut, E.; Bacsa, R. R.; Rousset, A. *Carbon* **2001**, *39*, 507.

(104)   Canete-Rosales, P.; Ortega, V.; Alvarez-Lueje, A.; Bollo, S.; Gonzalez, M.; Anson, A.; Martinez, M. T. *Electrochim Acta* **2012**, *62*, 163.

(105)   Lehman, J. H.; Terrones, M.; Mansfield, E.; Hurst, K. E.; Meunier, V. *Carbon* **2011**, *49*, 2581.

(106)   Zilli, D.; Bonelli, P. R.; Cukierman, A. L. *Nanotechnology* **2006**, *17*, 5136.

145

EDUCATION

Ph.D. Chemistry, Advisor: Dr. Mark S. Meier   April. 2014
University of Kentucky, Dept of Chemistry and Center for Applied Energy Research, KY

M.Sc. Organic Chemistry   May. 2006
University of Mumbai, India   1st Class with Distinction

B.Sc. Chemistry   May. 2004
University of Mumbai, India   1st Class with Distinction

Industrial Experience Summary

Research Chemist, Trainee with Galaxy Surfactants Ltd, Mumbai   Sep. 2006 - Apr. 2008
Research Chemist in Centaur Pharma Pvt. Ltd, Mumbai   Aug-2006
Q.C. Chemist, Trainee with Watson Pharma, Mumbai   Jul. - Aug. 2006

Publications/ Conference Presentations

- Patil, N. D.; Meier, M. S.;"An investigation of the fracturing process in nitrogen-doped multiwalled carbon nanotubes (N-MWCNTs). Evidence for directional unzipping", *Mater. Res. Express, 2014*, 1, 015603

- Patil, N. D.; Meier, M. S.; Yao, S.; Mobley, J.; Crocker, M. "Selective cleavage of the Cα-Cβ linkage in lignin model compounds via Baeyer-Villiger oxidation", *Organic and Biomolecular Chemistry* (submitted)

- Patil, N. D.; Meier, M. S.; Mobley, J.; Crocker, M. "Depolymerization of lignin by selective cleavage of the Cα-Cβ linkage via Baeyer-Villiger oxidation", *Green Chemistry*. (submitted)

- Patil, N. D.; Meier, M. S.; Mobley, J.; Crocker, M. "Depolymerization of lignin by selective cleavage of the Cα-Cβ linkage via Baeyer-Villiger oxidation" Preprint *ACS, 2013*. CELL-105

- Patil, N. D.; Meier, M. S.; Mobley, J. K.; Crocker, M.; Study of depolymerization in organosolv lignin by selective cleavage of the Cα-Cβ linkage, *RE3 2013*(Renewable energy and energy efficiency), Louisville, Kentucky

- Patil, N. D.; Meier, M. S.; Mobley, J. K.; Crocker, M.; Pace. R.; "Depolymerization of lignin by selective cleavage of the Cα-Cβ linkage via Baeyer-Villiger oxidation" *Naff symposium 2013*, Lexington, Kentucky

- Mobley, J. K.; Patil, N. D.; Crocker, M.; Meier. M. S.; "Towards Oxidative Catalytic Depolymerization of Lignin and Lignin Model Compounds" *NAM 2013*, Louisville, Kentucky

- Rodney Andrews, Mark Crocker, Seth DeBolt, Mark Meier, Samuel A Morton III. "Hydrocarbons from Biomass: Lignin Deconstruction for the Production of Liquid Fuels" *NSF* EFRI Grantees Meeting *2012*, Arlington, Virginia

- Mobley, J. K.; Patil, N. D; Pace, R; Crocker, M; Meier, M, S.. " GPC analysis of lignin and lignin oxidation products. Preprint *SERMACS, 2012,* SERM-636

- Patil, N. D.; Meier, M. S.; Qian, D. "Exploring the mechanism of longitudinal cutting in nitrogen-doped multiwalled carbon annotates (N-MWCNTs)", Preprint, *Carbon, 2010*

- Patil, N. D.; Qian, D.; Meier. M. S.; "Exploring the mechanism of longitudinal cutting in nitrogen-doped multiwalled carbon nanotubes (N-MWCNT)" Naff symposium 2010, Lexington, Kentucky

- Patil, N. D.; Mark S. Meier. "Longitudinal cutting of intact arrays of nitrogen-doped multiwalled carbon nanotubes", *KAS 2009*, Richmond, Kentucky